2024

Measuring, modeling, and manipulating the electrographic markers of disease in epilepsy

BOSTON UNIVERSITY

ARAM V. CHOBANIAN & EDWARD AVEDISIAN SCHOOL OF MEDICINE

Dissertation

MEASURING, MODELING, AND MANIPULATING THE ELECTROGRAPHIC MARKERS OF DISEASE IN EPILEPSY

by

DHINAKARAN MAHESWARAN CHINAPPEN

B.S.Eng., University of Pennsylvania, 2009
B.A., University of Pennsylvania, 2009
M.Eng., Cornell University, 2013
M.B.A, University of Illinois at Urbana-Champaign, 2019

Submitted in partial fulfillment of the

requirements for the degree of

Doctor of Philosophy

2024

Approved by

First Reader

Mark A. Kramer, Ph.D.
Professor of Mathematics and Statistics

Second Reader

Catherine J. Chu, M.D., M.A., M.M.S.C.
Associate Professor of Neurology and Neurologist
Harvard Medical School and Massachusetts General Hospital

Third Reader

Uri T. Eden, Ph.D.
Professor of Mathematics and Statistics

DEDICATION

I would like to dedicate this work to my parents, Veenah and Maghespren, the best human beings one could ever imagined, my ever supporting and loving sisters, Sandhya and Kanthimadi and their partners, and my wonderful nieces and nephews, Melvin, Anjali, Avissen, Shaivan and Avani to whom I wish this work can serve as an example one day that light will always win over darkness.

ACKNOWLEDGMENTS

Thank you to my main dissertation mentor, Dr. Catherine J. Chu, who has guided me professionally and provided the resources to accomplish this work as well as to Dr. Mark A. Kramer for his priceless guidance. I would like to extend my gratitude to all the members and affiliates of the ChuLab.

MEASURING, MODELING, AND MANIPULATING THE ELECTROGRAPHIC MARKERS OF DISEASE IN EPILEPSY

DHINAKARAN MAHESWARAN CHINAPPEN

Boston University Aram V. Chobanian & Edward Avedisian School of Medicine, 2024

Major Professor: Mark Kramer, Professor of Mathematics and Statistics

ABSTRACT

Epilepsy, a complex neurological disorder marked by repetitive and spontaneous seizures, is one of the leading drivers of neurological morbidity worldwide. This thesis investigates epilepsy using scalp electroencephalography (EEG), magnetoencephalography (MEG), intracranial EEG, and behavioral tasks in children and adult populations. The thesis consists of four studies that aim to improve our understanding of the disorder and develop better treatment options.

In a first study, we focused on predicting seizure risk. To do so, we analyzed interictal epileptiform discharge (IED) characteristics in 59 children with self-limited epilepsy with centrotemporal spikes (SeLECTS). We showed that specific features of the spike and slow wave complex of an IED – particularly average spike height, spike duration, slow wave rising slope, slow wave falling slope, and the most extreme values of slow wave rising slope – improve prediction of future seizure risk, beyond the expected resolution of SeLECTS with age. Moreover, longitudinal analysis showed the predictive value of spike

height. These findings hold clinical significance for patient care and offer insights into the underlying neuronal mechanisms that influence seizure risk.

Next, we examined the thalamocortical sensory motor circuit, a crucial communication pathway affected in SeLECTS. To do so, we used the MEG to measure the median nerve stimulation conduction time from the wrist to the sematosensory cortex. We found that children with SeLECTs exhibited slower nerve conduction times compared to healthy controls, and that the ventral thalamic volume predicted conduction time. In addition, we found more pronounced slowing in children with resolve epilepsy, suggesting that thalamocortical circuit dysfunction might persist even after seizures cease.

In a third study, we explored the electrophysiological response of the thalamus in patients with drug refractory epilepsy to auditory sensory gating, a filtering mechanism for incoming stimuli. While we found SG in the thalamus and at the scalp, we found that thalamic SG - but not scalp-recorded SG - predicted performance on an attention task. Additionally, thalamic and scalp spindle rates - indicators of memory consolidation and cortical development - also predicted attention. These findings highlight the importance of the thalamic reticular nucleus and its role in sensory inhibition and in modulating thalamic sleep spindles, demonstrating the link between thalamic function, sensory processing, and cognitive performance.

The final study investigated the optimization of Closed-Loop Auditory Stimulation (CLAS) for epilepsy. CLAS delivers sound timed to the upstate of the slow oscillation (SO) during sleep, with the goal of enhancing the endogenous brain rhythms – SOs and sleep spindles – that support memory consolidation. We explored the optimal timing and

detection parameters for CLAS to increase sleep spindles. We found that CLAS evokes SOs in both the thalamus and cortex. A higher success rate of evoked SOs occurred when the stimulation targeted the upstate of the endogenous SOs, with the impact on spindles depending on the targeted SO amplitude. CLAS during high amplitude SOs negatively impacted memory consolidation of a motor sequence task while CLAS targeting low amplitude SOs evoked a subsequent increase in spindle incidence and positively impacted memory consolidation. These findings indicate a new strategy to target CLAS for improved memory consolidation.

Conclusion: In this thesis, we identify new predictors of seizure risk and investigate the thalamocortical circuit dysfunction in SeLECTS. We also reveal the role of thalamus in sensory processing and attention in patient with refractory epilepsy and develop new approaches to optimize CLAS as a therapeutic avenue for cognitive symptoms in epilepsy.

TABLE OF CONTENTS

LIST OF TABLES

LIST OF FIGURES

LIST OF ABBREVIATIONS

AED ..... Anti-epileptic drug

ASM ..... Anti-seizure medication

CECTS ..... Childhood epilepsy with centrotemporal spikes

CLAS ..... Closed-loop auditory stimulation

DBS ..... Deep brain stimulation

EEG ..... Electroencephalogram

IED ..... Interictal epileptiform discharge

LA-CLAS ..... Low amplitude closed loop auditory stimulation

LGN ..... Lateral geniculate nucleus

MEG ..... Magnetoencephalography

MGH ..... Massachusetts General Hospital

MRI ..... Magnetic resonance imaging

NREM ..... Non-rapid eye movement

RE ..... Rolandic epilepsy

RNS ..... Responsive stimulation

SA ..... Statistical Analysis

SeLECTs ..... Self-limited epilepsy with centrotemporal spikes

SG ..... Sensory gating

SO ..... Slow oscillation

SO-CLAS ..... Slow oscillation closed loop auditory stimulation

SS ..... Sleep spindle

TRN..... Thalamic reticular nucleus

VEF ..... Visual evoked field

VNS..... Vagus nerve stimulation

CHAPTER ONE: Introduction

1. Epilepsy

1.1. Background

Epilepsy, a complex neurological disorder marked by repetitive and spontaneous seizures, is one of the leading drivers of neurological morbidity worldwide (World Health Organization, 2024). It occurs across demographic boundaries, affecting individuals of all ages and genders. Despite the historical recognition dating back to ancient civilizations, including records from Mesopotamia dating around 4000 BC, the underlying mechanisms, severity, and broader societal impact of epilepsy continue to pose significant challenges for healthcare providers and researchers alike (Kaculini, Tate-Looney and Seifi, 2021; Ostendorf and Gedela, 2017).

The global burden of epilepsy is substantial, with an estimated 50 million individuals affected worldwide (Beghi *et al.*, 2019; World Health Organization, 2024). Approximately 80% of those affected reside in regions classified as equal to or below middle-income countries. Within these populations, barriers to accessing adequate medical care, including diagnostic services and treatment options, contribute to a significant disparity in outcomes. With access to proper medical interventions, nearly three-quarters of epilepsy patients have the potential for significantly improved seizure control and a heightened quality of life (National Institute of Neurological Disorders and Stroke, 2024; World Health Organization, 2024; American Association of Neurological Surgeons, 2024).

Management of epilepsy encompasses a range of therapeutic approaches, tailored to individual patient needs and seizure characteristics. Anti-epileptic drugs (AEDs), which act to modulate neuronal excitability and inhibit abnormal electrical activity in the brain, are commonly prescribed as the first-line treatment strategy. However, despite the availability of numerous AEDs with varying mechanisms of action, approximately one-third of epilepsy patients struggle with seizure management when managed with medication as their sole therapeutic approach (Löscher *et al.*, 2020).

In cases where pharmacological interventions prove inadequate, alternative treatment modalities may be considered. Surgical resection of epileptogenic brain tissue, particularly in cases where seizures originate from well-defined, focal regions, can produce seizure freedom or significant reductions in seizure frequency. Additionally, neuromodulatory approaches such as electrical stimulation, including responsive stimulation (RNS), vagus nerve stimulation (VNS) and deep brain stimulation (DBS), have shown promise in reducing seizure burden and improving quality of life for select individuals with drug-resistant epilepsy.

The overarching goal of epilepsy management remains achieving optimal seizure control and minimizing the impact of seizures on daily functioning and quality of life. However, current treatment strategies for epilepsy primarily target symptom management rather than addressing the underlying pathophysiology of the disorder. Ongoing research efforts aimed at unraveling the underlying mechanisms of epilepsy (Nguyen, Moolchand and Soltesz, 2020) and developing novel therapeutic interventions (Nabbout and

Kuchenbuch, 2020) is laying the groundwork for novel treatment options, which hold promise for improved management and a higher quality of life for individuals living with with this challenging condition.

1.2. Seizures and spikes: understanding abnormal neurological events

A seizure represents a complex neurological phenomenon characterized by abnormal and synchronized electrical activity within the brain (Stafstrom and Carmant, 2015). Between seizures (i.e., interictally), epilepsy manifests in the brain's electrical activity in other ways. For example, interictal discharges – or spikes –manifest in brain voltage recordings as brief bursts of electrical activity, typically lasting less than 250 ms (Staley and Dudek, 2006). These spikes, which appear with a variety of shapes and sizes, exhibit significantly heightened amplitude compared to baseline levels and can emerge during any stage of consciousness. Other types of epileptiform activity that occur between seizures include bursts and slowing (Fernández *et al.*, 2015; *Epilepsy and Seizures | National Institute of Neurological Disorders and Stroke*, 2024; *Understanding different kinds of seizures*, 2024), high-frequency oscillations (Frauscher *et al.*, 2017) and the co-occurrence of high-frequency oscillations and spikes (Shi *et al.*, 2023) .

The consequences of such abnormal neuronal activity are diverse and difficult to track as they depend upon the specific regions of the brain impacted and the severity of the disturbances. Long-term implications of epilepsy-associated neurological events may

include a wide range of cognitive impairments, e.g., impairments in motor function can disrupt the circuits responsible for cognitive functioning and extend into disruptions in emotional regulation leading to mood disorders in certain types of epilepsy (van Rijckevorsel, 2006; Kanner, 2008; Prueter and Norra, 2005). Since spikes, high-frequency oscillations, and seizures can propagate throughout the brain, the importance in detecting the origin of these events and linking them to assessment of disease severity cannot be understated (Tamilia *et al.*, 2021; Gupta and Kadam, 2022; Schlafly *et al.*, 2022).

1.3. Rolandic epilepsy

Rolandic epilepsy (RE), also known as childhood epilepsy with centrotemporal spikes (CECTS) and Self-Limited Epilepsy with Centrotemporal Spikes (SeLECTS), represents the most prevalent form of focal developmental epilepsy observed in children. It is characterized by episodic occurrences of sleep-activated interictal spikes and seizures that originate from the lower half of the sensorimotor cortex, also referred to as the Rolandic region (Wickens, Bowden and D'Souza, 2017; Thorn *et al.*, 2020).

Most children with RE have cognitive deficits detected on formal testing. Affected children may exhibit a range of cognitive symptoms, comprising deficits in attention, difficulties in language processing, and challenges with fine motor skills (Garcia-Ramos *et al.*, 2015; Wickens, Bowden and D'Souza, 2017). However, many of these cognitive impairments improve or even resolve as the disease progresses into remission phases (Kim

et al., 2014). This natural progression offers an opportunity to study a natural model of epilepsy and its negative neurological impacts, as children with RE eventually grow out of the disease (Ross *et al.*, 2020). To that end, in Chapter 3 we investigate how the morphology of interictal spikes changes as children with RE reach seizure freedom and beyond.

1.4. Refractory epilepsy

Conducting simultaneous recordings on both the scalp and intracranial regions represents a rare and resource-intensive endeavor in the field of epilepsy research (Engel *et al.*, 2005). Patients suffering from refractory epilepsy, whose seizures do not respond to medication, are often candidates for alternative treatments, specifically resection or neuromodulation of the brain region producing seizures. To identify this surgical target often requires long-term monitoring with both scalp and intracranial recordings. Intracranial recordings require careful consideration and planning, as it involves the coordination of specialized equipment, skilled medical personnel, and dedicated resources. Following electrode implantation surgery, which involves the precise placement of electrodes within the brain, patients undergo extensive monitoring to capture and analyze neural activity associated with seizure events and epileptiform activity.

The data obtained from these recordings are invaluable for several reasons. First, these data serve the primary clinical purpose of identifying the epileptogenic zone, the

specific area responsible for generating seizures. By pinpointing this region, clinicians can tailor treatment strategies to target and potentially alleviate seizure activity. Moreover, these recordings guide the selection and implementation of therapeutic interventions, such as RNS, VNS, and DBS (Haneef and Skrehot, 2023). Through analysis of neural activity patterns and abnormal networks, clinicians can tailor stimulation parameters to modulate brain activity and reduce seizure frequency (Sisterson *et al.*, 2019). From a research perspective, data from simultaneous scalp and intracranial sources benefit our multiscale comprehension of the mechanisms driving epilepsy and possibly enrich our insights in other types of epilepsy.

2. Thalamocortical circuit dysfunction in epilepsy

2.1. Cortical and thalamic involvement

While epilepsy has traditionally been viewed as a primarily cortical disorder, recent evidence suggests that the thalamus also plays a pivotal role (Martín-López *et al.*, 2017; Caciagli *et al.*, 2020). The thalamus serves as a central hub for transmitting sensory and motor information as well as enabling communication between subcortical structures and cortical areas. It also contributes significantly to higher-level cognitive abilities such as attention, memory, and executive function (de Bourbon-Teles *et al.*, 2014; Fama and Sullivan, 2015; Wimmer *et al.*, 2015).

Disruption by epileptiform activity within both cortical and thalamic circuits has long been suspected to affect optimal cognitive functioning (Nicolai *et al.*, 2012; Horvath *et al.*, 2020). Cortical hyperexcitability, characteristic of epileptic seizures, can propagate aberrant neural signals to thalamic nuclei, leading to dysregulated thalamocortical interactions and subsequent cognitive impairments (Wodeyar *et al.*, 2024). Moreover, the thalamus itself can be a site of epileptogenic activity, contributing to the generation and propagation of seizures (Blumenfeld, 2002; Feng *et al.*, 2017). Seizure-induced alterations in thalamic circuitry can further exacerbate cognitive deficits, creating a complex interplay between cortical and thalamic involvement in epilepsy-related cognitive dysfunction (Lindquist *et al.*, 2023).

2.2. Focal epilepsy and cognitive deficit

Previous work in our group has shown that thalamocortical circuit dysfunction is implicated even in focal epilepsies (Ostrowski *et al.*, 2019; Thorn *et al.*, 2020; Kwon *et al.*, 2022; Spencer *et al.*, 2022). A spectrum of symptoms that extend beyond epileptiform activity, specifically beyond the focal dysfunction within the sensorimotor thalamocortical circuits, can be observed (Wickens, Bowden and D'Souza, 2017).

Direct measures of thalamocortical white matter connectivity show that children with RE have an abnormal developmental trajectory of thalamocortical structural connectivity to the sensorimotor cortex that persists beyond disease resolution (Ostrowski

et al. 2019). Electrophysiological and structural evidence implicates focal dysfunction of the sensorimotor thalamocortical circuits (Ostrowski *et al.*, 2019; Thorn *et al.*, 2020; Kwon *et al.*, 2022; Spencer *et al.*, 2022). Work in this area is described in Chapter 2, where we investigate the role of the thalamocortical circuit in RE via median-nerve and visual stimulation while recording brain magnetic activity (magnetoencephalography).

2.3. Leveraging insights from multiscale scalp-intracranial recordings in refractory epilepsy patients

Intracranial recordings from the thalamus in patients with epilepsy have recently become more common as part of clinical care. These recordings provide direct observations of deep brain (thalamic) voltage activity at high temporal resolution (e.g., 1,024 Hz). Combined with simultaneous invasive cortical recordings, these observations allow for detailed analysis of human thalamocortical circuits. In Chapter 4 and 5, we describe our analysis of thalamic recordings from patients performing passive auditory and active typing tasks and investigate the impact of these tasks on thalamocortical circuit activity.

3. Thalamocortical biomarkers and cognition

3.1. Sleep spindles

Sleep spindles are rhythmic bursts of neural activity that occur during specific stages of non-rapid eye movement (NREM) sleep, primarily in N2 and N3 sleep stages.

Alongside other prominent electrographic features like vertex waves, K-complexes, and slow oscillations, sleep spindles contribute to the highly complex architecture of sleep cycles (Andrillon *et al.*, 2011; Laura Fernandez and Anitha Luthi, 2019).

Typically observed in the alpha frequency band, ranging from 9 to 15 Hz, spindles durations typically span 0.5 to 2 seconds (Kostin *et al.*, 2017). Spindles are generated within the thalamus and modulated by the thalamic reticular nucleus (TRN) (Vantomme *et al.*, 2019). Sleep spindles are recognized for their vital role in memory consolidation during sleep and in cortical development, thereby crucial for learning (Herrera and Tarokh, 2024).

Recent studies have investigated the relationship between sleep spindle activity and neurological disorders in children affected by RE. Focal disruptions in sleep spindle patterns within the sensorimotor cortex (Kramer *et al.*, 2021) occur in children with RE, and spindle rates are linked with the severity of cognitive and motor symptoms observed. Understanding these disruptions in sleep spindle dynamics could offer valuable insights into the pathophysiology of RE and inform the development of targeted therapeutic interventions aimed at restoring normal sleep architecture and improving cognitive outcomes in affected individuals.

3.2. Thalamic reticular nucleus and sensory gating

Aside from being central to spindle generation during sleep, TRN neurons respond to novel sensory inputs during wakefulness, thereby showing rapid adaptability to changing

environments while simultaneously protecting the brain from overreacting to repetitive stimuli, conserving neural resources and preventing sensory overload (Khani *et al.*, 2019). This dynamic modulation underpins cognitive functions such as selective attention and sensory discrimination, crucial for navigating the complex sensory landscape of the external world (McAlonan, Cavanaugh and Wurtz, 2006).

However, when the ability of TRN-mediated inhibition is perturbed, the repercussions reverberate throughout the neural circuitry, precipitating aberrations in sensory gating. Experimental evidence from animal models shows that disruptions in TRN function, either through neuronal loss or dysfunction, can lead to a breakdown in the selective filtering of sensory inputs, culminating in an inundation of irrelevant stimuli inundating the cortex and compromising cognitive processes reliant on sensory discrimination (Ahrens *et al.*, 2015; Nakajima, Schmitt and Halassa, 2019).

Knowing that a spindle deficit exists in patients in epilepsy and that the TRN is involved, we performed a sensory gating (SG) experiment to investigate the two functions of the TRN - SG and spindle generation - and link these functions to a behavioral task measuring attention (Chapter 3).

4. Closed-Loop Auditory Stimulation and cognition

4.1 Existing Paradigms

Two approaches to brain stimulation include open-loop or closed-loop designs. In the open-loop paradigm, fixed stimuli are delivered without adapting to endogenous brain

activity, with stimulation parameters based on pre-calculated values, possibly from past experiments or theoretical modeling (Trapp, Schroll and Hamker, 2012). In contrast, a closed-loop paradigm is reactive to the state of the signal used as an input (Ghasemi, Sahraee and Mohammadi, 2018). The signal in question can be electrophysiological but also can multi-factorially encompass whole body reactions or intelligent feedback, among many (Potter, El Hady and Fetz, 2014; Zrenner *et al.*, 2016).

4.2 Closed Loop Auditory Stimulation and cognition

With the recent rise of brain-computer interfaces, the popularity of closed-loop approaches has grown, supported by increased computing power to assess complex signals in real-time (Sitaram *et al.*, 2017). Closed-loop auditory stimulation (CLAS) is a recent paradigm that applies acoustic sounds during sleep to increase slow oscillation and spindle incidences, with potential impacts on memory consolidation (Ngo *et al.*, 2015). Despite the initial promise of this approach, the impacts of CLAS on memory consolidation remain unclear (Wunderlin *et al.*, 2021). Knowing the disruption of the thalamocortical circuits can lead to spindle deficits in epilepsy, we investigated the impact of CLAS on patients with epilepsy (Chapter 5), with the aim to finding the impact in the thalamus as well as optimizing parameters for implementation.

CHAPTER TWO: Spike height improves prediction of future seizure risk[1]

Abstract

Objective: We evaluated whether interictal epileptiform discharge (IED) rate and morphological characteristics predict seizure risk.

Methods: We evaluated 10 features from automatically detectable IEDs in a stereotyped population with self-limited epilepsy with centrotemporal spikes (SeLECTS). We tested whether the average value or the most extreme values from each feature predicted future seizure risk in cross-sectional and longitudinal models.

Results: 10,748 individual centrotemporal IEDs were analyzed from 59 subjects at 81 timepoints. In cross-sectional models, increases in average spike height, spike duration, slow wave rising slope, slow wave falling slope, and the most extreme values of slow wave rising slope each improved prediction of an increased risk of a future seizure compared to a model with age alone ($p < 0.05$, each). In longitudinal model, spike rising height improved prediction of future seizure risk compared to a model with age alone ($p = 0.04$).

Conclusions: Spike height improves prediction of future seizure risk in SeLECTS. Several other morphological features may also improve prediction and should be explored in larger studies.

---

[1] Chapter Two, in full, is a reprint of the following published article as it appears in press: Chinappen, D. M., Xiao, G., Jing, J., Spencer, E. R., Eden, U. T., Kramer, M. A., Westover, M. B., & Chu, C. J. (2023). Spike height improves prediction of future seizure risk. Clinical neurophysiology: official journal of the International Federation of Clinical Neurophysiology, 150, 49–55. https://doi.org/10.1016/j.clinph.2023.02.180

Significance: Discovery of a relationship between novel IED features and seizure risk may improve clinical prognostication, visual and automated IED detection strategies, and provide insights into the underlying neuronal mechanisms that contribute to IED pathology.

Keywords: Electroencephalography (EEG) biomarker; Interictal epileptiform discharges; Rolandic epilepsy; Self-limited epilepsy with centrotmporal spikes (SeLECTS).

1. Introduction

Interictal epileptiform discharges (IEDs) recorded on the scalp EEG are a well-recognized biomarker of epilepsy. Defined as brief (<250 ms) electrical discharges, IEDs are present in nearly all cases of epilepsy, independent of etiology (Staley and Dudek, 2006). The presence of IEDs is the most widely utilized, and sensitive, biomarker to estimate seizure risk (Shinnar *et al.*, 1994; Wirrell, 1998; Staley and Dudek, 2006; Kanemura *et al.*, 2015). However, IEDs are not specific for epilepsy. For example, IEDs are present in 0.5–2.4% of the general population without a seizure history (Bennett, 1967; Eeg-Olofsson, Petersén and Selldén, 1971; Gregory, Oates and Merry, 1993) and can persist for years after seizure resolution (Bouma *et al.*, 1997; Kobayashi *et al.*, 2011; van Klink *et al.*, 2016; Xie *et al.*, 2018; Chen and Koubeissi, 2019; Kramer *et al.*, 2019). Thus, improved non-invasive biomarkers are required to better classify patients at risk of a future seizure (Engel, 2011).

IEDs are composed of a large negative spike followed by a slow wave. Due to the low inter-rater reliability between experts in detecting individual IED events (13–18%) (Webber *et al.*, 1993; Scheuer, Bagic and Wilson, 2017), but improved agreement when determining whether at least one IED is present (kappa 0.83, (Stroink *et al.*, 2006)), prior work evaluating IEDs as a biomarker for seizure risk focused on the presence or absence of IEDs as a binary classifier. However, IEDs are highly variable in rate and several other quantifiable morphological characteristics, such as the amplitude, duration, and slope of both the spike and slow-wave components (Halford, 2009; Bagheri *et al.*, 2017; Kural *et al.*, 2020). With the introduction of reliable, reproducible, automated approaches to detect IEDs (Jing *et al.*, 2020, 2020), these variable and rich features can now be more accurately quantified. However, the utility of spike morphological measurements even with reliable approaches to quantification may be limited by the impact of spike location and brain anatomy on surface measures. This challenge can be mitigated by analyzing spikes across subjects with normal cerebral anatomy and the same spike location.

To determine whether distinct IED morphological characteristics improve prediction of seizure risk among patients with IEDs, we evaluated the relationships between IED rate and morphological features and seizure risk in a cohort of children with self-Limited Epilepsy with centrotemporal spikes (SeLECTS, also called Rolandic epilepsy) (Specchio *et al.*, 2022). Focusing on SeLECTS provides several advantages for this analysis. First, this common, non-lesional developmental epilepsy has a well-characterized and self-limited seizure course (Ross *et al.*, 2020) allowing us to test the

ability of IED features to predict seizure risk over the course of resolving disease. Second, SeLECTS is electrographically stereotyped, characterized by distinct focal spikes in the centrotemporal regions, thereby minimizing the impact of variations in brain anatomy on morphological measures (Herman *et al.*, 2011; Tenney *et al.*, 2016).

We hypothesized that IED rate and morphological features would predict seizure risk in children with SeLECTS with persistent IEDs, thereby improving prediction beyond the presence of IEDs alone. Identification of a relationship between novel IED features and seizure risk would directly improve patient care, help inform automated IED detection strategies, and provide insights into the underlying neuronal mechanisms that contribute to IED pathology.

2. Methods

2.1. Subjects

This project was approved by the institutional review board at Massachusetts General Hospital (MGH). EEG and clinical data from two databases were reviewed for inclusion in this study. These included: 1) All subjects with a diagnosis of SeLECTS seen between June 2001 and June 2017 at MGH with available clinical information on the date of the most recent seizure relative to an EEG recording (n = 130), and 2) All subjects with SeLECTS enrolled in a prospective study between 01/2014 and 06/2019 that included the date of the most recent seizure relative to an EEG recording (n = 34). For 1), patients were

identified via search of the institutional EEG database for the words “rolandic,” “sleep-activated,” “sleep activated,” “benign,” “BECTS,” “ECTS,” “centrotemporal,” “centro-temporal,” or “horizontal dipole” and clinical chart review confirming the history of a seizure, sleep-activated centrotemporal discharges on EEG, and a clinical diagnosis of SeLECTS by a child neurologist (Xie *et al.*, 2018). For 2), subjects enrolled in the prospective study with a clinical diagnosis of SeLECTS by a child neurologist following International League Against Epilepsy criteria, including both a history of focal motor or generalized seizure and an EEG showing sleep-activated centrotemporal spikes were included (Berg *et al.*, 2010). Subjects with a history of only a single clinical seizure were included (n = 1) if clinical and EEG features led to the diagnosis of SeLECTS (Fisher *et al.*, 2014). For both 1) and 2), patients with a history of autism spectrum disorder, mental retardation, or other unrelated neurological disease were excluded while children with attention disorders and mild learning difficulties were included, as these profiles are consistent with known SeLECTS comorbidities (Wickens, Bowden and D’Souza, 2017).

Of the 164 subjects identified for inclusion, 48 were excluded because raw EEG recordings were not available, leaving 178 raw EEG recordings from 116 subjects available for analysis. Of these, 40 EEGs were excluded because stage 2 non-rapid eye movement sleep (N2) was not recorded, leaving 138 EEG recordings from 93 subjects. Of these, 25 EEGs were excluded because these recordings had no IEDs or IEDs were not maximal in the centrotemporal regions (e.g., C3, C4, T3, or T4) resulting in 112 EEG recordings from 79 unique subjects. After manual removal of grossly artifactual detections, 80 EEG

recordings from 59 unique subjects had persistent IED detections and were included in the subsequent analysis.

2.2. EEG data acquisition

EEG data obtained in the clinical MGH EEG lab included electrooculogram (two channels), EEG (19 channels, Ag/AgCl electrodes placed according to the 10–20 international system referred to the second cervical spinous process: FP2, F4, C4, P4, O2, F8, T4, T6, Fz, Cz, Pz, Fp1, F3, C3, P3, O1, F7, T3, and T5), and electrocardiogram using a standard clinical recording system (Xltek, a subsidiary of Natus Medical). Signals were sampled at 256 or 512 Hz. In database 2, EEG data were recorded with a 70-channel cap based on the 10–10 electrode placement system at a 2,035 Hz sampling rate (Easycap, Vectorview, Elekta-Neuromag, Helsinki, Finland) with additional electrodes placed at T1 and T2 locations.

All EEG data were visually inspected by a board-certified neurophysiologist (CJC) and channels with significant artifact were excluded from analysis. Since IEDs are activated during non-rapid eye movement sleep in this disease, to maintain a consistent state of consciousness across recordings, all available N2 data per EEG were selected for analysis following standard sleep staging criteria (Grigg *et al.*, 2007). Additional clinical data were collected for each subject, including age, sex, medication use, and duration seizure free. In a large prospective cohort of 60 children with SeLECTS followed for a

mean of 16 years from epilepsy onset through resolution, we have previously demonstrated that duration seizure free provides a reliable measure of future seizure risk (see Figure 4 in Ross et al., 2020). For example, after 1 month seizure free, the risk of future seizure is 86% and after 60 months seizure free, the risk of a future seizure is ~ 0.

2.3. Automated IED detection

For automated IED detection, only the 10–20 channels were used. IEDs were detected using SpikeNet, a validated automated spike detection program found to perform equivalent to human experts, but with better reproducibility (Jing et al., 2020a). Briefly, SpikeNet's preprocessing steps include 0.0–64.0 Hz band-pass filtering, application of a notch filter, downsampling to 128.0 Hz and referencing channels to the average reference. The SpikeNet detector had lower calibration errors than other commercially available detectors (Jing *et al.*, 2020). Since children with SeLECTS can have unilateral or bilateral involvement, for each EEG, we focused our analysis on the hemisphere with the highest spike rate. To reduce noise due to false detections, but also minimize subjectivity in IED detection, candidate IEDs (n = 12,838) were manually reviewed and only false detections due to gross artifacts were removed (n = 2,160, 16.73%).

2.4. IED morphologic features

After IED detection, for each subject, we evaluated IED rate along with 9 morphological features in each IED spike, including: spike falling height, spike rising

height, spike rising slope, spike falling slope, spike duration, slow wave rising slope, slow wave falling slope, slow wave duration, slow wave falling height (Fig. 2.1). For each subject, we then computed the mean for each feature across all IEDs. Then, we computed the mean of the largest 10% of values (e.g., the largest 10% of spike heights), provided at least 10 spike detections were present in the EEG recording. If only 10 spikes were available, the single largest value from the 10 spikes was included for each feature.

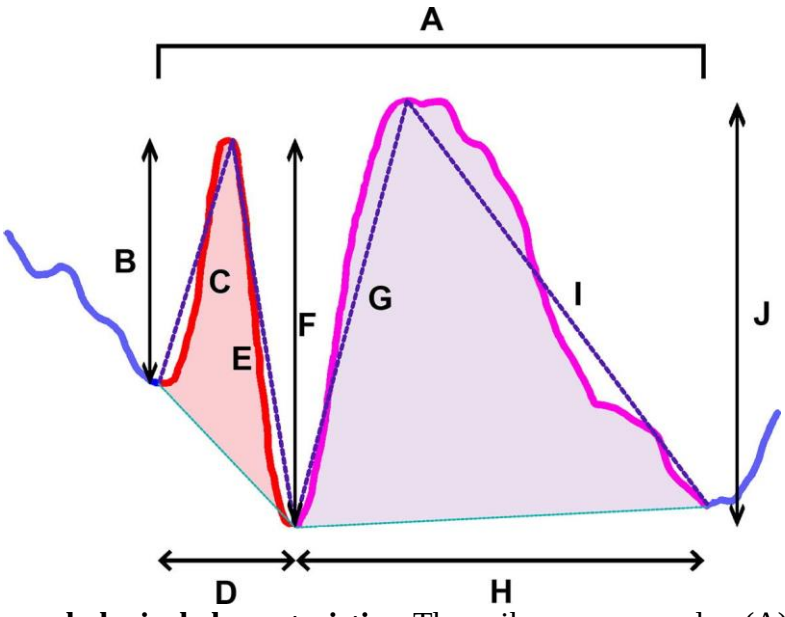

Fig. 2.1. IED morphological characteristics. The spike wave complex (A) consists of 9 features: (B) Spike rising height, (C) Spike rising slope, (D) Spike duration, (E) Spike falling slope, (F) Spike falling height, (G) Slow wave rising slope, (H) Slow wave duration, (I) Slow wave falling slope, (J) Slow wave falling height.

2.5. Statistical analysis

We hypothesized that, among patients with IEDs, IED rate and measures of spike and slow wave morphological features would predict seizure risk. To test this hypothesis,

we developed generalized linear mixed effects models (gamma distribution, log link) of duration seizure free with subject-specific intercepts to account for multiple EEG visits by some subjects.

As age strongly predicts seizure risk in this self-limited disease, we constructed a baseline model with predictor age for comparison to all other models (Equation (1). We evaluated whether antiseizure medication (ASM) or each IED feature improved prediction of seizure risk compared to the model with age alone (Equation (2). To identify collinear IED features among the IED features that improved prediction of seizure risk, we applied hierarchical clustering using a distance measure of one minus the sample correlation between features. Then, among the IED features that improved prediction of seizure risk, we created models for all pairs of non-collinear features (Equation (3). We express the models for seizure risk as,

$$log(Seizure\ risk) \sim 1 + age + (1|subject) \quad (1)$$

$$log(Seizure\ risk) \sim 1 + age + IED\ feature\ or\ ASM + (1|subject) \quad (2)$$

$$log(Seizure\ risk) \sim 1 + age + IED\ feature\ X + IED\ feature\ Y + (1|subject) \quad (3)$$

where age, each IED feature (spike rate, spike rising height, spike rising slope, spike duration, spike falling slope, spike falling height, slow wave rising slope, slow wave duration, slow wave falling slope and slow wave falling height), and antiseizure medication use (ASM) are fixed effects and (1|subject) is a subject specific intercept (i.e., random effect). Nested model comparisons were performed using the log likelihood ratio test, and

goodness-of-fit was evaluated by inspecting the quantile–quantile (Q-Q) plot of the deviance residuals (Lee, Nelder and Pawitan, 2006).

To test whether IED features found significant in the cross-sectional model remained significant in a longitudinal model, we analyzed the relationships including only the subset of subjects with multiple visits, using Eq (1), (2), (3).

3. Results

3.1. Data and characteristics

80 EEG recordings from 59 subjects (26F, ages at recording: 2.9–15.1 years old) were included. A total of 10,748 individual centrotemporal IEDs during N2 sleep were analyzed. EEG N2 sleep duration was an average of 17.7 minutes per subject (range: 1.9–79.5 minutes). The mean number of IEDs per EEG was 134 (range of 1–1419). The mean duration seizure free for the subjects at the time of the EEG visits was 11.3 months (range 0–51 months). 30 subjects (50.9%) were taking antiseizure medications (ASMs) at the time of the EEG recording.

3.2. Spike morphological features vary across and within patients

Visual inspection of IEDs revealed marked morphological diversity in spike and wave amplitude, duration, and slopes both within the same subject and across different

subjects (Fig. 2.2A-C). Distributions of the mean IEDs features across subjects tended to be unimodal (Fig. 2.2D).

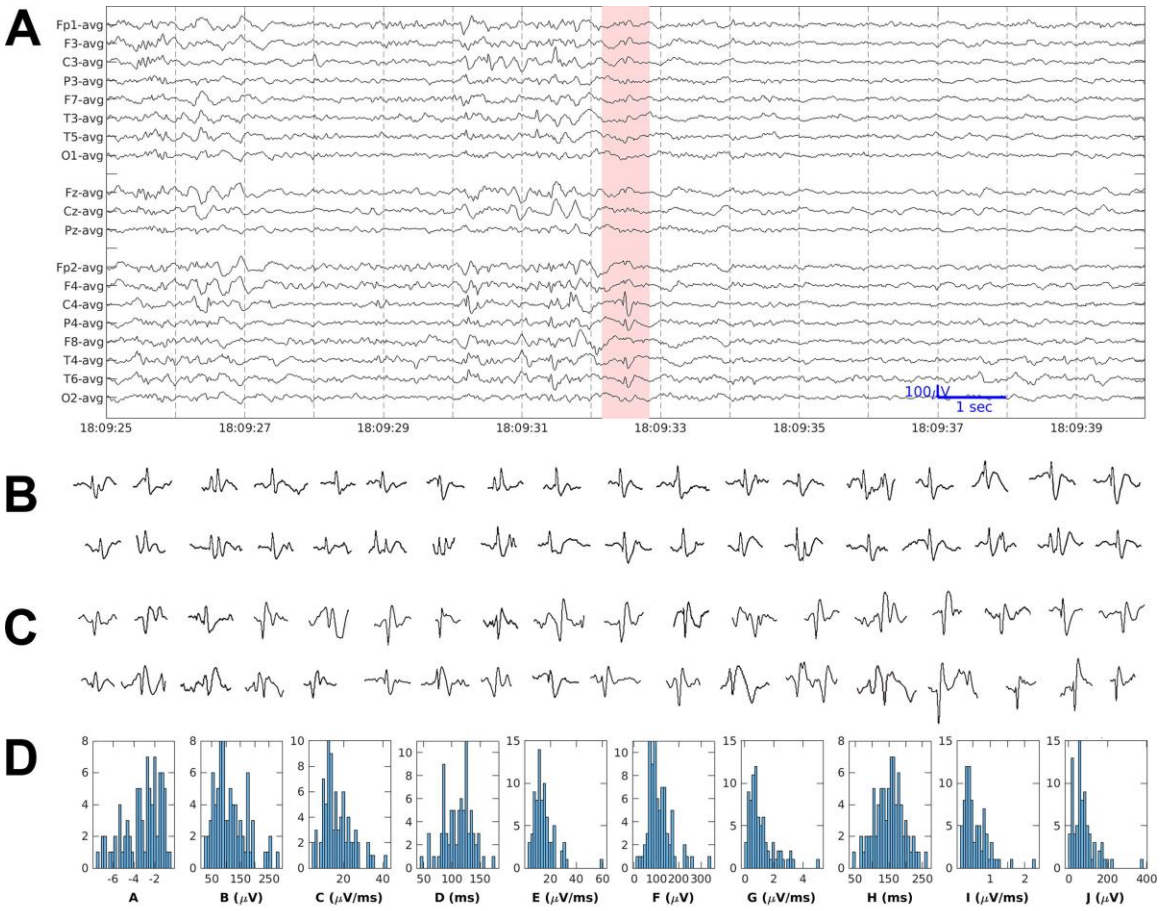

Fig. 2.2. Example IED detections and distributions of IED features. A) An example IED detection (time indicated by red shading) at C4. B, C) Several examples of IED detections (B) within the same recording in one subject, or (C) across different subjects, reveal marked variability in IED morphology across events. D) Distributions of the IED features across subjects are approximately unimodal. Here, A (natural logarithm of spike rate), B (Spike rising height), C (Spike rising slope), D (Spike duration), E (Spike falling slope), F (Spike falling height), G (Slow wave rising slope), H (Slow wave duration), I (Slow wave falling slope) and J (Slow wave falling height) correspond to the morphological features in Fig. 2.1.

3.3. Age predicts seizure risk

Consistent with prior reports (Callenbach *et al.*, 2010), we found that in this self-limited developmental epilepsy, age ($p = 0.001$, effect size 0.245 days/year, 95% CI [0.111 0.380]) had a strong positive relationship with duration seizure free in cross-sectional analysis. In SeLECTS, for each year increase in age, the duration to the next seizure increased by a factor of 28%. Current ASM use was not a significant predictor of seizure risk ($p = 0.14$) and inclusion of ASM was not found to improve the model with age alone (likelihood ratio test $p = 0.14$). Similarly, in longitudinal analysis, age had a strong positive relationship with duration seizure free ($p = 0.008$, effect size 0.235 days/year, 95% CI [0.064 0.406]); for each year increase in age, the duration seizure free increased by a factor of 26%. Current ASM use was not a significant predictor of seizure risk ($p = 0.4$) and inclusion of ASM did not improve the model with age alone (likelihood ratio test $p = 0.4$).

3.4. IED morphological features improve prediction of seizure risk in cross-sectional models

Several IED morphological features improved prediction of seizure risk compared to a model with age alone. Among the spike features (B-F in Fig. 1), spike rising height (B, likelihood ratio test: $p = 0.011$) and spike duration (D, likelihood ratio test: $p < 0.001$) improved prediction of seizure risk compared to the model with age alone. Among the slow wave features (G-J in Fig. 1), slow wave rising slope (G, likelihood ratio test: $p = 0.048$)

and slow wave falling slope (I, likelihood ratio test: p = 0.025) improved prediction of seizure risk compared to the model with age alone (Table 2.1).

	Fixed Effect	p-value (Beta)	AIC	BIC	LLL	p-value (Compare)
All	Age	0.001	903.24	912.77	−447.62	
	B	0.011	898.75	910.66	−444.38	0.011
	D	0.006	891.21	903.12	−440.61	0.002
	G	0.033	901.35	913.26	−445.67	0.048
	I	0.014	900.24	912.15	−445.12	0.025
Largest 10%	Age	0.001	658.51	666.82	−325.25	
	G	0.029	650.65	661.04	−320.33	0.002

Table 2.1. IED features improve prediction of seizure risk beyond age alone. Using the average IED values, four features (B, D, G, and I) improve prediction of seizure risk. Using only the extreme 10% of IED values, one feature (G) improves prediction of seizure risk. B: spike height, D: spike duration, G: slow wave rising slope, I: slow wave falling slope.

3.5. Spike height improves prediction of seizure risk in longitudinal analysis

In subjects with multiple visits, spike height improved prediction of future seizure risk compared to the model with age alone (p = 0.040) and was found trending (p = 0.073, effect size −0.011 per μV, 95% CI [-0.024 0.0011]). None of the other IED features identified from cross-sectional analysis improved the prediction of future seizure in the longitudinal model compared to the model with age alone.

3.6. Multicollinearity in IED morphological features

Visual inspection of scatterplots and clustering analysis revealed that spike rising height (B) and spike duration (D) were collinear and slow wave rising height (G) and slow wave falling height (I) were collinear (Fig. 2.3). To test whether combinations of IED

features improved prediction of seizure risk, we considered each combination of non-collinear features (i.e., B and G; B and I, D and G, D and I; Fig. 2.3). We found no combination of features improved model fit compared to the model with age and spike duration alone in cross-sectional or longitudinal analysis.

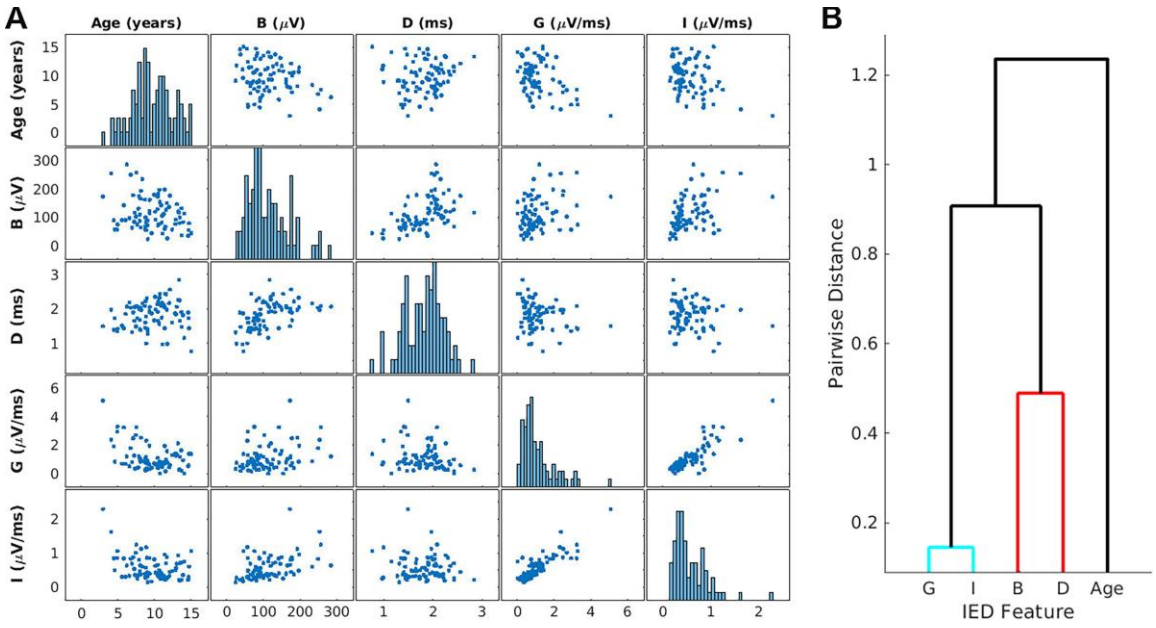

Fig. 2.3. IED features cluster into two correlated groups. A) Distributions (diagonal) and scatter plots (off-diagonal) of age and the four IED features identified to improve the model fit. B) Two clusters identify high correlation between G (slow wave rising slope) and I (slow wave falling slope), and high correlation between B (spike rising height) and D (spike duration).

3.7. The most extreme IED morphological features do not improve prediction of seizure risk

To evaluate whether extreme IED morphological values predict seizure risk, we considered the largest 10% of measurements from subjects with at least 10 IEDs to evaluate

(n = 59). In this cohort, age was again found to have a positive linear relationship with seizure risk (p = 0.001, effect size 0.213 days/year, 95% CI [0.053 0.373]). Following a similar analysis approach as above, we find only one feature - slow wave rising slope - improved prediction of seizure risk compared to the model with age alone (log likelihood ratio test, p = 0.002, Table 1).

4. Discussion

Reliable, non-invasive biomarkers are required to predict seizure risk in both epileptogenesis and epilepsy remission and inform treatment decisions (Engel, 2011). Here, we studied a unique population of patients with a self-limited epilepsy syndrome and identified several IED features that improved prediction of seizure risk beyond the presence of IEDs alone. These findings leverage new features of this canonical non-invasive epilepsy biomarker to improve estimates of seizure risk and our understanding of the components of epileptiform activity that may be most pathogenic.

Consistent with previous studies in SeLECTS, here we also did not find a significant relationship between spike rate and seizure risk (Kramer *et al.*, 2019; Xie *et al.*, 2018; van Klink *et al.*, 2016). Outside of SeLECTS, the relationship between spike rate and seizure frequency has been mixed. Some studies have found increased spike rate correlates with increased seizure frequency and the development of chronic epilepsy (White *et al.*, 2010; Kanemura *et al.*, 2015) while others found that interictal activity

increases after a seizure but does not predict the probability of future seizure occurrence (Gotman and Marciani, 1985; Gotman and Koffler, 1989). These mixed results may be due at least in part to spike detection approaches. Prior studies have relied on visual analysis, where inter-rater agreement in identifying spikes is low (Black *et al.*, 2000; Barkmeier *et al.*, 2012; Scheuer, Bagic and Wilson, 2017). Here we used an automated approach and only removed false detections due to clear artifactual activity, allowing for reproducibility of detection criteria and results. We also focused on a stereotyped idiopathic focal epilepsy and evaluated only the most active spike population in the centrotemporal regions during N2 sleep. Despite reducing variability due to etiology, localization, state of consciousness, and spike detection, we were unable to identify a relationship between spike rate and seizure risk.

Observations from animal models suggest that IEDs represent abnormally enhanced synchronization of large neuronal populations (Truccolo *et al.*, 2014; Bragin, Wilson and Engel Jr, 2000). Thus, IED morphological features are expected to directly reflect the underlying pathological neuronal dynamics, including the size of the network and the degree of the synchronization. In this study, after controlling for age, we found a negative relationship between four IED morphological features and duration seizure free. In each case, an increase in each measure (spike height, spike duration, slow wave rising slope, slow wave falling slope) predicted a shorter duration seizure free, which strongly correlates with increased future seizure risk in SeLECTS (Ross *et al.*, 2020). Together, these results indicate that the shape of the spike and slow wave changes dynamically with

disease resolution. This could be related to factors such as size and synchronization of neuronal networks underlying spike generation or potentially a change in the orientation of the cortical spike source (Gregory and Wong, 1984).

In our cross-sectional and longitudinal analysis, we found that spike height consistently improved prediction of future seizure risk. In the cross-sectional model, when considering the average of all IED features, a 10 μV decrease in spike height corresponds to a 9% increase in duration seizure free. In the longitudinal model, a 10 μV decrease in spike height corresponds to a 10% increase in duration seizure free. Duration seizure free is directly related to the probability of a future seizure, for example an increase in duration seizure free from 10 months to 11 months decreases the probability of a future seizure from 47% to 44% (Ross *et al.*, 2020). Thus, relatively small incremental changes in these morphological features can have a measurable impact on future seizure risk. In our cross-sectional analysis, our findings suggest that several other morphological features may also improve prediction of future seizure risk, however this relationship was not observed in the longitudinal model. This may be related to the small number of longitudinal subjects included in our analysis and these features could be further explored in future studies.

A potential limitation of this cross-sectional study is the use of duration seizure-free as a surrogate for seizure risk. A longitudinal study across the course of epilepsy could further validate our observations by directly recording changes in spike frequency and morphology within subjects compared to direct measures of their future seizure rate. In this investigation, studying SeLECTS provided several advantages, however, our focus on a

homogeneous population limits the generalizability of our findings to other types of epilepsy. In addition, future work utilizing electrical source imaging could more precisely localize the epileptogenic focus and propagation of spikes over disease resolution (Nemtsas *et al.*, 2017).

5. Conclusion

We conclude that the morphological features of IEDs predict seizure risk in children with SeLECTS with persistent IEDs, thereby improving prediction beyond the presence of IEDs alone. These findings have direct implications for patient care, help inform visual and automated IED detection strategies, and ultimately may provide insights into the underlying neuronal mechanisms that contribute to IED pathology.

6. Funding Information

This work was supported by NIH NINDS R01NS115868.

7. Disclosure

CJC has consulted for Biogen Inc and Ovid Pharmaceuticals. MAK has consulted for Biogen Inc. None of the other authors have any disclosures to report.

8. Author contributions

CJC conceived and designed the analysis and wrote the paper. DMC and GX collected the data, performed the analysis, and wrote the paper. JJ and MBW contributed analysis tools. MAK, ERS, and UTE designed the analysis.

9. Declaration of competing interest

The authors declare that they have no known competing financial interests or personal relationships that could have appeared to influence the work reported in this paper.

CHAPTER THREE: Decreased thalamocortical connectivity in resolved Rolandic epilepsy[2]

Abstract

Objective: Median nerve somatosensory evoked fields (SEFs) conduction times reflect the integrity of neural transmission across the thalamocortical circuit. We hypothesized median nerve SEF conduction time would be abnormal in children with Rolandic epilepsy (RE).

Methods: 22 children with RE (10 active; 12 resolved) and 13 age-matched controls underwent structural and diffusion MRI and median nerve and visual stimulation during magnetoencephalography (MEG). N20 SEF responses were identified in contralateral somatosensory cortices. P100 were identified in contralateral occipital cortices as controls. Conduction times were compared between groups in linear models controlling for height. N20 conduction time was also compared to thalamic volume and Rolandic thalamocortical structural connectivity inferred using probabilistic tractography.

Results: The RE group had slower N20 conduction compared to controls ($p = 0.042$, effect size 0.6 ms) and this difference was driven by the resolved RE group ($p = 0.046$). There was no difference in P100 conduction time between groups ($p = 0.83$). Ventral thalamic volume positively correlated with N20 conduction time ($p = 0.014$).

---

[2]Chapter Three, in full, is a reprint of the following published article as it appears in press: Chinappen, D. M., Ostrowski, L. M., Spencer, E. R., Kwon, H., Kramer, M. A., Hämäläinen, M. S., & Chu, C. J. (2023). Decreased thalamocortical connectivity in resolved Rolandic epilepsy. *Clinical neurophysiology: official journal of the International Federation of Clinical Neurophysiology*, 153, 21–27. https://doi.org/10.1016/j.clinph.2023.05.013

Conclusions: Children with resolved RE have focally decreased Rolandic thalamocortical connectivity.

Significance: These results identify a persistent focal thalamocortical circuit abnormality in resolved RE and suggest that decreased Rolandic thalamocortical connectivity may support symptom resolution in this self-limited epilepsy.

Keywords: BECTS; CECTS; Idiopathic focal epilepsy; SeLECTS; Self-limited epilepsy with centrotemporal spikes; Thalamus.

1. Introduction

Rolandic epilepsy (RE, also called self-limited epilepsy with centrotemporal spikes, SeLECTS) is the most common focal developmental epileptic encephalopathy, characterized by a transient period of mild to severe cognitive symptoms and sleep-potentiated interictal spikes and seizures arising from the sensorimotor cortex (Wickens, Bowden and D'Souza, 2017; Thorn *et al.*, 2020). Rolandic epilepsy overlaps clinically with more severe epilepsy aphasia syndromes, and sparse cases have been linked to a monogenic gene mutation (Carvill *et al.*, 2013). Electrographic features are highly penetrant between first-degree relatives, but disease symptoms can also be discordant between monozygotic twins suggesting a complex interplay between genes, environment, and development may contribute to symptom expression in RE (Bray Patrick F. *et al.*, 1964; Bray and Wiser, 1965; Vadlamudi *et al.*, 2006). RE symptoms and electrophysiology lie on a spectrum with

continuous spike-wave during slow wave sleep, Landau-Kleffner syndrome, and centrotemporal spikes and sharp waves without epilepsy (Lemke *et al.*, 2013). Most children with RE have cognitive deficits detected on formal testing during the active phase of the disease (Wickens, Bowden and D'Souza, 2017). Seizures and cognitive symptoms are both self-limited (Ross *et al.*, 2020).

Electrophysiological and structural evidence implicate focal dysfunction of the Rolandic thalamocortical circuits in RE. Children with RE have focally abnormal white matter microstructure near the sensorimotor cortex (Ciumas *et al.*, 2014; Kim *et al.*, 2014; Ostrowski *et al.*, 2019). Sleep spindles, which are generated in the reticular nucleus of the thalamus and entrained in thalamocortical circuits, are focally decreased in the sensorimotor cortex in children with RE during the active phase of the disease (Beenhakker and Huguenard, 2009; Kramer *et al.*, 2021). Clinical symptoms -- seizures and cognitive symptoms – and electrographic features – epileptiform spikes and sleep spindle deficits – resolve in disease resolution (Xie *et al.*, 2018; Ross *et al.*, 2020; Kramer *et al.*, 2021). Direct measures of thalamocortical white matter connectivity reveal that children with RE have abnormal structural and functional thalamocortical connectivity to the Rolandic cortex (Kwon *et al.*, 2022), and an aberrant developmental trajectory of thalamocortical structural connectivity to the sensorimotor cortex persists beyond disease resolution (Thorn *et al.*, 2020). Taken together, these findings demonstrate that alterations in thalamocortical connectivity persist beyond symptoms, potentially providing compensatory mechanisms that support symptom resolution.

Somatosensory evoked magnetic fields (SEFs) are summated neural responses to peripheral nerve sensory stimulation measured in the Rolandic cortex. In the case of median nerve somatosensory stimulation, neural activity arrives at the primary somatosensory cortex after transmission along peripheral nerves, dorsal medial lemniscus, and thalamocortical white matter as a dominant surface-negative signal (e.g., N20) approximately 20 ms after stimulation. This evoked potential thus provides a direct assay of integrity of the Rolandic thalamocortical circuit. In contrast, visual evoked fields (VEFs) are summated neural responses to visual stimulation measured in the primary visual cortex. Neural activity arrives at the primary visual cortex after transmission from the retina, along the optic nerves and thalamocortical optic tracts as a dominant positive signal (e.g., P100) approximately 100 ms after stimulation. Cortical visual evoked potentials are sensitive to subtle structural deficits along the visual pathway but are not expected to be disrupted by a disease that affects focal thalamocortical Rolandic circuits (Toosy, Mason and Miller, 2014).

Given converging evidence for Rolandic thalamocortical circuit dysfunction in RE, we hypothesized that median nerve SEF conduction time would be abnormal in children with RE compared to controls, reflecting aberrant functional and structural connectivity of the thalamocortical sensorimotor circuit. We further hypothesized that conduction time along the visual pathway would be similar in children with RE and controls, confirming that the thalamocortical dysfunction in RE is focal to the sensorimotor circuit. After identifying a difference in N20 conduction time, we explored the relationships between

N20 conduction time and thalamic volume, ventral nucleus volume, and white matter connectivity to help localize the anatomical source of this dysfunction. Identification of focally impaired thalamocortical conduction time to the Rolandic cortex provides a novel biomarker for RE, helps localize the anatomical disruption, and provides further insight into the pathophysiology of symptoms and resolution in this common childhood disease.

2. Methods

2.1. Subjects

Children 4–15 years of age who received a clinical diagnosis of RE by a child neurologist following 1989 International League Against Epilepsy criteria, confirmed to have a history of focal motor or generalized seizures, and an EEG showing sleep-activated centrotemporal spikes were eligible for this prospective study (‘Proposal for Revised Classification of Epilepsies and Epileptic Syndromes’, 1989; Fisher *et al.*, 2014; Scheffer *et al.*, 2017). Control subjects without a history of seizure or known neurologic disorder were also recruited (n = 13). RE and control subjects with a history of unrelated neurologic disease were excluded, although children with attention disorders and mild learning difficulties consistent with known RE comorbidities were included (Wickens, Bowden and D’Souza, 2017). Children with RE were grouped into two categories of seizure risk: Active, defined as having had a seizure within 12 months (n = 10); and Resolved, defined as being seizure free for >12 months (n = 12) because most children who have been seizure

free for 12 months have entered terminal remission (Ross *et al.*, 2020). Two subjects who were initially enrolled during active disease returned after disease resolution and were included in the Resolved group.

Subject age, sex, current medications, and date of last seizure were collected at the time of visit. Subject height on the visit date was extrapolated from the subjects' individualized growth curve available from the electronic medical record (n = 29, Center for Disease Control and Prevention, 2017) or from an estimate of the height provided by the child'ss guardian on the visit date (n = 6). Subjects and their guardians gave age‐appropriate informed consent according to standards reviewed by the Institutional Review Board at Massachusetts General Hospital.

2.2. Magnetoencephalogram (MEG) acquisition and processing

MEG data were recorded with a 306-sensor system at 2,035 Hz sampling rate (Elekta-Neuromag, 204 planar gradiometers and 102 magnetometers) inside a magnetically shielded room. For each recording session, the head position was recorded approximately every four minutes and deemed satisfactory based on reasonable distance values of the head and the MEG helmet.

During MEG acquisition, left and right median nerve evoked fields were collected at random median nerve inter-stimulation intervals ranging from 100 to 140 ms over a period of approximately four minutes. Subjects were instructed to stay awake and

monitored via live video feed. For these data, the minimum necessary stimulation amplitude required to trigger a visibly confirmed thenar contraction was used. Following median nerve stimulation, visual evoked field data were collected during the same visit. For this, subjects were instructed to keep their eyes open and affixed to a plus sign projected on a screen in the middle of their visual field while flashing checkered patterns appeared on the screen, randomly switching across four quadrants corresponding to the right and left upper and lower visual fields with interstimulation intervals ranging from 333-525 ms.

2.3. Magnetic resonance imaging (MRI) acquisition

All subjects underwent structural and diffusion MRI recording as close to the day of MEG acquisition as possible (median 0.0 days between MEG and MRI, range: −22.0 to 36.0 days). All images were visually inspected by a neuroradiologist to confirm no gross structural abnormalities. All images were acquired in the same Siemens 3.0T MRI with a 64-channel head coil at the Martinos Center for Biomedical Imaging and included: 1) T1 MultiEcho Magnetization Prepared RApid Gradient Echo (MEMPRAGE) images (176 slices, 1.0 mm slice thickness, 1.0 × 1.0 × 1.0 mm3 voxel size, repetition time (TR): 2,530 ms, inversion time (TI): 1,100 ms, flip angle: 7°) with 4 different Echo Times (TE), 1.69 ms, 3.55 ms, 5.41 ms and 7.27 ms; 2) T2 Fluid Attenuated Inversion Recovery (FLAIR) (192 slices, 0.9 × 0.9 × 0.9 mm3 voxel size, 5,000 ms TR, 1,800 ms TI, and TE 7 ms; 3) Diffusion Weighted Imaging (DWI) (64 diffusion-encoding directions, 82 ms TE, 8,080

ms TR, flip angle:90°, voxel size = 2.0 × 2.0 × 2.0 mm3, diffusion sensitivity of b = 2,000 s/mm2, number of slices = 74, no skip).

2.4. Magnetic source imaging of SEFs and VEFs

Averaged evoked fields were detected and measured in source space. Using FreeSurfer, each participant's cortical surface was tessellated using a combination of T1 and T2-FLAIR images when available (n = 31), or only the T1 images (n = 2) otherwise, and decimated to 10,242 dipoles per hemisphere, corresponding to approximately 5 mm spacing between adjacent source locations (Hamalainen and Sarvas, 1987; Fischl, Sereno and Dale, 1999). To compute the MEG forward solution, a three-compartment boundary-element model was employed following the assumed geometrical intracranial space (FreeSurfer). Inner and outer skull and inner skin triangulations were generated using a watershed algorithm applied onto the T1 images of each participant. Minimum-norm estimate (MNE) software was applied to estimate cortical current distribution, assuming orientation of the source to be fixed perpendicular to the cortical mesh (Mamashli *et al.*, 2017).

After acquisition, in off-line analysis, channels contaminated with artifact were identified and not considered during analysis. The noise covariance matrix was estimated from each MEG recording and the cortical generators then estimated using anatomically constrained dynamic statistical parametric mapping (dSPM). Data were filtered between 0.1 Hz and 500 Hz for somatosensory evoked responses and 1.5 Hz and 70 Hz for visually

evoked responses. The data were then epoched into single trials beginning 200 ms prior to stimulus onset and ending 500 ms after stimulus onset. Epochs were rejected if the peak-to-peak amplitude during the epoch exceeded 2,000 fT/cm and 10,000 fT in any of the gradiometer or magnetometer channels, respectively. Averaged trials were subsequently analyzed from 20 ms prior to stimulus onset to 100 ms after stimulus onset for SEF, and from 20 ms prior to stimulus to 200 ms after stimuls onset for VEF.

The averaged median nerve N20 evoked potentials were contralaterally detected in the somatosensory cortex by identifying the distinct N20-P35 shape (Fig. 2.1). Following the identification of the first clear N20 signal, the localization and tangential orientation of each dipole in the hand region of the somatosensory cortex was visually confirmed for accuracy. Subjects without an identifiable N20 evoked potential in the somatosensory cortex were excluded. For each subject, the vertex with the largest amplitude at the N20 peak was selected and the conduction time recorded contralaterally. The visual evoked potentials were detected in the occipital cortex by identifying the P100 signal. The localization and orientation of each dipole was visually confirmed to be adjacent to the pericalcarine fissure, inverted and contralateral to the corresponding visual field stimuli. Subjects without an identifiable P100 evoked potential in the visual cortex were excluded. The vertex with the largest amplitude at the P100 peak was selected and the conduction time recorded for each subject. Upper and lower quadrant results were averaged for a single measure per hemisphere.

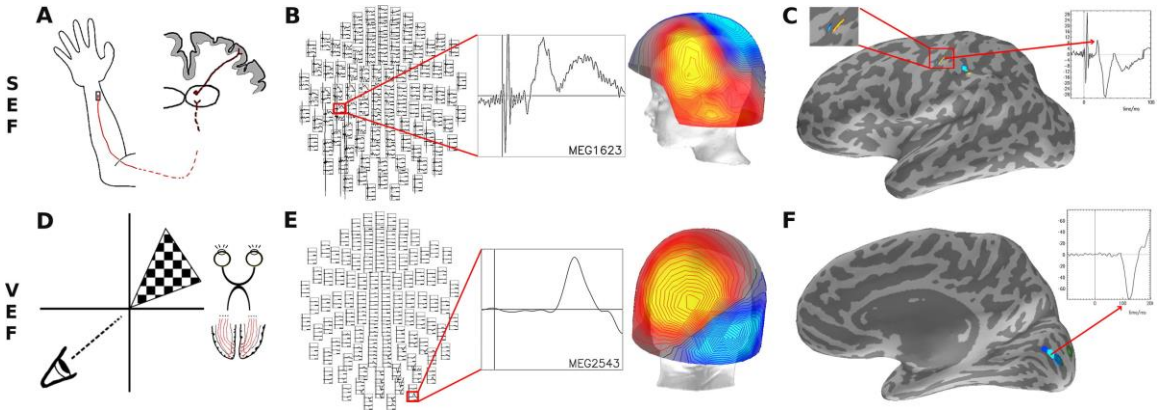

Fig. 3.1. Experimental set up and processing. A) For somatosensory evoked field (SEF) testing, the distal median nerve was stimulated, resulting in an evoked response that synapses in the ventroposteriolateral thalamus and then arrives as an N20 signal in the sensory cortex. B) Magnetoencephalogram (MEG) cortical recordings were averaged across trials in each hemisphere and visually inspected for a N20 dipole in sensor space. C) The peak N20 response was confirmed to localize to the hand representation area of the contralateral primary sensory cortex, and the N20 conduction time was measured as the time of the peak of the N20 amplitude deflection in source space. D) For visual evoked field (VEF) testing, checkered visual stimuli were displayed randomly in the four quadrants, resulting in an evoked response that synapses in the lateral geniculate nucleus of the thalamus and then arrives as a P100 signal in occipital cortex. E) MEG cortical recordings were averaged across trials in each hemisphere and visually inspected for a P100 dipole in sensor space. F) The peak P100 response was confirmed to localize in the contralateral pericalcarine cortex in source space and the P100 conduction time was measured as the time of the peak of the negative P100 amplitude deflection.

2.5. Posthoc analyses

2.5.1 Thalamic volume and cortical surface measurements

Intracranial anatomical landmarks along the three-neuron pathway that median nerve evoked fields traverse from the wrist to the cortex were analyzed. This pathway includes synapses in the ipsilateral dorsal root ganglion and the contralateral ventral posterolateral nucleus of the thalamus. Thalamic volume estimates were performed on the

T1-MEMPRAGE volumes using thalamic segmentations tools in FreeSurfer 7.1.1 (Iglesias *et al.*, 2018; *FreeSurfer*, no date). The combination of T1-MEMPRAGE and T2-FLAIR volumes were used, when available, to estimate the entire thalamic volume and regional thalamic volumes (anterior, lateral, ventral, intralaminar and posterior) (Iglesias et al., 2018). Two subjects did not complete MRI (n = 33 available for analysis). Two subjects had only T1-MEMPRAGE available.

2.5.2 Probabilistic tractography

From the thalamus, median nerve sensory evoked fields travel through the corona radiata white matter to the sensory cortex. To evaluate the thalamocortical structural connectivity of this circuit, probabilistic tractography was performed on available MR diffusion data (n = 33).

To evaluate the Rolandic sensorimotor thalamocortical white matter, we computed the structural connectivity to the postcentral gyrus target region of interest (ROI) from two seed ROIs: a) the entire ipsilateral thalamus; and b) the ventral region of the ipsilateral thalamus. We applied ball-and-stick model-based probabilistic diffusion tensor tracking (Probtrackx2 through Functional Magnetic Resonance Imaging of the Brain (FMRIB) Software Library (FSL) 5.0.4 / FMRIB Diffusion Toolbox (FDT) (Behrens *et al.*, 2003)). The Desikan-Killiany atlas was used to segment the postcentral gyrus (Desikan *et al.*, 2006).

2.5.3 White Matter Connectivity

BedpostX (Bayesian Estimation of Diffusion Parameters Obtained using Sampling Techniques for modeling Crossing Fibers) was used to estimate the principal diffusion direction per voxel. 500 streamlines per seed ROI voxel were sampled using Probtrackx2 with a 0.2 curvature threshold with distance correction on. A step length of 0.5 mm was used for each streamline with a maximum of 2000 steps per streamline. Streamlines were terminated when they reached the target ROI or they met the rejection criteria by each hemisphere. Loop checks were performed to prevent streamlines from looping back on themselves, and a subsidiary fiber volume threshold of 0.01 of the parent fiber volume was applied to exclude negligible volumes. Using the number of streamlines launched from the seed ROI and the number of voxels in the target ROI a Connectivity Index (CI) was calculated (Chu et al., 2015). The CI was then normalized by the volume (number of voxels) of the seed ROI. Appropriate tracts were confirmed with visual analysis.

2.6. Statistical analyses

To detect a difference in the distributions of SEF conduction times between children with RE and controls, we estimated a linear mixed effects model with group as predictor and a random subject specific intercept to account for two observations per subject (left and right SEF conduction time). Height was included as a covariate. We note

that height and age are collinear and because height is expected to directly impact SEF measures, we included height instead of age as a covariate in the models.

To evaluate whether duration of epilepsy remission (duration seizure free), thalamic volume, or Rolandic thalamocortical structural connectivity predicted SEF conduction time, we estimated mixed effects models of a similar form; in separate models, we included each of these variables as a predictor, a random subject specific intercept, and height as a covariate.

To test if conduction times in the active and remission groups differed from the control subjects, we estimated linear mixed effects models with conduction time as the dependent variable, group and height as independent variables, and a random subject-specific intercept to account for two observations per subject (left and right hemisphere SEF conduction time). Equivalent control tests were done using VEF conduction time, group, and LGN volume.

3. Results

3.1. Participant information

For SEF, 22 children with RE (mean age 11.9 years, range: 8.0–16.9 years, 3F; active RE: mean age 11.0 years, range: 9.0–14.7 years; resolved RE: mean age 12.7 years, range: 8.0–16.9) were included, of whom 8 were on anti-seizure medication (ASM). Thirteen control children (mean age 11.9 years, range 8.0–15.1 years, 7F) were included.

For VEF, 22 children with RE (mean age 11.8 years, range: 9.0–16.9 years, 4F; active RE: mean age 10.5 years, range: 9.0–14.6 years; resolved RE: mean age 13.4 years, range: 10.4–16.9) were included, of whom 7 were on anti-seizure medication (ASM). Fourteen control children (mean age 12.5 years, range 9.0–15.1 years, 8F) were included. Subject characteristics are provided in Table 3.1.

ID	Group	Age (years)	Sex	Duration Seizure Free (Months)	Anti-Seizure Medication	Centrotemporal Spikes	Experiment
1	RE	8.0	M	29	None	Left, Bilateral	SEF
2	RE	9.0	M	4	None	Right, Bilateral	SEF, VEF
3	RE	9.1	F	1	Keppra, Lamictal	Left, Bilateral	VEF
4	RE	9.1	M	0	None	None	SEF, SEF
5	RE	9.6	M	7	None	None	SEF, VEF
6	RE	9.8	M	0	Valproate; Vimpat	Right, Bilateral	SEF, VEF
7	RE	9.9	M	6	None	Right, Bilateral	SEF, VEF
8	RE	10.1	M	5	None	Not available	VEF
9	RE	10.4	M	26	Keppra	Right, Bilateral	SEF, VEF
10	RE	10.9	M	10	None	Left, Bilateral	SEF, VEF
11	RE	11.0	F	2	None	Left, Bilateral	SEF, VEF
12	RE	11.3	M	1	None	Right, Bilateral	VEF
13	RE	11.5	M	20	None	Left, Bilateral	SEF, VEF
14	RE	11.6	M	2	Keppra	None	SEF, VEF
15	RE	11.8	M	17	None	Left	SEF
16	RE	11.9	M	24	Keppra	Right, Bilateral	SEF, VEF
17	RE	12.8	M	18	Keppra	Right, Bilateral	SEF
18	RE	12.8	F	34	None	None	SEF, VEF
19	RE	13.3	M	26	Keppra	Left	SEF, VEF
20	RE	13.7	M	51	None	Right, Bilateral	SEF
21	RE	14.6	M	0	Onfi	Left	SEF, VEF
22	RE	14.7	M	0	Keppra	Left, Bilateral	SEF
23	RE	14.8	F	5	None	Right, Bilateral	VEF
24	RE	14.8	M	40	None	None	SEF, VEF
25	RE	14.9	M	38	None	Left	SEF, VEF
26	RE	16.9	M	26	None	Left	SEF, VEF
27	Control	8.0	M				SEF
28	Control	8.7	M				SEF
29	Control	9.0	F				SEF, VEF
30	Control	9.4	F				SEF
31	Control	9.4	M				SEF
32	Control	10.5	F				SEF, VEF
33	Control	10.9	M				VEF
34	Control	11.5	M				VEF
35	Control	12.2	F				VEF
36	Control	12.9	F				VEF
37	Control	12.9	F				SEF, VEF
38	Control	13.4	F				VEF
39	Control	13.6	F				VEF
40	Control	14.0	F				SEF
41	Control	14.2	F				SEF, VEF
42	Control	14.3	M				SEF, VEF
43	Control	14.3	F				SEF, VEF
44	Control	14.4	M				SEF, VEF
45	Control	15.1	M				SEF, VEF

Table 3.1. Subject characteristics. RE: Rolandic Epilepsy; SEF: Somatosensory Evoked Fields; VEF: Visual Evoked Fields.

3.2. Children with resolved RE have delayed median nerve sensory conduction time

Children with RE have delayed median nerve SEF conduction time compared to controls ($p = 0.042$; effect size 0.6 ms, 95% CI [0.021, 1.201], average conduction time of RE group: 21.3 ± 1.6 ms, average conduction time of controls: 20.4 ± 1.0 ms, Fig. 3.2A). Separating RE subjects into active or remission groups, only the SEF conduction time in the remission group differed from controls ($p = 0.046$, effect size 0.7 ms, 95% CI [0.0, 1.4]; active group $p = 0.48$, effect size 0.5 ms, 95% CI [−0.2, 1.2]).

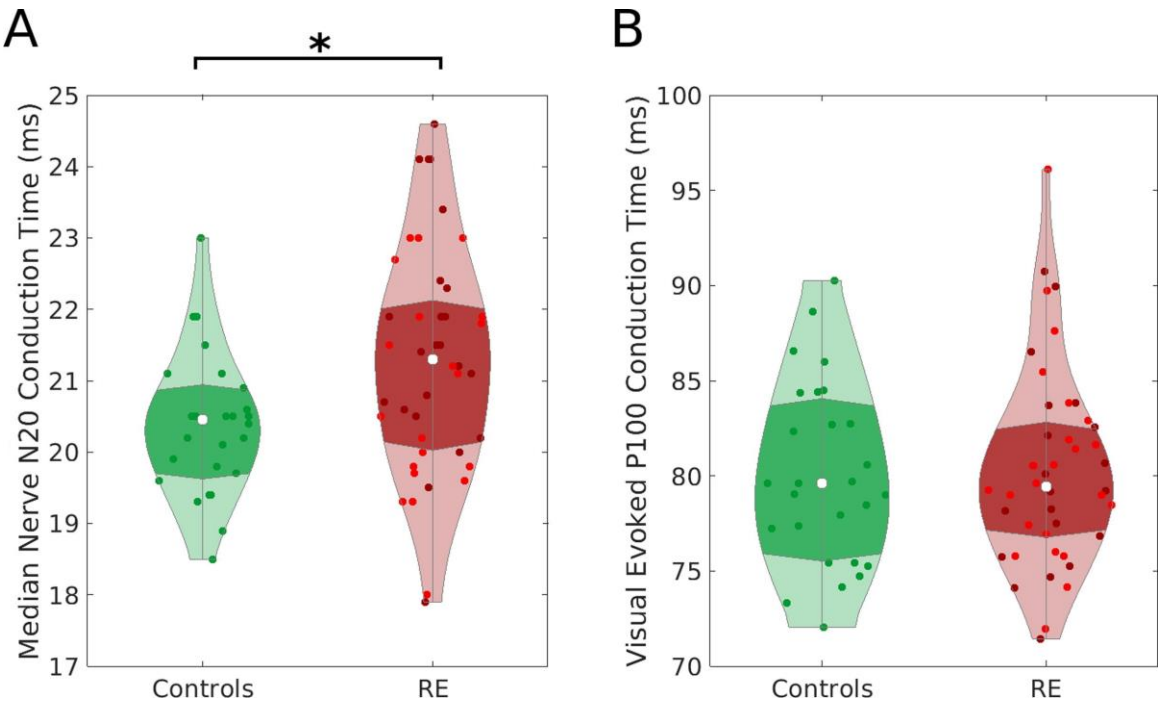

Fig. 3.2. Somatosensory Evoked Fields (SEF), but not Visual Evoked Fields (VEF), conduction times differ in children with Rolandic epilepsy and controls. A) Children with Rolandic Epilepsy (RE) have delayed SEF median nerve N20 conduction time compared to controls ($p = 0.042$) B) There is no evidence of a difference in VEF P100 conduction times across groups ($p = 0.8$). Points indicate individual hemisphere

measurements. For RE, bright red indicates the active RE and darker red indicates remission RE. Violin plots (Bechtold, 2016) indicate the density of conduction time values, the violin width represents the number of points at each value, the white represents the median value, and the darker shading indicates the interquartile range.

3.3. No difference in VEF conduction between RE and controls

There was no evidence of a difference in visual field P100 conduction time to the occipital cortex between RE and controls ($p = 0.83$, Fig. 3.2B). Taken together, these results identify a focal conduction delay along the Rolandic thalamocortical white matter circuit in children with resolved RE.

3.4. Ventral thalamic volume predicts SEF conduction time

We found no evidence that thalamic volume predicts SEF conduction time ($p = 0.11$, effect size 0.0003 ms/mm3, 95% CI [−0.0001, 0.0007]). However, the ventral thalamic region, through which the median nerve stimulus travels, was larger in RE compared to controls ($p = 0.037$, effect size 239 mm3, 95% CI [15, 462] mm3, Fig. 3.3A) and had a positive relationship with conduction time ($p = 0.023$, effect size 0.0008 ms/mm3, 95% CI [0.0001, 0.0015] ms/mm3, Fig. 3.3B).

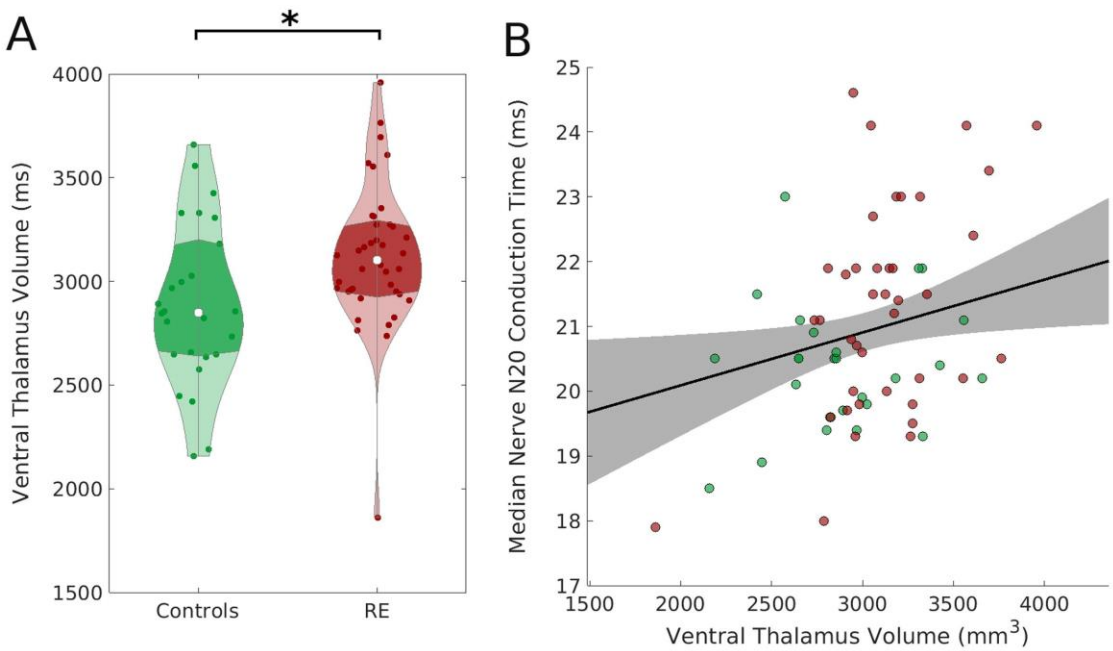

Fig. 3.3. Ventral thalamic volume is larger in Rolandic epilepsy and positively correlates with Somatosensory Evoked Fields (SEF) conduction time. A) Children with Rolandic Epilepsy (RE) have a larger ventral thalamic volume than controls ($p = 0.037$). Violin plots (Bechtold, 2016) indicate the density of conduction time values, the violin width represents the number of points at each value, the white dot represents the median value, and the darker shading indicates the interquartile range. B) The ipsilateral ventral thalamic volume correlates with N20 median nerve conduction time ($p = 0.023$). Points indicate individual subjects (green: controls, red: RE). The black line (shaded gray region) indicates linear mixed effects model fit (95% confidence interval).

3.5. Thalamocortical white matter structural connectivity does not predict SEF conduction time

To evaluate whether white matter structural connectivity predicted SEF conduction time, we used probabilistic tractography to compute the CI between somatosensory cortex and the whole thalamus, and between somatosensory cortex and the ventral thalamus (Table 3.2). We found no evidence of a relationship between either CI and SEF conduction time ($p > 0.3$).

Group	Connectivity Index
	Whole thalamus to postcentral gyrus - Left
RE	0.040 ± 0.016
Control	0.033 ± 0.016
	Whole thalamus to postcentral gyrus - Right
RE	0.042 ± 0.015
Control	0.024 ± 0.009
	Ventral thalamus to postcentral gyrus - Left
RE	0.035 ± 0.012
Control	0.040 ± 0.023
	Ventral thalamus to postcentral gyrus-Right
RE	0.037 ± 0.017
Control	0.028 ± 0.012

Table 3.2. Diffusion MRI-based Connectivity Measurements.

4. Discussion

In this prospective cross-sectional study, we found evidence for a conduction delay in the median nerve somatosensory evoked fields in children with resolved RE compared to control subjects. We found no evidence for a conduction abnormality in visual evoked

potentials between children with RE and control subjects. Taken together, these data demonstrate an emergent abnormality in the Rolandic thalamocortical circuit in RE and suggest that focally decreased Rolandic thalamocortical connectivity may support symptom resolution in this transient focal epilepsy.

Median nerve sensory responses travel along a three-neuron pathway where the terminal neuron lies in the VPL nucleus and projects to the sensory Rolandic cortex through the corona radiata. The ventral thalamus further includes the VL thalamic nucleus which regulates sensory integration for motor control and projects to the supplementary motor regions, the VA nucleus which has projections to premotor cortex, and the VM nucleus which has projections to the somatosensory cortex and limbic structures. Investigation of this intracranial portion of the pathway revealed that the volume of the contralateral ventral thalamus positively correlated with conduction time in RE. We have previously reported abnormal Rolandic white matter structural connectivity in RE in disease resolution (Kwon *et al.*, 2022). Increased structural connectivity would typically reflect increased myelinated fibers and support faster conduction time. Here, however, we found delayed conduction time in resolved RE. Further, conduction time correlated with ventral thalamic volume, which were larger in children with RE. Notably, prior work that has identified that children with smaller thalamic volumes and abnormal thalamocortical metabolic connectivity are at increased risk of sleep-potentiated epileptic encephalopathies (Moeller *et al.*, 2013; Sánchez Fernández *et al.*, 2017; Agarwal *et al.*, 2016). Thus, the positive relationship between ventral thalamic size and SEF conduction time may reflect a compensatory

strategy to help inhibit the abnormal activity in this thalamocortical circuit (Li *et al.*, 2021). Thus, the increased conduction time we see here in resolved RE may potentially reflect increased inhibitory processing at the level of the thalamus. Future mechanistic work is required to better understand this relationship.

5. Conclusion

We found that children with RE have a focal conduction delay in median nerve somatosensory evoked responses. These data suggest that the functional integrity of the thalamocortical sensorimotor circuit is abnormal in RE, and that a decrease in thalamocortical conduction may be a feature of disease resolution. Conduction time delays correlates with increased thalamic volume, implicating this node of the circuit in compensatory responses that may support symptom resolution.

6. Disclosures

None of the authors has any conflict of interest to disclose.

7. Acknowledgements

This work was supported by grants NIH NINDS K23NS092923 and R01NS115868. The authors would like to thank Dan Y. Song, Wenting Xie, Emily L.

Thorn, McKenna Parnes, Erin E. Ross, Sally M. Stoyell and Grace Xiao for participating in data collection. Gratitude also goes to the MEG Core team at MGH.

8. Ethical publication statement

We confirm that we have read the Journal's position on issues involved in ethical publication and affirm that this report is consistent with those guidelines.

CHAPTER FOUR: Sensory gating responses in human thalamus predict performance on attention task

Abstract

Introduction: Experimental evidence from animal models demonstrates that disruptions in thalamic reticular nucleus (TRN) function during wakefulness reduce selective gating of redundant sensory inputs. This "sensory gating" (SG) safeguards the integrity of higher cognitive functions from irrelevant stimuli. The TRN also initiates sleep spindles, cardinal sleep oscillations during stages 2 and 3 non-rapid eye movement (NREM) sleep. Whether sensory gating can be measured in the human thalamus and how it relates to attention is not known. We evaluated electrophysiological responses to a paired auditory stimulus in the thalamus and evaluated whether sensory gating predicted performance on an attention task in patients with drug refractory epilepsy.

Methods: Subjects undergoing direct thalamic recording during epilepsy surgery evaluation were prospectively enrolled (n=26). Thalamic stereoEEG (SEEG) electrode localization was confirmed by manual co-registration of post-operative head CTs or MRIs and pre-operative MRIs and FreeSurfer segmentation. Thalamic SEEG recordings from the pulvinar (Pul), centromedian nucleus (CM), and anterior nucleus (ANT) were analyzed referenced to ipsilateral white matter. Scalp EEG recordings from FZ were analyzed referenced to the second cervical spinous process. Subjects passively listened to 240-300

paired auditory stimuli comprised of an initial auditory click, stimulus 1 (S1), and a second click, stimulus 2 (S2) separated by 500 ms, with intertrial intervals of 8-10 s. Data were bandpass filtered (6.0-50.0 Hz) and epoched by trial. Trials were rejected if the peak-to-peak amplitude exceeded ±100 μV, the remaining trials were averaged, and the latency and amplitude of the P50 auditory evoked response were recorded. Sensory gating was computed as the ratio of the P50 response to S2 versus S1. The Connors Continuous Performance Task (CCPT) was performed following the SG task. Sleep spindle rates were estimated during stages 2 and 3 NREM sleep from the overnight record prior to the SG task using a validated automated sleep staging algorithm and spindle detector.

Results: A clear thalamic P50 response to S1 preceded the scalp response by 18.0 ms on average ($p<0.001$; by thalamic region relative to scalp: CM -20.5 ms, $p<0.001$; ANT -13.7 ms, $p<0.001$; Pul -12.7 ms, $p=0.015$). SG was detected (ratio<1) in the scalp (0.58, $p<0.001$) and in the thalamus (0.60, $p<0.001$; CM 0.64, $p<0.001$; ANT 0.50, $p<0.001$; Pul 0.72, $p=0.024$). The SG ratio in the ANT trended to be lower than in the Pul ($p=0.040$). The auditory SG ratio decreased as the distance from the thalamic medial geniculate nucleus increased ($p=0.015$). Thalamic SG ($p=0.048$), but not scalp SG ($p=0.14$), predicted accuracy on the CCPT. Both thalamic ($p=0.019$) and scalp ($p=0.027$) overnight sleep spindle rate predicted accuracy on the CCPT. Thalamic SG predicted thalamic spindle rate ($p=0.015$), but scalp SG did not predict scalp spindle rate ($p=0.23$).

Conclusions: These results demonstrate that thalamic reticular nucleus function mediates performance on an attention task and can be assessed using thalamic SG or non-invasive sleep spindle measures.

1. Introduction

During wakefulness, the thalamic reticular nucleus functions as a modulatory filter, regulating the flow of sensory and motor information directed towards, as well as from, the cerebral cortex. Encasing the other thalamic nuclei, the TRN is responsible for "sensory gating" (SG), a mechanism to discern signal from noise, thereby safeguarding the integrity of higher cognitive functions from irrelevant stimuli (Crabtree, 2018; Li *et al.*, 2020).

TRN neurons exhibit the capability of responding to novel sensory inputs, thereby showing rapid adaptability to changing environments while simultaneously protecting the brain from overreacting to repetitive stimuli, thus conserving neural resources and preventing sensory overload (Khani *et al.*, 2019). This dynamic modulation underpins cognitive functions such as selective attention and sensory discrimination, crucial for navigating the complex sensory landscape of the external world (McAlonan, Cavanaugh and Wurtz, 2006).

However, if the ability of the TRN to exercise inhibition is perturbed, the repercussions can impact SG ability. Experimental evidence from animal models shows that disruptions in TRN function, either through neuronal loss or dysfunction, can lead to

a breakdown in the selective filtering of sensory inputs, culminating in an inundation of irrelevant stimuli propagating to the cortex and increasing the chances of compromising cognitive processes reliant on sensory discrimination (Ahrens et al., 2015; Nakajima et al., 2019).

In conditions such as attention deficit hyperactivity disorder (ADHD), characterized by deficits in attentional control and cognitive function, aberrant SG mechanisms have been linked to cognitive dysfunction and symptomatic manifestations of inattention (Holstein *et al.*, 2013; Micoulaud-Franchi *et al.*, 2015). Similarly, schizophrenia, marked by disturbances in perception, cognition, and social functioning, is often accompanied by impaired SG, reflecting a breakdown in the neural mechanisms responsible for ignoring irrelevant sensory inputs and preserving cognitive integrity (Judd *et al.*, 1992). Conversely, in select cohorts, augmented sensory gating has been associated with favorable cognitive outcomes. For instance, investigations into the cognitive profiles of gifted children have unveiled a positive correlation between robust sensory gating abilities and enhanced impulse control, underscoring the pivotal role of sensory processing mechanisms in shaping cognitive and behavioral phenotypes (Shi *et al.*, 2013).

Given the intricate interplay between thalamocortical circuitry and diverse neurological pathologies, it is conceivable that deviations in sensory gating may manifest in refractory epileptic patients. Therefore, interrogating the status of sensory gating in this population can help elucidate the underlying mechanisms driving cognitive dysfunction in epilepsy.

2. Methods

2.1. Participants and EEG recordings

All patients who underwent stereotactically placed depth electrode EEG (sEEG) recordings targeting the thalamus as part of their clinical care for drug refractory epilepsy at Massachusetts General Hospital between August 2020 and August 2023, were approached for enrollment. The electronic medical record was reviewed for demographic information, epilepsy etiology, results of clinical neuropsychological evaluations, and antiseizure medication exposure within 24 hours of the experiment.

Depth electrodes (PMT Corporation, Chanhassen, MN, USA) were placed with robotic stereotactic assistance (ROSA, Zimmer Biomet, Warsaw, IN, USA) based on the clinical indications for seizure network localization as determined by a multidisciplinary clinical team. 21 scalp EEG electrodes were also placed following the 10-20 international system. All EEG recordings were obtained with a sampling rate of 1024 Hz using an XLTEK digital system (Natus Medical Incorporated, Pleasanton, CA).

This study was approved by the Massachusetts General Hospital Institutional Review Board.

2.2. Tasks

2.2.1 Sensory gating task

Paired auditory stimuli (240-300 events) separated by 8-10 s (uniformly distributed) were delivered to the subject via in-ear wired earbud headphones, and simultaneously to the EEG recording system as electrical triggers during the awake state. The stimuli include two identical auditory clicks separated by 500 ms (6.6 ms in duration, 1,500 Hz wave frequency, 44,100 Hz sample rate, 16 bits per sample).

2.2.2. Attention Task

Enrolled subjects who were able to follow instructions were asked to participate in a continuous performance task to assess attention as soon as possible following the sensory gating task (Epstein *et al.*, 2010; Vaughn *et al.*, 2011). Briefly, the task involved displaying letters to the subject, who was instructed to press the spacebar for every letter but X. The task was organized into a series of 18 blocks of 20 trials where 360 letters are individually displayed for 250 ms on a computer screen, including 36 X's and 324 non-X letters across all blocks. The interstimulus intervals (ISI) between letter presentations within each trial was either 1 s, 2 s, or 4 s, and block order was randomized. The number of omission errors (OE, not pressing the spacebar when non-'X' letters are displayed) and commission errors (CE, pressing the spacebar when the letter 'X' was displayed) were computed. Accuracy

was calculated as the proportion of correct responses to the total number of possible responses.

2.3. Electrode localization

For electrode localization, the pre-implantation T1 and T2 scans were processed for whole brain segmentation and thalamic segmentation using FreeSurfer (Fischl *et al.*, 2002, 2004). Each subject's post operative CT or MRI scan with implanted electrodes was co-registered to their pre-operative sagittal T1 MRI. For CT-to-MRI registration, Slicer was used to align the pre-implantation T1 scans, and the General Registration (BRAINS) was used for automated registration (Johnson, Harris and Williams, 2007). The results were visually inspected and manually adjusted as needed to confirm satisfactory registration. For MRI-to-MRI registration, FreeSurfer's automatic registration processing module was used and manually adjusted as needed based on visual review. Electrodes were localized in FreeSurfer's Freeview overlaid on the pre-implantation MRI scan. Each electrode contact was manually marked (raw locations). Then, using all manually marked contacts per depth electrode, a single-value decomposition (SVD) algorithm was also used to distribute the electrodes along a straight line of best fit (corrected localizations). The FreeSurfer label for each contact was recorded for both the raw and corrected contact locations.

2.4. EEG processing

Electrodes localized to the thalamus and scalp electrodes at Fz and Cz were included for analysis. Intracranial thalamic electrodes were referenced to an intracranial electrode contact localized to the ipsilateral corona radiata white matter and Fz was referenced to the left mastoid.

Data were bandpass filtered (6.0-50.0 Hz) then epoched into single trials. Trials from scalp or intracranial sources were rejected if the amplitude exceeded ±100 μV. Epileptic spikes were automatically detected using Persyst13 software and trials rejected if spikes occurred within 100 ms after the stimulus. Eye-blinks with a minimum amplitude threshold of 40 μV were automatically detected at frontal electrodes Fp1 and Fp2 and trials were rejected if eye-blinks were detected within ±100 ms of the stimulus (Sovierzoski, Argoud and De Azevedo, 2008; Chang *et al.*, 2016; Kanoga, Nakanishi and Mitsukura, 2016).

P50 evoked auditory responses at Fz were required for inclusion. This required: 1) Flat baseline (e.g., the 95% confidence interval from times -0.1 s to 0.0 included zero; and 2) A discernible P50 evoked response (e.g., the 95% confidence interval of the first positive deflection after 25 ms and before 100 ms excluded zero (Lijffijt *et al.*, 2009)). Among electrodes in the thalamus, the contact with the highest amplitude evoked response within 50 ms of the scalp P50 was chosen for analysis. The amplitude (relative to the preceding

negative trough) of the P50 responses were recorded following the first (S1) and second (S2) auditory stimuli to calculate an S2 to S1 P50 amplitude ratio.

2.5. Spindle detection

For sleep spindle analysis, the overnight EEG from 11P to 7A preceding the sensory gating experiment was staged for N2 and N3 using a validated sleep staging algorithm (Ellenrieder *et al.*, 2022). Sleep spindles were detected at FZ referenced to a common average reference and bipolar referenced adjacent thalamic channels using an automated detector validated for use in EEG containing epileptiform spikes (Kramer *et al.*, 2021).

2.6. Statistical Analysis (SA)

SA.A To compare the timing of the auditory evoked response between the scalp and thalamus, a linear mixed effects model (LME) was applied with electrode location (scalp or thalamus) as a fixed effect, the P50 arrival time as the response variable, and a random-effects term to account for repeat observations (i.e., multiple thalamic electrodes) within subjects

$$P50\ Arrival\ Time = \beta_0 + \beta_1 * I + (1|subject) \quad \text{[Eq. 1]}$$

where *I* is an indicator function with $I = 0$ indicating scalp and $I = 1$ indicating thalamus, β_0 and β_1 are unknown parameters to estimate, and $(1|subject)$ indicates a random-effects term indexed by subject.

SA.B To compare the evoked response times between the scalp and each thalamic nucleus, the difference between the scalp P50 arrival time and each thalamic P50 arrival time was computed for each subject. To test if these adjusted thalamic P50 arrival times differed from 0, Wilcoxon rank sum tests were applied, as the data violated the null hypothesis of normality ($p<0.05$, Lillie test).

SA.C To test for difference in the amplitudes of the S1 and S2 evoked responses, Wilcoxon rank sum tests were applied, as the thalamic S1 and S2 P50 responses violated the null hypothesis of normality ($p<0.05$, Lillie test).

SA.D To test for the presence of sensory gating at the scalp, at the thalamus, and at each thalamic nucleus, the mean SG ratio (no evidence of deviation from normality, $p>0.05$ Lillie test) was compared to 1 (equivalent to no sensory gating) using one-sample t-tests.

SA.E To compare the means of the SG ratios between the scalp and thalamus, a linear mixed effects model of SG ratio was estimated:

$$Sensory\ Gating\ Ratio = \beta_0 + \beta_1 * I + (1|subject) \qquad \text{[Eq. 2]}$$

where *I* is an indicator function with $I = 0$ indicating scalp and $I = 1$ indicating thalamus, β_0 and β_1 are unknown parameters to estimate, and $(1|subject)$ indicates a random-effects term indexed by subject.

SA.F To compare the means of the SG ratios between the thalamic nuclei, three linear mixed effects models of SG ratio were estimated:

$$Sensory\ Gating\ Ratio = \beta_0 + \beta_1 * I + (1|subject) \quad \text{[Eq. 3]}$$

where I is an indicator function with: (1) $I = 0$ indicating ANT and $I = 1$ indicating CM, or (2) $I = 0$ indicating ANT and $I = 1$ indicating Pul, or (3) $I = 0$ indicating CM and $I = 1$ indicating Pul. For each model, β_0 and β_1 are unknown parameters to estimate, and $(1|subject)$ indicates a random-effects term indexed by subject.

SA.G To test if the SG ratio in the thalamus depended on distance from the medial geniculate nucleus (MGN), the linear distance between the center of mass of the MGN and the coordinates of the localized thalamic electrode was calculated for. A linear mixed-effects model (LME) of the thalamic SG ratio with predictor distance was estimated,

$$Sensory\ Gating\ Ratio = \beta_0 + \beta_1 * (Distance\ from\ MGN) + (1|subject) \quad \text{[Eq. 4]}$$

where β_0 and β_1 are unknown parameters to estimate and $(1|subject)$ indicates a random-effects term indexed by subject.

SA.H To estimate the relationship between sensory gating and attention, a linear model of the CCPT accuracy was estimated with average thalamic SG or scalp SG as predictor:

$$Accuracy\ on\ Attention\ Task = \beta_0 + \beta_1 * Sensory\ Gating\ Ratio \quad \text{[Eq. 5]}$$

where β_0 and β_1 are unknown parameters to estimate.

SA.I To estimate the relationship between sensory gating and commission and omission errors, a generalized linear model (Poisson distribution, log link) of the commission or omission errors was estimated with average thalamic SG or scalp SG as predictor

$$\log\left(Commission\ or\ Omission\ Errors\right) = \beta_0 + \beta_1 * Sensory\ Gating\ Ratio \quad \text{[Eq. 6]}$$

where β_0 and β_1 are unknown parameters to estimate.

SA.J To estimate the relationship between attention and spindle rate, a linear model of the CCPT accuracy was estimated with average thalamic spindle rate or scalp spindle rate as predictor:

$$Accuracy\ on\ Attention\ Task = \beta_0 + \beta_1 * Spindle\ Rate \quad \text{[Eq. 7]}$$

where β_0 and β_1 are unknown parameters to estimate.

SA.K To estimate the relationship between spindle rate and commission and omission errors, a generalized linear model (Poisson distribution, log link) of the commission or omission errors was estimated with average thalamic spindle rate or scalp spindle rate as predictor:

$$\log(Commission\ or\ Omission\ Errors) = \beta_0 + \beta_1 * Spindle\ Rate \quad \text{[Eq. 8]}$$

SA.L To investigate the relationships between thalamic SG ratio and thalamic spindle rate, a GLME of spindle rate (gamma distributed, log link) was estimated with SG ratio as the predictor:

$$Spindle\ Rate = \beta_0 + \beta_1 * Sensory\ Gating\ Ratio + (1|subject) \quad \text{[Eq. 9]}$$

where β_0 and β_1 are unknown parameters to estimate and $(1|subject)$ indicates a random-effects term indexed by subject.

SA.M To investigate the relationships between scalp SG ratio and scalp spindle rate, a GLM of spindle rate (gamma distributed, log link) was estimated with SG ratio as the predictor:

$$Spindle\ Rate = \beta_0 + \beta_1 * Sensory\ Gating\ Ratio \quad \text{[Eq. 10]}$$

where β_0 and β_1 are unknown parameters to estimate.

Within each hypotheses, multiple comparisons were corrected using the Benjamini-Hochberg procedure (Benjamini and Hochberg, 1995).

3. Results

3.1. Subject demographics

Of the 31 patients approached to participate in this study, 26 agreed to participate. Five of these patients had noisy signal without evident P50 at Fz. Thus, 26 subjects (13F, average 24.9 years old, ages 8.2 – 60.6 years old) with epilepsy from a variety of etiologies were included. Patients had electrodes targeting the centromedian nucleus (CM, n=12), anterior nucleus (ANT, n=3), both the CM and ANT (n=4), both the CM and Pul (n=2), or both the

ANT and Pul (n=5). Eighteen patients had bilateral thalamic implantations. See Table 4.1 for additional patient details.

Subject	Sex	Age Group	Thalamic Target(s)	Epilepsy Etiology	Anti-seizure medications	Attention assessment on pre-surgical neuropsychological evaluation+
1	F	Adult	CM	Bilateral nodular periventricular heterotopia	clobazam, cannabidol, lacosamide, levetiracetam	Average
2	F	Adult	CM	Perinatal anoxic brain injury	lacosamide, topimarate	Low average to average
3	F	Adult	CM	HSV encephalitis post left frontotemporal resection and anterior corpus callosotomy	clobazam, cannabidol, lamotrigine, levetiracetam	Low to extremely low
4	M	Ped	CM	Bilateral polymicrogyria	lamotrigine, levetiracetam, topimarate, valproic acid	Extremely low
5	M	Adult	ANT	Non-lesional	clobazam, lamotrigine, modafinil	Superior
6	M	Adult	ANT	Non-lesional; post right temporal lobectomy and right frontal topectomy	lamotrigine	High average to exceptionally high
7	M	Ped	CM	Non-lesional	lamotrigine, valproic acid	Evaluation not completed evaluation due to difficulty to sustain attention; ADHD+
8	M	Ped	CM	Stroke	clobazam, cannabidol, lamotrigine	Average

9	M	Ped	CM	Neonatal hypoglycemia	clobazam, cannabidol, lacosamide	No evaluation of attention performed due to visual impairment; ADHD+
10	F	Adult	CM	GLUD1	clonazepam, lacosamide, parempanel	No evaluation performed
11	M	Ped	CM	Non-lesional	clobazam, levetiracetam	Good
12	F	Ped	CM, Pul	Bilateral polymicrogyria	clobazam, cannabidol, levetiracetam	No evaluation performed
13	F	Ped	CM	Non-lesional	lamotrigine, oxcarbazepine	Low average to below average
14	F	Adult	CM, ANT	Non-lesional	lamotrigine, oxcarbazepine	Average to Exceptionally High
15	F	Ped	ANT	Non-lesional	lamotrigine, levetiracetam, oxcarbazepine	No problems with attention, within or above age expectations
16	M	Adult	CM	Hippocampal sclerosis	carbamzepine, lamotrigine, zonisamide	Above to high average
17	M	Adult	CM	Non-lesional	lamotrigine, oxcarbazepine	Average to very low
18	F	Adult	CM, ANT	Left frontal astrocytoma	cannabidol, brivaracetam, cenobamate, zonisamide	Below average
19	M	Adult	CM, ANT	Non-lesional	clobazam, divalproex, leveritacetam, valproic acid	Mild inefficiency in complex attentional functions
20	F	Ped	CM, ANT	MCD; epileptic encephalopathy	lamotrigine, oxcarbazepine	Exceptionally low to below average; ADHD+
21	F	Adult	ANT, Pul	Non-lesional	clonazepam, lamotrigine, levetiracetam	High Average to Exceptionally Strong.
22	M	Adult	ANT, Pul	Non-lesional	lacosamide, lamotrigine, levetiracetam, zonisamide	Low average to average, difficulties in sustained attention

23	M	Adult	ANT, Pul	Non-lesional	lamotrigine, topimarate	Low average
24	M	Ped	ANT, Pul	Bilateral subependymal gray matter heterotopia	lamotrigine, levetiracetam, topimarate	Low average to average
25	F	Adult	CM, Pul	non-lesional	cenobamate	Average to high average
26	F	Adult	ANT, Pul	Structural (PMG/PVNH/SOD)	clonazepam, eslicarbazepine	Significant weaknesses with attention

Table 4.1. Subject details. Ped: Pediatric; CM: centromedian nucleus; ANT: anterior nucleus; Pul: pulvinar nucleus; GLUD-1:glutamate dehydrogenase 1; ; HSV: herpes simplex virus; PMG: polymicrogyria; PVNH: periventricular nodular heterotopia; SOD: septo-optic dysplasia; TSC: tuberous sclerosis complex; ADHD+: positive diagnosis for attention deficit hyperactivity disorder; MCD: malformation of cortical development . Anti-seizure medication taken in the 24 hr prior to sensory gating experiment. +: Overall impression of attention per most recent neuropsychological evaluation.

3.2. Thalamic auditory evoked response morphological characteristics

The human thalamic auditory evoked response across all thalamic contacts and across all subjects had similar morphological characteristics to the auditory evoked response observed at Fz for subjects with evoked responses on the scalp and in the thalamus (n=16 subjects, n=32 thalamic recordings). At Fz, the population average auditory evoked response was characterized by a triphasic wave with an initial large positivity at 58.6 ms (P50), a negativity at 116.2 ms (N100), and a second positivity at 168.0 ms (P200). In the thalamus, the population average auditory evoked response was similarly characterized by

an initial large surface positivity at 39.1 ms, a negativity at 88.9 ms, and a second positivity at 152.3 ms (Fig. 4.1A).

The initial P50 potential in the thalamus preceded the scalp signal by 18.0 ms (95% CI [13.2, 22.8] ms, p<0.001, **SA.A**). When thalamic nuclei were analyzed separately, on average, the P50 in the pulvinar was detected at 29.9 ms (range: [26.4, 36.1] ms), in the CM at 48.8 ms (range: [23.9, 85.0] ms), and in the ANT at 43.6 ms (range: [26.4, 80.1] ms; Figure 4.1B). Compared to the scalp P50, the thalamic P50 was observed earlier in each thalamic nucleus evaluated (pulvinar: n=5, median: -12.7 ms, range: [-33.2, -12.7] ms, p=0.015; centromedian: n=16, median: -20.5 ms, range: [-38.0, 0.0] ms, p<0.001; anterior nucleus: n=11, median: -13.7 ms, range: [-38.0, 0.0] ms, p<0.001; Wilcoxon rank sum tests; Figure 4.1C, **SA.B**).

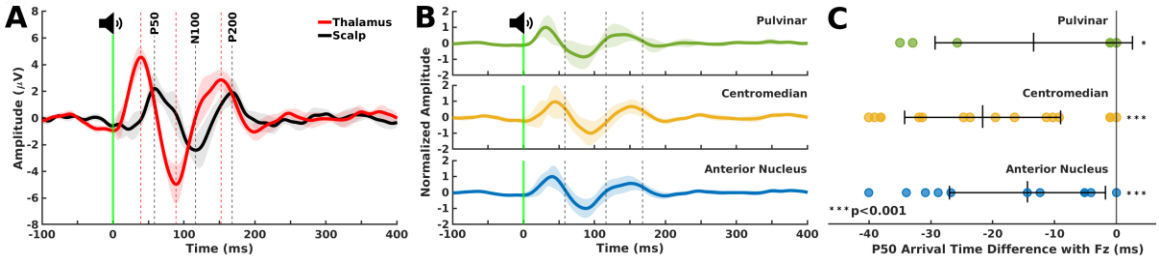

Figure 4.1. Scalp P50 detected in the thalamus. A) Thalamic responses (n=32, red curve) to the first auditory stimulus of the paired click paradigm precedes the scalp P50 response by 18.0 ms (n=16 subjects). Solid (shaded) curves indicate mean (95% confidence intervals). **B)** Average of normalized evoked responses to the first auditory stimulus in the thalamus based on nuclei targets (pulvinar, centromedian nucleus, anterior nucleus). **C)** The thalamic response to the corresponding scalp P50 response is shown with respect to the scalp P50 (where the arrival time is set to zero) and separated by the target in the thalamus. Crosses indicate median (center tick) and lower and upper quartiles.

3.3 Sensory gating responses in human thalamus

Sixteen subjects had detectable auditory evoked responses (see Methods: EEG Processing) on the scalp and were included in subsequent analysis (S1 amplitude: median 4.1 μV, range [1.2, 11.6] μV; S2 amplitude: median 2.8 μV, range [0.5, 7.8] μV). In the scalp, the S1 response was larger than the S2 response, as expected (n=16, p=0.03, Wilcoxon rank sum test, **SA.C**). All 16 of these subjects also had a detectable auditory evoked response (see Methods: EEG Processing) in the thalamus (mean of 2 thalamic nuclei observed per subject; S1 amplitude: median 6.0 μV, range [1.7, 23.8] μV; S2 amplitude: median 3.0 μV, range [0.7, 38.7] μV). In the thalamus, the S1 response was larger than the S2 response (p=0.0029, Wilcoxon rank sum test, **SA.C**).

Sensory gating was present at the scalp (n=16, mean 0.58, range [0.16, 0.86], p<0.001, one-sample t-test, **SA.D**) and at the thalamus (n=32, mean: 0.60, range: [0.11, 0.96], p<0.001, one-sample t-test, **SA.D**; Fig. 4.2D). These results remained significant after correcting for multiple comparisons (2 tests). No difference in the mean SG ratios at the scalp and thalamus were detected (p=0.995, **SA.E**). Sensory gating was also detected in all three nuclei targets: Pul (n=5, mean 0.72, range [0.52, 0.96], p=0.024, one-sample t-test, **SA.D**), CM (n=16, mean 0.64, range [0.11, 0.92], p<0.001, one-sample t-test, **SA.D**), and ANT (n=11, mean 0.50, range [0.14, 0.80], p<0.001, one-sample t-test, **SA.D**; Figure 4.2D). These results remained significant after correcting for multiple comparisons (3 tests). The sensory gating ratio was higher in Pul than in ANT (effect size 0.29, 95% CI [0.14, 0.44], p=0.001, **SA.F**). No differences in SG ratio were detected between Pul and

CM (p=0.60, **SA.F**) or between ANT and CM (p=0.034, **SA.F**) after correcting for multiple comparisons (3 tests).

Thalamic sensory gating ratio decreased with distance from the medial geniculate nucleus (MGN); observations further from the MGN demonstrated stronger gating with lower sensory gating ratios (-0.010 change in SG per mm, 95% CI [-0.019, -0.002] per mm, p=0.015, **SA.G,** Fig. 4.2E).

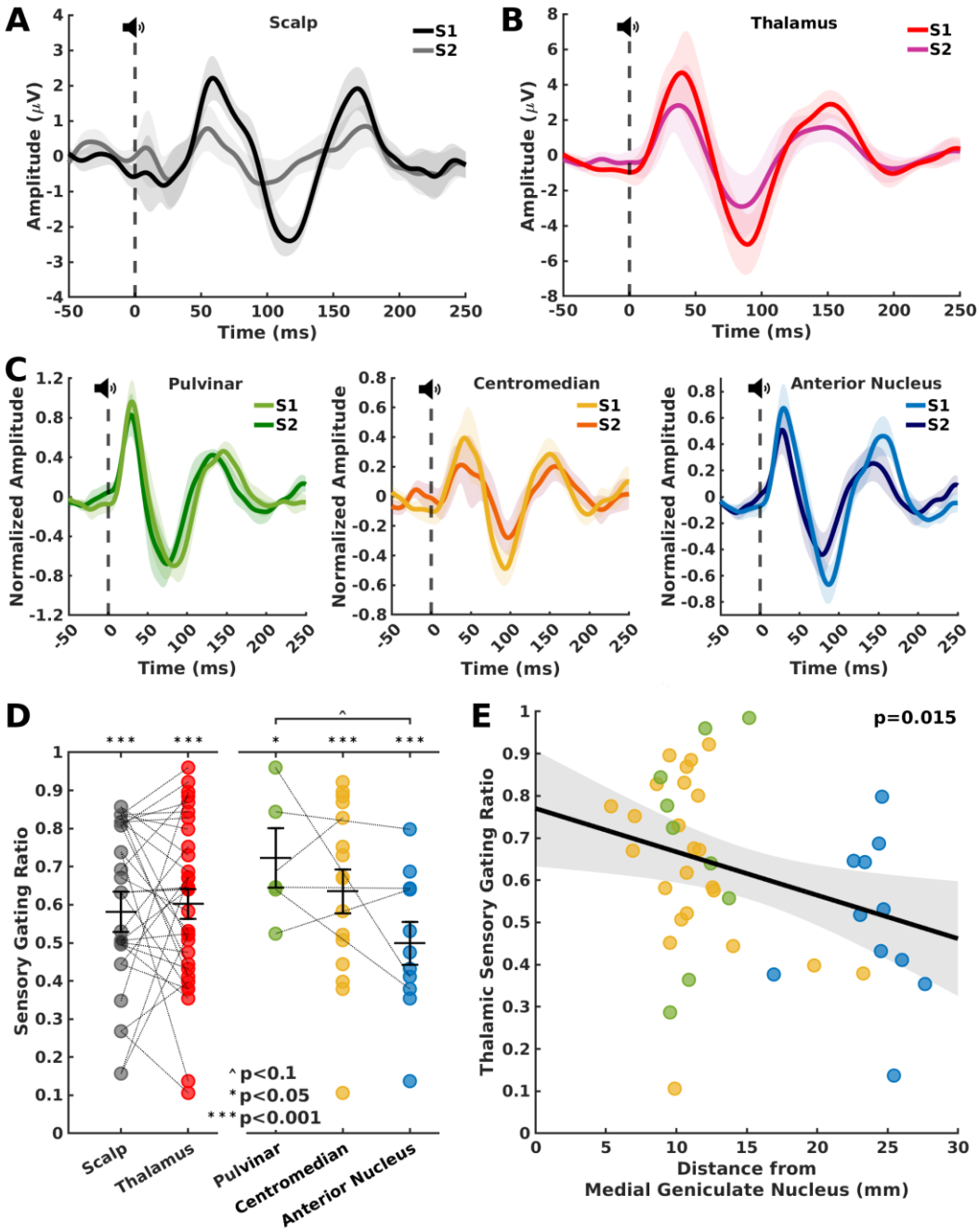

Figure 4.2. Sensory gating in the thalamus. (A-C) Average evoked responses at the **(A)** scalp, (**B**) thalamus, and (**C**) each thalamic nucleus following auditory stimuli (±95%CI across subjects). **(D)** SG ratios (mean±SEM) in the scalp and thalamus, and each thalamic nucleus (lines connect measurements from the same subject). **(E)** SG ratio plotted versus distance from the medial geniculate nucleus (colors as labeled in D).

3.4. Thalamic sensory gating predicts attention

Of the 26 subjects who completed the auditory SG task, 15 subjects completed the attention task (5 subjects chose not to participate in the attention task, 5 were excluded due to intellectual disability and inability to follow instructions, and 1 due to poor visual acuity). Of these 15 subjects, 11 subjects had detected thalamic evoked responses and 9 had both thalamic and scalp detected evoked responses. Lower averaged thalamic sensory gating predicted worse accuracy on the attention task (effect size -0.14, 95% CI [-0.28, -0.001], p=0.048, **SA.H**); a 0.1 unit decrease in thalamic sensory gating ratio corresponded to a 0.014 decrease in accuracy. Because observed accuracy values vary between 0.875 and 0.975 (Figure 4.3B), this corresponds to a 13% decrease on this scale. An increased thalamic sensory gating ratio was associated with increased commission errors (effect size 1.94, 95% CI [0.30, 3.58], p=0.025, **SA.I**); a 0.1 increase in thalamic sensory gating ratio corresponded to 21% increase in commission errors (see Fig 4.4C and Table 4.2). No evidence of a relationship between thalamic sensory gating ratio and omission errors was detected (p=0.27, **SA.I**). When sensory gating was measured at the scalp, no relationship was detected between sensory gating ratio and accuracy on the attention task (p=0.14, **SA.H**) or commission errors (p=0.63, **SA.I**). However, an increased scalp sensory gating ratio was associated with increased omission errors (effect size 5.7, 95% CI [2.1, 9.2], p=0.007, **SA.I**, Fig. 4.5E, Table 4.2); a 0.1 increase in scalp sensory gating ratio corresponded to a 76% increase in omission errors.

3.5 Spindle rate predicts attention

In the thalamus, higher overnight sleep spindle rate predicted increased accuracy on the attention task (effect size 0.007, 95% CI [0.002, 0.013], p=0.019, **SA.J**, Figure 4.3B); an increase of 1 spindle per minute corresponded to a 0.007 increase in accuracy, or approximately a 7% increase over the range of values observed (0.87 to 0.975, see Figure 4.3B). A decrease in averaged thalamic overnight spindle rate was also associated with an increase in omission errors (effect size -0.38, 95% CI [-0.71, -0.05], p=0.030, **SA.K**, Figure 4.4F); an increase of 1 spindle per minute in the averaged thalamic overnight spindle rate corresponded to a 31% decrease in omission errors. No evidence of a relationship between spindle rate and commission errors was detected (p=0.22, **SA.K**, Fig. 4.4D, Table 4.2).

At the scalp, higher overnight sleep spindle rate predicted higher accuracy on the attention task (effect size 0.006, 95% CI [0.0008, 0.01], p=0.027, **SA.J**, Figure 4.3C). An increase of spindle rate of 2 events per minute corresponded to a 0.01 increase in accuracy, or an approximate 10% change over the range of accuracies observed (Fig 4.4F). Decreased scalp overnight sleep spindle rate was associated with increased commission errors (effect size -0.07, 95% CI [-0.13 -0.01], p=0.021, **SA.K**, Figure 4.5D); an increase of 1 spindle per minute in the scalp overnight spindle rate corresponded to a 7% decrease in omission errors. No evidence of a relationship between scalp spindle rate and omission errors was detected (p=0.17, **SA.K**, Fig. 4.5F, Table 4.2).

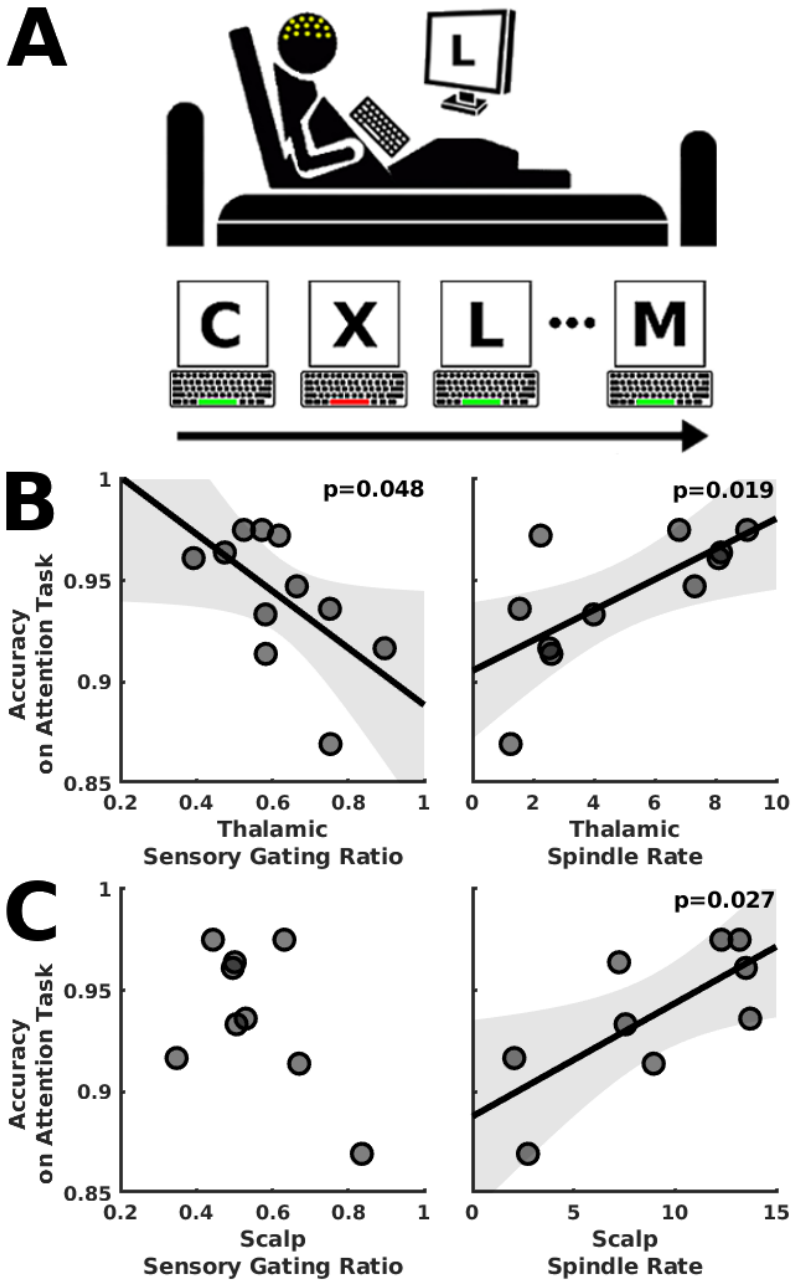

Figure 4.3. Sensory gating and attention. A) A continuous performance task was performed to assess attention. B) **Left:** Thalamic sensory gating ratio predicts accuracy on the attention task. **Right**: Thalamic sleep spindle rate predicts accuracy on the attention task C) **Left**: No relationship was detected between scalp sensory gating ratio and attention task accuracy. **Right**: Scalp spindle rate predicts attention task accuracy.

	Sensory Gating Ratio		Spindle Rate	
	Effect Size [95% CI]	p-value	Effect Size [95% CI]	p-value
Thalamus				
Accuracy	-0.141 [-0.90, -0.001]	0.048	0.001 [0.001, 0.001]	0.019
Commission Errors	1.94 [0.30, 3.58]	0.025	-0.060 [-0.162, 0.043]	0.218
Omission Errors	3.05 [-2.81, 8.91]	0.270	-0.038 [-0.708, -0.046]	0.030
Scalp				
Accuracy	-0.13 [-0.32, -0.05]	0.135	0.001 [0.001, 0.010]	0.027
Commission Errors	-0.60 [-3.35, -2.16]	0.626	-0.070 [-0.127, -0.014]	0.020
Omission Errors	5.66 [2.15, 9.17]	0.007	-0.11 [-0.292, 0.064]	0.173

Table 4.2: Attention Task Results predicted by thalamic and scalp sensory gating and overnight spindle rates. Thalamic sensory gating predicts accuracy and commission errors on attention task, overnight thalamic spindle rate predicts accuracy and omission errors, scalp sensory gating predicts omission errors and scalp sensory gating predicts accuracy and commission errors.

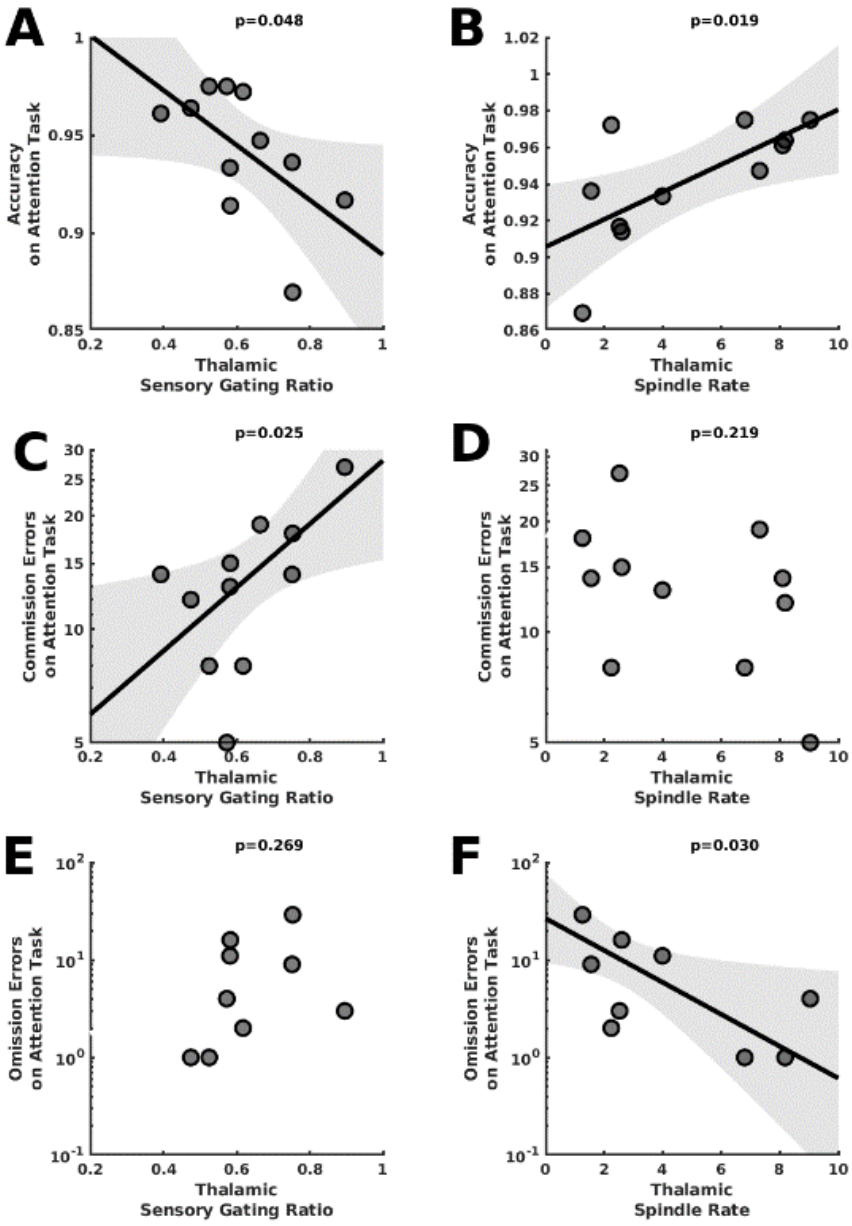

Figure 4.4. Thalamic sensory gating, spindle rate and attention. A) Thalamic sensory gating ratio predicts accuracy on the attention task. B) Thalamic spindle rate predicts accuracy C) Thalamic sensory gating predicts commission errors on attention task D) No relationship was detected between thalamic spindle rate and commission errors E) No relationship was detected between thalamic spindle rate and omission errors F) Thalamic spindle rate predicts omission errors

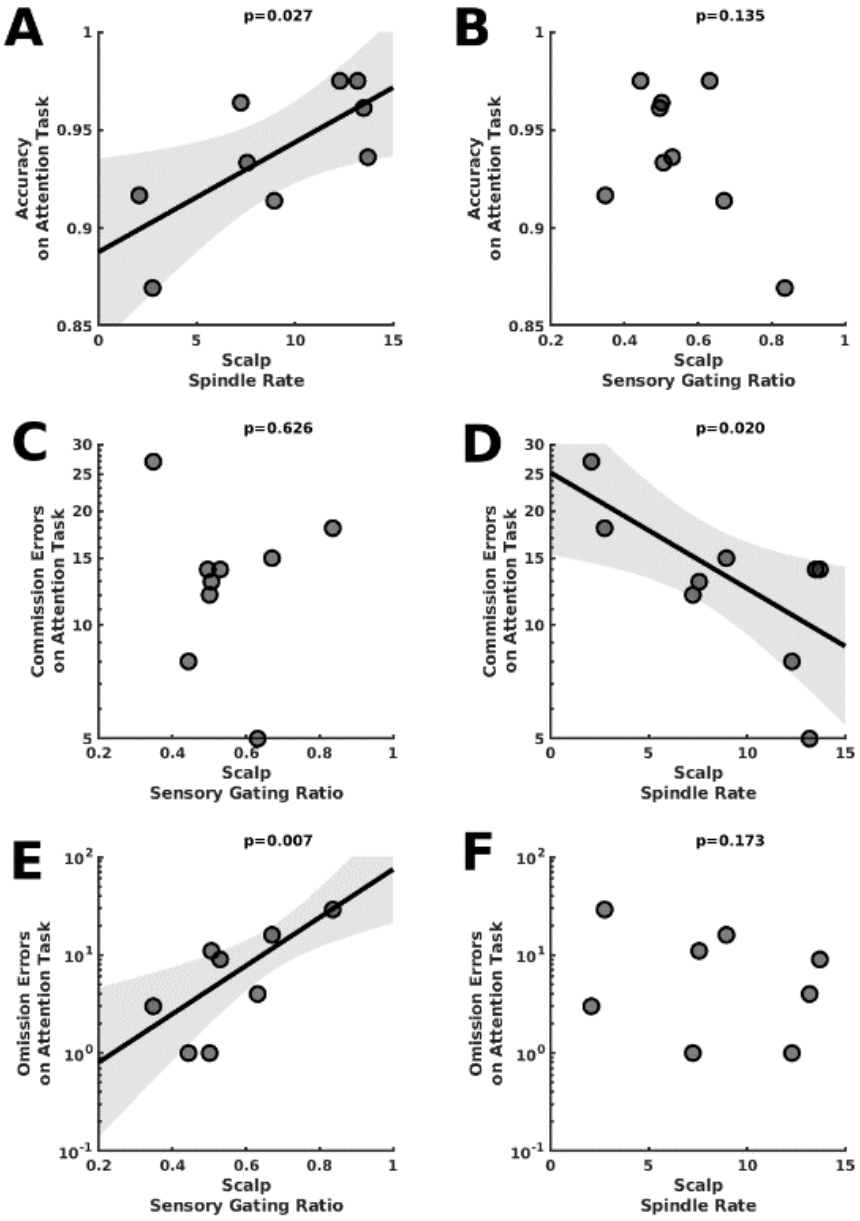

Figure 4.5. Scalp sensory gating, spindle rate and attention. A) Scalp sensory gating ratio predicts accuracy on the attention task. B) No relationship was detected between scalp spindle rate and accuracy C) No relationship was detected between thalamic sensory gating and commission errors on attention task D) Scalp spindle rate predicts commissions errors E) Scalp sensory gating predicts omission erros on attention task F) No relationship was detected between scalp spindler ate and omission errors

3.6. Thalamic sensory gating ratio correlates with thalamic sleep spindle rate.

The thalamic SG ratio and spindle rate both predict task performance, but in opposite directions; lower SG ratios predict improved performance, while higher spindle rates predict improved performance. To investigate the relationship between the thalamic SG ratio and thalamic spindle rate, a generalized linear mixed effects model was estimated. Higher thalamic sensory gating ratios predicted lower thalamic spindle rates (effect size -1.8, 95% CI [-2.9, -0.7], p=0.0025, **SA.L**, Figure 4.6); a 0.1 increases in thalamic sensory gating ratio corresponded to a 19% increase in thalamic spindle rate. This relationship was only detected at the thalamus; no evidence of a relationship between the scalp SG ratio and scalp spindle rate was detected in this cohort (p=0.23, **SA.M**).

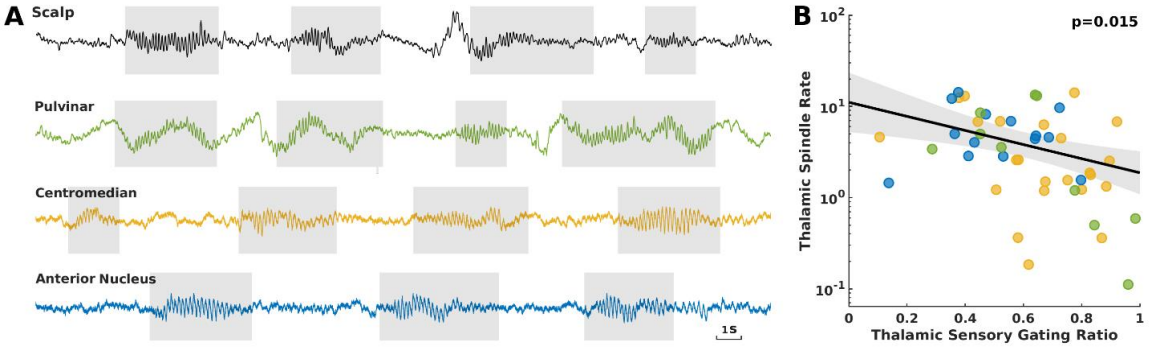

Figure 4.6. Thalamic sensory gating ratio predicts thalamic spindle rate. A) Examples of spindle detections in N2 and N3 stages of non-rapid eye movement sleep in the scalp and in three thalamic nuclei targets (pulvinar, centromedian nucleus and anterior nucleus). B) There is an exponential negative relationship between thalamic spindle rate and thalamic sensory gating ratio: the higher the spindle rate, the higher is the ability to gate redundant auditory information.

4. Discussion

In this study, we investigated the dynamics of thalamic SG and its implications for attentional processes. We observed that the thalamic response to the initial auditory stimulus in a paired click paradigm precedes that of the scalp, indicating the role of the thalamus in early auditory processing. Sensory gating was consistently present across all thalamic nuclei and scalp, emphasizing the integral involvement of thalamic networks in this phenomenon. However, our findings also revealed regional variations in SG, with lower gating observed in the anterior region of the thalamus. This discrepancy indicates the nuanced nature of sensory processing within the thalamus, suggesting specialized roles for different nuclei. The higher auditory SG ability detected in the ANT of the thalamus is consistent with previous findings showing that the ANT is involved in attention control (de Bourbon-Teles *et al.*, 2014; Wright *et al.*, 2015; Leszczyński and Staudigl, 2016).

Our study establishes a link between thalamic sensory gating and behavioral attentional performance. The predictive relationship between thalamic sensory gating ratio, and attentional task performance confirms the critical role of the thalamus in attention networks(Portas *et al.*, 1998; de Bourbon-Teles *et al.*, 2014). Similarly, the relationship between spindle rate and attention is consistent with previous findings at the scalp, and in the thalamus where spindles are generated (Sonnleitner *et al.*, 2012; Chen *et al.*, 2016). This convergence of behavioral assessment and direct physiological measurements underscores the central role of the thalamus in attentional processes, which are at risk in epilepsy (Hesdorffer *et al.*, 2004; Williams *et al.*, 2016).

Our findings also shed light on the disrupted neural circuits producing cognitive impacts in patients with epilepsy. Patients with epilepsy often exhibit spindle deficits and impaired cognitive abilities, as well as an increased risk of attention deficit hyperactivity disorder (Urakami *et al.*, 2012; Williams *et al.*, 2016; Kramer *et al.*, 2021; Schiller *et al.*, 2022; Spencer *et al.*, 2022; Zhang *et al.*, 2023). The involvement of the TRN, essential for spindle generation and attentional gating, suggests a common underlying root cause for these deficits (Steriade *et al.*, 1987; McAlonan, Brown and Bowman, 2000). Thus, our study underscores the importance of thalamocortical circuitry in cognitive function and suggests potential avenues for therapeutic intervention in epilepsy-related cognitive impairments.

5. Conclusion

This study investigates the intricate relationship between thalamic auditory sensory gating, attentional processes, and epilepsy. Our findings demonstrate that thalamic sensory gating is consistent across different nuclei and is closely linked to thalamic spindle rate, highlighting the thalamic contribution to sensory processing and attentional modulation. The observed increase in auditory gating towards the anterior portion of the thalamus underscores the regional specificity of sensory processing within this structure. Furthermore, our study suggests that deficits in thalamic sensory gating may contribute to

attention deficit disorder commonly observed in epilepsy, pointing towards potential therapeutic targets for cognitive impairments in this patient population.

CHAPTER FIVE: Evoked thalamic spindles following Closed-Loop Auditory Stimulation increase memory consolidation

Abstract

Rationale: Slow oscillations (SOs) and sleep spindles (SSs) are prominent brain oscillations during non-rapid eye movement (NREM) sleep that support sleep-dependent memory consolidation. Quiet sounds timed to the upstate of SOs (closed-loop auditory stimulation or CLAS) during NREM is a non-invasive method to increase SOs and SSs with potential applications across many neurological and psychiatric disorders, including epilepsy. SOs are thought to be initiated in the cortex and SSs in the thalamus. The optimal timing of CLAS to induce SOs and SSs across thalamocortical circuits is not known. Further, the impact of CLAS on these thalamocortical rhythms in patients with epilepsy is not known. We performed CLAS on participants with simultaneous scalp EEG and intracranial thalamic recordings to study the optimal detection parameters and timing of CLAS to increase SOs and SSs in the thalamus and the cortex in patients with epilepsy.

Methods: We performed CLAS on 33 subjects (16 F, average 25.3 years old, ages 5.1 – 66.1 years old) with epilepsy from a variety of etiologies undergoing direct thalamic recordings during their epilepsy surgery evaluations. In each case, subjects wore headphones that delivered a quiet auditory click timed to the upstate of SOs (0.5-4 Hz) detected in the scalp EEG (Fz) during NREM sleep. Following a night of CLAS, subjects slept with headphones and SOs were detected, but no stimulation was delivered for these

control sessions (sham, n=22). Electrode locations were confirmed on post-operative MRI or co-registration of pre-operative MRI and post-operative CT. Thalamic nuclei were reconstructed using FreeSurfer. Data were divided into single trials centered on auditory stimulation. Trials were rejected as artifact if the amplitude exceeded ±500 μV. In scalp and thalamic recordings, evoked responses were compared between SO-CLAS (stimulation targeting SOs with negative peak voltages lower than -50 μV) and sham nights, and similarly for low amplitude (LA)-CLAS (stimulation targeting slow waves with negative peak voltage between -25 μV and -50 μV) and sham nights.

Results: Evoked SOs are present in both thalamic and scalp recordings compared to sham stimulation for both SO-CLAS and LA-CLAS ($p<0.001$), with larger amplitude responses in the thalamus compared to the scalp following SO-CLAS ($p<0.002$). Stimuli that evoked a subsequent SO were closer to the upstate peak of the endogenous SO compared to stimuli that failed to induce a subsequent SO for both SO-CLAS (thalamus: -0.08 rad vs. -0.83 rad, $p<0.001$; scalp: 0.13 rad vs. -0.28 rad, $p<0.001$) and LA-CLAS (thalamus: -0.12 rad vs. -0.61 rad, $p<0.001$; scalp: 0.05 rad vs. -0.25 rad, $p<0.001$). No difference in evoked spindles coupled to slow oscillations were detected between SO-CLAS and sham nights ($p>0.05$), and application of SO-CLAS trends to reduced memory consolidation ($p=0.096$). Alternatively, LA-CLAS increases evoked spindles coupled to slow oscillations in the thalamus ($p<0.001$) and increases memory consolidation ($p=0.019$).

Conclusion: We find that CLAS evokes both cortical and thalamic SOs in patients with epilepsy. CLAS delivered closer to the peak of the upstate produces a higher yield of evoked SOs. SSs can be supported depending on the amplitude of the endogenous thalamic SOs. These findings support development of this non-invasive therapeutic tool to increase the brain rhythms that support memory in patients with epilepsy.

1. Introduction

Epilepsy's impact stretches beyond the immediate hurdle of seizure control, a affecting millions globally with a web of neurological challenges. Memory and cognitive function are often compromised, impacting patients' quality of life (Mazarati, 2008; Holmes, 2015). While standard treatments focus on seizure control, there is a growing need for interventions that address these cognitive deficits. The research in this chapter explores a non-invasive approach targeting specific brain rhythms during sleep to enhance memory consolidation in epilepsy patients.

During non-rapid eye movement (NREM) sleep, brain rhythms orchestrate memory consolidation, the process of solidifying short-term memories into long-term storage (Cowan, 2008). Two key rhythms in this process are slow oscillations (SOs) and sleep spindles (SSs). SOs - large, slow waves (0.5-4 Hz) believed to originate in the cortex - act as a conductor, creating windows of increased communication efficiency between different brain regions (Massimini et al., 2004). Riding on these slow oscillations are SSs, brief

bursts of higher frequency activity (12-16 Hz) thought to be generated in the thalamus (Urakami *et al.*, 2012). SSs have been proposed to organize neural firing and support strengthening of connections essential for memory formation (Laura Fernandez and Anitha Luthi, 2019).

Disruptions within the thalamocortical circuit, the pathway connecting the cortex and thalamus, are a hallmark of epilepsy (Martín-López *et al.*, 2017). These disruptions can lead to memory impairments by hindering the synchronized activity of SOs and SSs, compromising communication and memory consolidation processes (Kramer *et al.*, 2021; Schiller *et al.*, 2022; Wodeyar *et al.*, 2024).

Closed-loop auditory stimulation (CLAS) is a promising, non-invasive intervention that may improve memory function in epilepsy. CLAS delivers quiet sounds precisely timed to the peak (upstate) of SOs during NREM sleep (Ngo *et al.*, 2013). This precise timing is crucial because it optimizes the window of opportunity for communication within the thalamocortical circuit. By delivering a sound cue at this precise moment, CLAS may enhance communication and potentially boost SS activity, leading to improved memory consolidation. While boosting healthy brain rhythms were proven to be replicable, the impacts on memory using similar techniques have yield mixed results (Wunderlin *et al.*, 2021).

How to optimize CLAS for the treatment of cognitive impairments in epilepsy remains unknown. To address this challenge requires optimizing features of CLAS (e.g.,

stimulation timing) to maximize the impact on SSs in epilepsy patients. To that end, patients undergoing CLAS with simultaneous scalp EEG and intracranial thalamic recordings were observed to characterize the impact of auditory stimulation on SOs and SSs in the brain regions that generate these rhythms. This investigation holds potential for not only improving memory function in epilepsy but also for optimizing CLAS as a non-invasive therapeutic tool for memory deficits in other neurological and psychiatric disorders.

2. Methods

2.1. Participants and EEG recordings

Patients who underwent stereotactically placed depth electrode EEG (sEEG) recordings targeting the thalamus as part of their clinical care for drug refractory epilepsy at Massachusetts General Hospital between August 2020 and August 2023, were approached for enrollment in this study. Depth electrodes (PMT Corporation, Chanhassen, MN, USA) were placed with robotic stereotactic assistance (ROSA, Zimmer Biomet, Warsaw, IN, USA) based on the clinical indications for seizure network localization as determined by a multidisciplinary clinical team. Twenty-one scalp EEG electrodes were also placed following the 10-20 international system. All EEG recordings were obtained with a sampling rate of 1024 Hz using an XLTEK digital system (Natus Medical Incorporated, Pleasanton, CA). Of the 40 subjects approached for enrollment, 33 subjects

agreed to participate. This study was approved by the Massachusetts General Hospital Institutional Review Board.

The electronic medical record for each patient was reviewed for demographic information, epilepsy etiology, results of clinical neuropsychological evaluations, and antiseizure medication exposure within 24 hours of the experiment.

2.2. Experimental setup

Subjects wore in-ear headphones that delivered a quiet auditory click timed to the upstate of SOs (0.5-4 Hz) detected in the scalp electroencephalogram (Fz) during NREM sleep (n=33), following the methodology in (Ngo *et al.*, 2013). Following a night of CLAS, subjects slept with headphones and SOs were detected, but no stimulation (sham) delivered (n=22).

2.3. Real-time detection of slow oscillations

Scalp data were read in real-time, updated in data packets of duration 40 ms, Butterworth filtered between 0.5 to 4.0 Hz in 1 s intervals, before automatic slow oscillation detection (Mölle and Born, 2011). CLAS was performed targeting oscillations with two different amplitudes. For slow oscillation CLAS (SO-CLAS), a slow oscillation was detected if the negative peak was less than -50 μV. For low amplitude slow oscillation

CLAS (LA-CLAS), stimulations were delivered only if the negative peak was between -25 μV and -50 μV. There was a minimum of 4 s between detections.

2.4. Motor sequence task (MST)

Subjects were instructed to complete the motor sequence task (MST) before and shortly after a night of CLAS or sham. The MST consists of typing a 5-digit sequence as many times as possible in 12 rounds of 30 s duration, with 30 s of rest between rounds. Subjects completed the task in the evening before sleep (training) and in the morning after sleep (testing) (Fig. 5.1). Task performance (i.e., the number of correct typed sequences) was normalized by the average of the last 3 trials in the training phase. Memory improvement was calculated by comparing the average number of correct sequences in the first three trials during testing after sleep to the average number of correct sequences during the last three trials during training before sleep (Tucker, Nguyen and Stickgold, 2016), as follows:

$$MST\ Improvement = \frac{Average\ of\ First\ \ 3\ trials\ during\ testing - Average\ of\ Last\ 3\ trials\ during\ training}{Average\ of\ Last\ 3\ trials\ during\ training}$$

[Eq. 1]

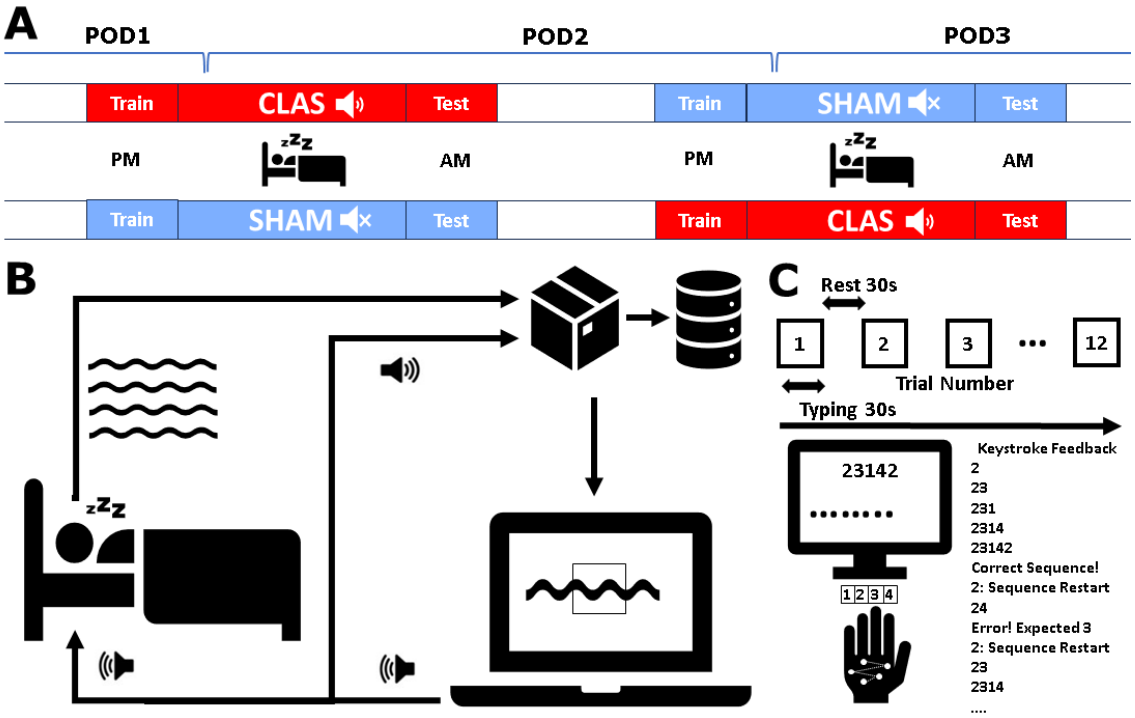

Figure 5.1. Cross-study design and setup. A) Patients undergoing monitoring in the epilepsy unit were approached on post-operative day 1, 2 and 3 (POD1,2,3) to participate in the experiement in a cross-study design. Half of the approached patients received closed-loop auditory stimulation (CLAS) then no stimulation (SHAM), and vice-versa for the rest. Patients were also approached to complete a motor sequence task (MST) shortly before and after sleep. B) CLAS consisted of real-time data acquisition during sleep by streaming data packets from the clinical recording system. C) MST training and testing consisted of 12 trials of 30 s duration, with 30 s of rest between trials. Keystrokes were monitored in real-time to ensure that experimental instructions were followed and to provide the typing sequence result (correct or error) and reward after each round to the patient.

2.5. Electrode localization

Using FreeSurfer or Slicer, each subject's post-operative CT or MRI scan with implanted electrodes was registered to the subject's most recent available sagittal T1 MRI scan preceding implantation (Fedorov *et al.*, 2012; Fischl, 2012). The pre-implantation T1

and T2 scans were processed with FreeSurfer for whole brain segmentation and thalamic segmentation, which estimates thalamic nuclei based on a human probabilistic thalamic atlas (Fischl *et al.*, 2002; Iglesias *et al.*, 2018). For CT-to-MRI registration, Slicer was used to align the pre-implantation T1 scans, and the General Registration (BRAINS) was used for automated registration (Johnson, Harris and Williams, 2007). The results were visually inspected and manually adjusted as needed to confirm satisfactory registration. For MRI-to-MRI registration, FreeSurfer's automatic registration processing module was used and manually adjusted as needed based on visual review. Electrodes were localized in FreeSurfer's Freeview overlaid on the pre-implantation MRI scan. Each electrode contact was manually marked (raw locations). Then, using all manually marked contacts per depth electrode, a single-value decomposition (SVD) algorithm was also used to distribute the electrodes along a straight line of best fit (corrected localizations). For each seizure type included, the FreeSurfer label for each contact in the cortical seizure onset zone and in the ipsilateral thalamus was recorded for both the raw and corrected contact locations.

2.6. Evoked response analysis

Thalamic and scalp electrodes were referenced to a non-cephalic electrode placed on the second spinous process. In two subjects, electrical noise was present upon visual inspection and the channel signal was filtered with a low pass filter of 4 Hz (finite impulse response using the Kaiser window method with a maximum passband ripple of 0.1 and stopband attenuation of at least 60 db; filter order: 48). Data were divided into single trials

centered on auditory stimulation. Trials were rejected as artifact if the amplitude exceeded ± 500 μV.

2.6. Offline slow oscillation detection

For offline slow oscillation detection, sleep staging was first performed using a validated sleep staging algorithm before applying an automatic slow oscillation detector (Mölle and Born, 2011; Ellenrieder *et al.*, 2022).

2.7. Spindle detection

For sleep spindle analysis, sleep staging was performed using a validated sleep staging algorithm (Ellenrieder *et al.*, 2022). Sleep spindles were then detected using an automated detector validated for use in EEG containing epileptiform spikes (Kramer *et al.*, 2021). Before application of the sleep spindle detector, thalamic electrodes were referenced to an adjacent electrode on the same intracranial lead and the scalp electrode (Fz) referenced to the scalp common average reference. Spindle rate was computed and averaged across all N2 and N3 sleep stages for the duration of CLAS or during control recordings (sham).

2.8. Phase estimator

The EEG signal was bandpass filtered (0.5-2 Hz), the Hilbert transform applied to compute the analytic signal, and the smoothed phase was estimated after removing waveform distortions due to a narrowband filter (Davis *et al.*, 2020).

2.9. Spindle incidence

To measure the impact of stimulation at each thalamic target, spindle detections following an evoked slow oscillation - identified using the offline slow oscillation detector - were considered. For each spindle with an offline detected and evoked slow oscillation, a binary array of length 2 s before stimulation and 5 s after stimulation was constructed, where each time point (sampling rate 1,024 Hz) indicated the absence or presence of a spindle. The average spindle incidence was then calculated for each subject as the average of these binary arrays across all spindle detections with an offline detected and evoked slow oscillation. The average spindle incidence was then scaled by subtracting the average spindle incidence in the baseline between -2 and -1 s before simulation. For each subject, the spindle incidence was averaged across all thalamic targets.

2.10. Statistical analysis (SA)

SA.A. To compare the efficacy of stimulation on the night of CLAS, slow oscillations detected by the online detector were first compared to offline SO detections.

Evoked slow oscillations were included if: (i) the stimulation occurred at a slow oscillation also detected by the offline slow oscillation detector, and (ii) the negative peak of the evoked slow oscillations was less than or equal to -50 μV and within 0.75 s of the stimulation. The number of stimulations that evoked SOs were counted at the scalp and for each thalamic recordings for each subject. To compare the phase of the endogenous SO when an auditory stimulation successfully evoked a subsequent SO, versus when stimulation failed to evoke a subsequent SO, a two-sided t-test was applied to compare the mean phase of the endogenous SOs at the time of simulation (no deviation from normality using Lillie test, $p>0.05$).

SA.B. To compare the evoked responses during CLAS compared to sham recordings across patients, a Wilcoxon ranksum test was applied at each time point, from -2 s before stimulation to 5 s after stimulation. The Wilcoxon ranksum test was applied because more than 5% of the data violated the null hypothesis of normality ($p<0.05$, Lillie test). Multiple comparison correction was performed to control the false discovery rate (FDR) using the Benjamini-Hochberg procedure with a false discovery control level of 0.05. Thalamic responses were averaged across all thalamic targets for each subject before comparison.

SA.C. To compare the amplitude and time of occurrence of the averaged evoked responses for each subject between the thalamus and scalp, and between the amplitude of the preceding endogenous events and evoked responses, paired t-tests were applied unless

the data violated the null hypothesis of normality, in which case a Wilcoxon ranksum test was applied.

SA.D. To compare the spindle incidence in a night of CLAS versus a night of sham CLAS, the average spindle incidences per subject were averaged across the population of subjects. The resulting population averaged spindle incidences were compared at each time point using Wilcoxon ranksum tests because more than 5% of the data violated the null hypothesis of normality ($p<0.05$, Lillie test). Multiple comparison correction was performed to control the false discovery rate (FDR) using the Benjamini-Hochberg procedure with a false discovery control level of 0.05. Thalamic spindle incidences were averaged across all thalamic targets for each subject before comparison.

SA.E. To compare the memory improvement after a night of CLAS versus a night a sham CLAS, a paired t-test was applied.

3. Results

3.1. Subject Demographics

Thirty-three subjects (16 F, average 25.3 years old, ages 5.1 – 66.1 years old) with epilepsy from a variety of etiologies were included. Patients had electrodes targeting the centromedian nucleus (CM, n=11), anterior nucleus (ANT, n=4), the pulvinar (Pul, n=1), both the CM and ANT (n=5), both the CM and Pul (n=5), both the ANT and Pul (n=6), or all three targets (n=1). Twenty-five patients had bilateral thalamic implantations. Among

subjects with both CLAS and sham recordings (n=26), 20 had identical anti-seizure medications on both days of the experiment, 4 had at least 1 overlapping anti-seizure medication, and 2 only had anti-seizure medications on the day of the sham.

Subj #	**Sex**	**Age Group**	**Thal. Target**	**Epilepsy etiology**	**Anti-Seizure medication on day of CLAS**	**Anti-Seizure medication on the day of sham CLAS**
1	M	Ped	Pul	Structural (PMG)	lamotrigine, levetiracetam, topiramate (morning, evening)	N/A
2	M	Adult	ANT	Unknown	lamotrigine (morning)	N/A
3	M	Adult	ANT	Unknown	lamotrigine (morning, evening)	N/A
4	M	Ped	CM	Unknown	lamotrigine, levetiracetam, valproic acid (morning, evening)	N/A
5	M	Ped	CM	Structural (encephalomalacia, stroke)	clobazam (evening); cannabidol, lamotrigine (morning, evening)	N/A
6	M	Ped	CM	Structural (encephalomalacia, neonatal hypoglycemia)	clobazam, cannabidol, lacosamide (morning, evening)	N/A
7	M	Ped	CM	Unknown	clobazam (morning, afternoon, evening), levetiracetam (morning, evening)	N/A

8	M	Adult	ANT, CM	Structural (FCD, HS)		lacosamide, oxcarbazepine (morning, evening)
9	F	Ped	CM, Pul	ACC, PMG	clobazam, cannabidol, levitiracetam (morning, evening)	clobazam, cannabidol, levitiracetam (morning, evening)
10	F	Ped	CM	Structural (PMG)	cannbidol, fenfluramine, lamotrigine, levetiracetam (morning, evening); perampanel (evening)	cannbidol, fenfluramine, lamotrigine, levetiracetam (morning, evening); perampanel (evening)
11	F	Ped	CM	Unknown	lamotrigine (morning, evening)	lamotrigine (morning, evening)
12	F	Adult	CM	Unknown	lamotrigine, oxcarbazepine (morning, evening)	lamotrigine, oxcarbazepine (morning, evening)
13	F	Ped	CM	Unknown	lamotrigine, levetiracetam, oxcarbazepine (morning, evening)	lamotrigine, levetiracetam, oxcarbazepine (morning, evening)
14	M	Adult	CM	Structural (HS)	zonisamide (morning)	carbamazepine, lamotrigine, zonisamide (morning, evening)
15	M	Adult	CM	Unknown	lamotrigine, oxcarbazepine (morning, evening)	lamotrigine, oxcarbazepine (morning, evening)
16	F	Adult	ANT, CM	Unknown	cannabidol, brivaracetam (morning, evening); cenobamate, zonisamide (evening)	cannabidol, brivaracetam (morning, evening); cenobamate,

						zonisamide (evening)
17	M	Adult	ANT, CM	Unknown	clobazam, levetiracetam, valproic acid (morning, evening)	clobazam, levetiracetam, valproic acid (morning, evening)
18	F	Adult	ANT, Pul	Unknown	clonazepam, lamotrigine, levetiracetam (morning, evening)	clonazepam, lamotrigine, levetiracetam (morning, evening)
19	M	Adult	CM, Pul	Unknown	lamotrigine, levetiracetam, zonisamide (morning)	lamotrigine, levetiracetam (morning)
20	M	Adult	ANT, Pul	Unknown	lamotrigine, topiramate (morning, evening)	lamotrigine (morning, evening)
21	M	Ped	ANT, Pul	Unknown	levetiracetam, topiramate (morning, evening)	levetiracetam, topiramate (morning, evening)
22	F	Adult	CM, Pul	Unknown	None	None
23	F	Adult	ANT, Pul	Structural (PMG/PVNH/SOD)		clonazepam (morning, evening), eslicabazepine (evening)
24	M	Adult	ANT	Structural (encephalomalacia)	lamotrigine (morning, evening)	lamotrigine (morning, evening)
25	F	Adult	CM, ANT	Structural (encephalomalacia)	lamotrigine, levetiracetam (morning, evening)	lamotrigine (morning, evening), levetiracetam (morning)
26	F	Adult	ANT	Unknown	lamotrigine, oxcarbazepine (morning, evening)	lamotrigine, oxcarbazepine (morning, evening)

27	F	Ped	ANT, Pul	Structural (FCD, HS)	fenfluramine, rufinamide (morning, evening); eslicarbazepine , cenobamate (evening)	eslicarbazepine, fenfluramine, rufinamide (morning, evening); cenobamate (evening)
28	M	Adult	CM, Pul	Structural (MCD, PMG)	levetiracetam (morning, evening)	levetiracetam (morning, evening)
29	M	Ped	CM, ANT	Structural (MCD, PMG)	cannabidol, fenfluramine, gabapentin, levetiracetam, lacosamide, rufinamide (morning, evening)	levetiracetam, fenfluramine, lacosamide (evening)
30	F	Adult	CM, Pul	Unknown	lamotrigine (morning, evening)	lamotrigine (morning, evening)
31	F	Adult	AN, Pul	Encephalomalacia	clonazepam (morning, evening)	clonazepam (evening)
32	F	Adult	ANT, CM, Pul	Unknown	levetiracetam (morning, evening)	levetiracetam (morning, evening)
33	F	Adult	CM	Unknown	lacosamide, oxcarbazepine (afternoon, evening)	lacosamide, oxcarbazepine (morning, evening)

Table 5.1. Subject details. Subj #: Subject number; Ped: Pediatric; Thal: Thalamic; CM: centromedian nucleus; ANT: anterior nucleus; Pul: pulvinar nucleus; FCD: focal cortical dysplasia; GM: gray matter; HS: hippocampal sclerosis; HSE: herpes simplex encephalitis; MCD: malformation of cortical development; PMG: polymicrogyria; PVNH: periventricular nodular heterotopia; SOD: septo-optic dysplasia; SOZ: seizure onset zone; TSC: tuberous sclerosis complex; WM: white matter. GLUD-1:glutamate dehydrogenase 1; ; HSV: herpes simplex virus; PMG: polymicrogyria; PVNH: periventricular nodular heterotopia; SOD: septo-optic dysplasia; TSC: tuberous sclerosis complex; ADHD+: positive diagnosis for attention deficit hyperactivity disorder; MCD: malformation of cortical development . Anti-seizure medication taken in the 24 hr prior to sensory gating experiment.

3.2. Efficacy of SO-CLAS depends on SO phase

Eighteen subjects completed SO-CLAS nights. Across these subjects, 14,292 auditory stimulations were delivered in N2 and N3 sleep stages (mean per subject: 1286, range: [10, 3174]), resulting in 12,638 evoked SOs in the thalamus and 8,856 evoked SOs at the scalp. SO-CLAS administered closer to the upstate of the SO oscillation evoked more SOs compared to earlier stimulation times (i.e., before the upstate) in the thalamus (phase of stimulations with evoked SO: average -0.08 rad, interquartile range [-0.81, 0.58] rad; phase of stimulations without evoked SO: average -0.83 rad, range: [-1.78, -0.30] rad; $p<0.001$, t-test, **SA.A**) and on the scalp (phase of stimulations with evoked SO: average 0.13 rad, range [-0.46, 0.69] rad; phase of stimulations without evoked SO: average -0.28 rad, range [-0.98, 0.31] rad; $p<0.001$, t-test **SA.A**) (Fig. 5.2AB).

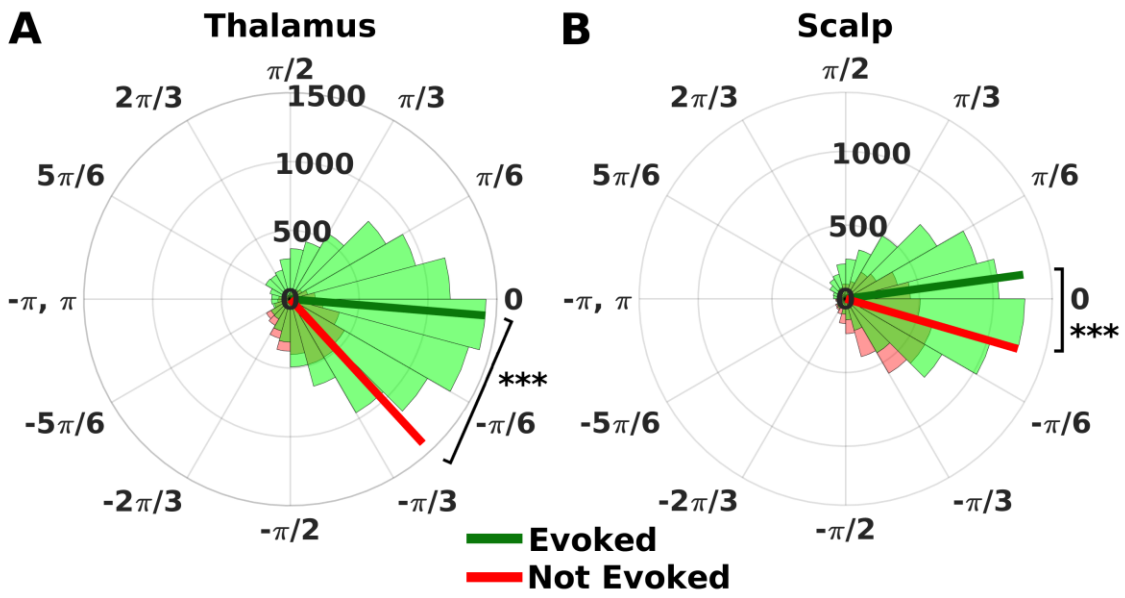

Figure 5.2. Success of CLAS is influenced by phase of stimulation. A) Auditory stimulation aligned with the SO upstate is more likely to evoke a SO (green) than auditory stimulation not aligned with the SO upstate (red, $p<0.001$) in the thalamus. **B)** Auditory stimulation aligned with SO upstate is more likely to evoke a SO (green) than auditory stimulation not aligned with the SO upstate (red, $p<0.001$) at the scalp.

3.3. SO-CLAS evokes larger slow oscillations in the thalamus than scalp

Twelve subjects completed both SO-CLAS and sham SO-CLAS. A larger evoked response followed auditory stimulation on the CLAS night (mean -59.3 μV, 95% CI [-85.6, -32.9] μV) compared to sham night (mean 9.8 μV, 95% CI [4.3, 15.6] μV) at the thalamus ($p<0.001$, Wilcoxon ranksum test and correction for multiple comparisons using FDR, **SA.B**). A similar result was observed at the scalp; a larger evoked response following auditory stimulation on the CLAS night (mean -39.4 μV, 95% CI [-53.3, -25.5] μV) compared to the sham night (mean 4.3 μV, 95% CI [-2.4, 11.0] μV; $p<0.001$; Wilcoxon ranksum test and correction for multiple comparisons using FDR, **SA.B**; Fig 5.3).

The average arrival time of the negative peak of the evoked response was 488.9 ms in the thalamus (range [210.9, 696.3] ms) and 494.0 ms at the scalp (range [86.9, 698.2] ms); no difference between these arrival times was detected ($p=0.9$, Wilcoxon ranksum test, **SA.C**). At the scalp, the evoked response had a smaller negative peak (mean -43.0 μV, range [-104.1, -5.3] μV) than the preceding endogenous slow oscillation (mean -73.3 μV, range [-117.9, -11.2] μV; $p<0.001$, **SA.C**, paired t-test). At the thalamus, no difference was detected in the negative peak of the evoked response (mean -64.3 μV, range [-134.3, -1.1] μV) compared to the preceding endogenous slow oscillation (mean -78.0 μV, range [-

188.7, -25.8] µV; p=0.3, paired t-test, **SA.C**). However, the evoked thalamic response had a deeper downstate than the evoked scalp response (p=0.002, paired t-test **SA.C**).

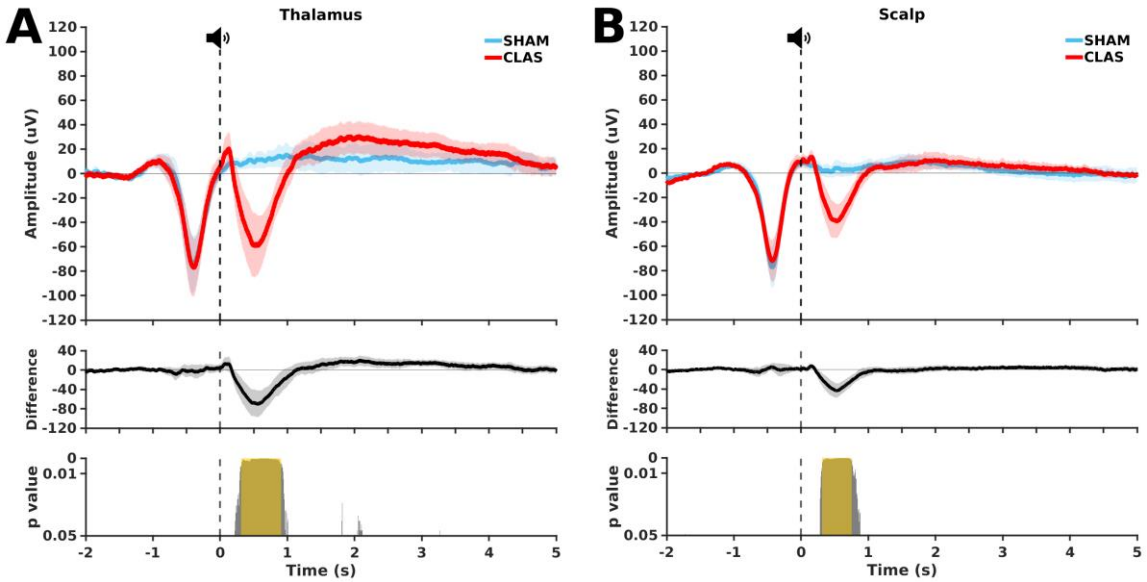

Figure 5.3. Thalamic and scalp auditory responses to closed-loop stimulation. At the **(A)** thalamus and **(B)** scalp, there is a large, evoked oscillation, following stimulation targeting the upstate of the slow oscillation (CLAS, red in upper panels) compared to the sham night (SHAM, blue in upper panels). The difference between the CLAS and SHAM conditions (middle panels) is significant (bottom panel, where yellow indicates significance after correction for multiple comparisons). In all figures, thick solid lines indicate the mean and shading indicates 95% confidence intervals.

3.4. SO-CLAS does not increase spindle incidence and may decrease performance on a memory task

No differences were detected between the average spindle incidence during CLAS and sham nights (p>0.05, Wilcoxon ranksum test and correction for multiple comparisons using FDR, **SA.D**; Fig 5.4A). Comparing performance on the MST for each hand, there

was a trend toward reduced memory improvement after a night of CLAS compared to a night of SHAM stimulation (p=0.096, paired t-test, **SA.E**; Fig 5.4B,C).

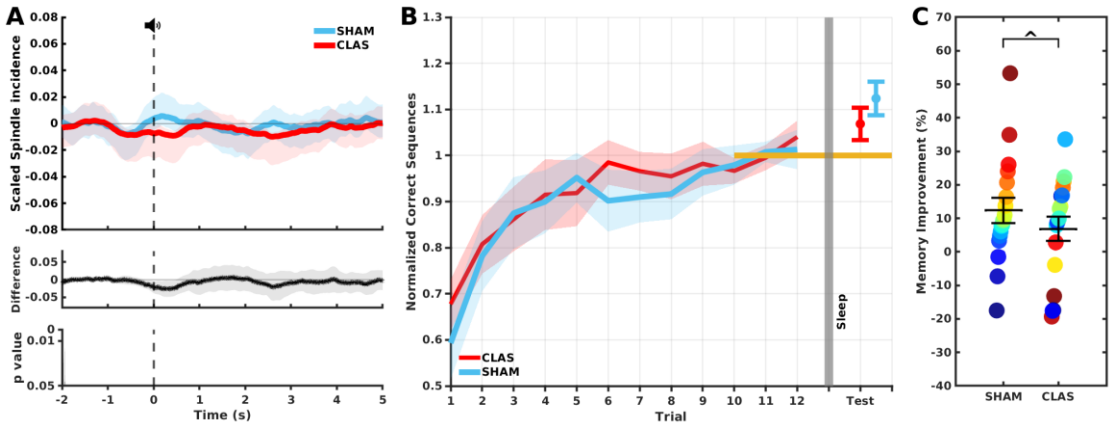

Figure 5.4. Impact of SO-CLAS on spindle incidence and sleep-dependent memory consolidation. A) No differences were detected between the average spindle incidence curves of CLAS and sham nights. Shading indicates 95% confidence intervals. **B)** The learning curves of MST before CLAS and sham show typical responses of diminished returns of learning towards the 12th trials, with CLAS showing a lesser mean increase in performance after sleep compared to sham. thick solid lines indicate the mean and shading indicates 95% confidence intervals. Performance was normalized by the average of the last trials in training before sleep (orange line). **C)** Comparing the performance on each hand, memory improvement trends worse following a CLAS night compared to sham. In this panel, each dot indicates a subject, the thick horizonal line indicates the mean, and the thin horizontal lines indicate standard error of the mean. ^p=0.1.

3.5. Efficacy of LA-CLAS also depends on SO phase

Ten subjects completed LA-CLAS nights. Across these subjects, 5,515 auditory stimulations were delivered in N2 and N3 sleep stages (mean per subject: 552, range: [129, 1299]), resulting in 4,018 evoked SOs in the thalamus and 1,582 evoked SOs at the scalp. LA-CLAS administered closer to the upstate of the SO oscillation evoked more SOs

compared to earlier stimulation times (i.e., before the upstate) in the thalamus (phase of stimulations with evoked SO: average -0.12 rad, interquartile range [-0.88, 0.54] rad; phase of stimulations without evoked SO: average -0.61 rad, interquartile range [-1.59, 0.11] rad; p<0.001, t-test, **SA.A**) and on the scalp (phase of stimulations with evoked SO: average 0.05 rad, interquartile range [-0.49, 0.49] rad; phase of stimulations without evoked SO: average -0.25 rad, interquartile range [-0.84, 0.28] rad; p<0.001, t-test, **SA.A**; Fig. 5.5AB).

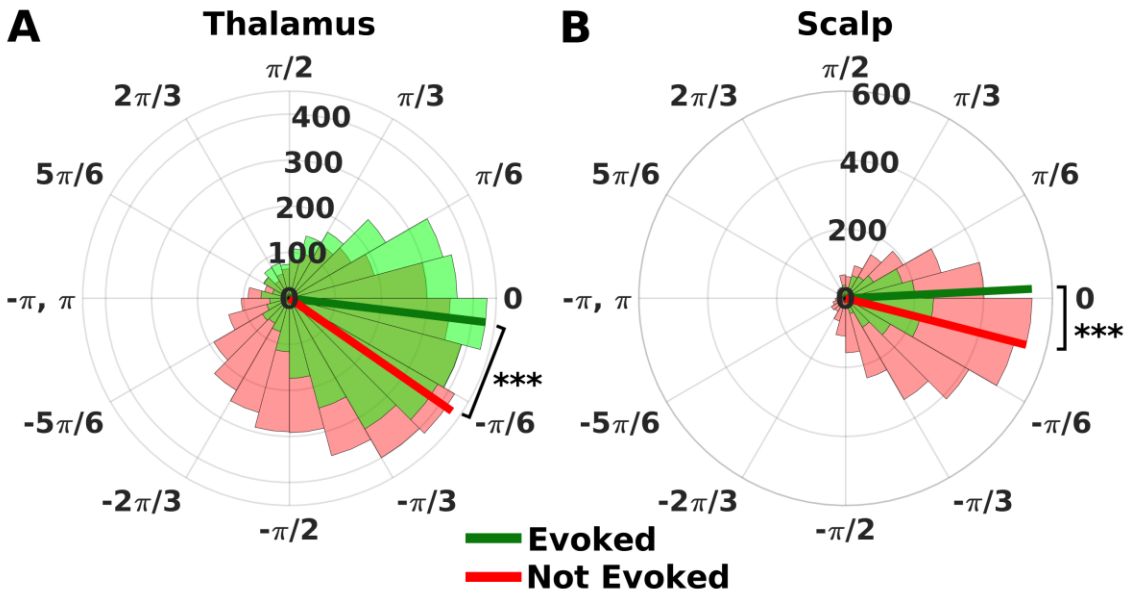

Figure 5.5. Success of LA-CLAS is influenced by phase of stimulation. A) Auditory stimulation aligned with the SO upstate is more likely to evoke a SO (green) than auditory stimulation not aligned with the SO upstate (red) in the thalamus. **B)** Auditory stimulation aligned with the SO upstate is more likely to evoke a SO (green) than auditory stimulation not aligned with the SO upstate (red) at the scalp.

3.6. LA-CLAS evokes thalamic slow oscillations

Ten subjects had both LA-CLAS and LA-CLAS sham nights. In the thalamus, we found a larger evoked slow oscillation averaged across all subjects following auditory stimulation on the CLAS night (mean -56.2 μV, 95% CI [-86.2, -26.1] μV) compared to the sham night (6.4 μV, 95% CI [2.6, 9.9] μV; $p<0.001$, Wilcoxon ranksum test and correction for multiple comparisons using FDR, **SA.B**). We found a similar result at the scalp; a larger evoked response averaged across all subjects following auditory stimulation on the CLAS night (mean -32.7 μV, 95% CI [-47.4, -18.1] μV) compared to the sham night (mean -4.0 μV, 95% CI [-8.1, -0.0] μV;, $p<0.001$ (uncorrected), $p>0.05$ (corrected), Wilcoxon ranksum test and correction for multiple comparisons using FDR, **SA.B**; Fig 5.6).

Considering the evoked response for each individual subject, no difference was detected between the average arrival time of the negative peak of the evoked response at the thalamus (mean 535.4, range: [296.9, 626.0] ms) compared to the scalp (mean 547.8, range [467.8, 600.6] ms, $p=0.9$, Wilcoxon ranksum test). No difference was found in the amplitude of the evoked response detected in the thalamus (mean -52.9 μV, range [-143.7 -2.9] μV) compared to the scalp (mean: -35.0 μV, range: [-80.6, -10.8] μV, $p =0.47$, Wilcoxon ranksum test).

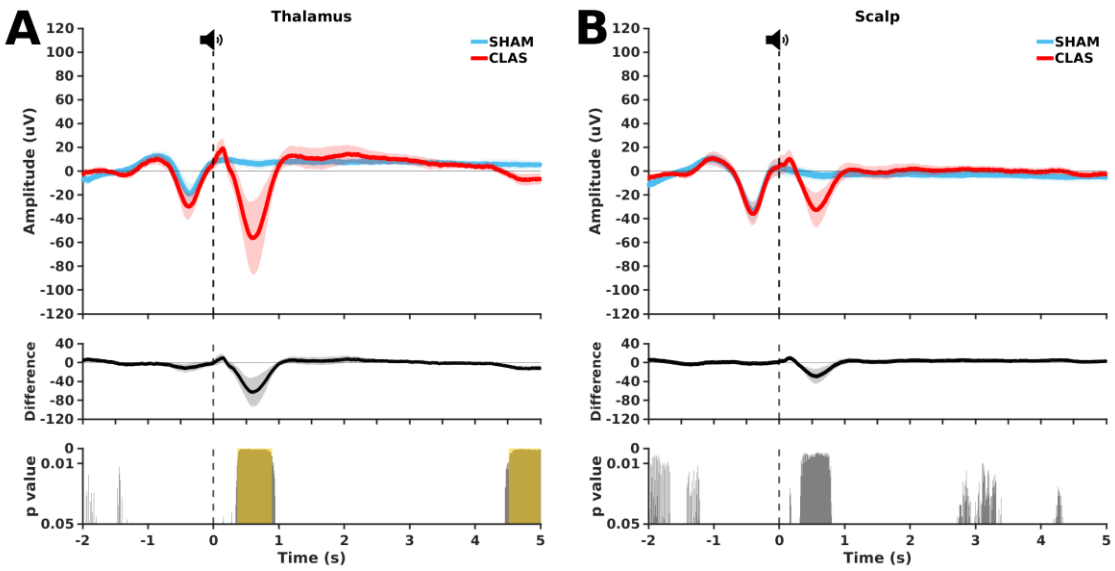

Figure 5.6. Thalamic and scalp auditory responses to modified closed-loop stimulation. At the **(A)** thalamus and **(B)** scalp, there is a large, evoked oscillation, following stimulation targeting the upstate of the slow oscillation (CLAS, red in upper panels) compared to the sham night (SHAM, blue in upper panels). The difference between the CLAS and SHAM conditions (middle panels) is significant (bottom panel, where yellow indicates significance after correction for multiple comparisons). In all figures, thick solid lines indicate the mean and shading indicates 95% confidence intervals.

3.7. LA-CLAS increases spindle incidence and performance on a memory task

There was an increase in spindle incidence after CLAS stimulation compared to sham (p=0.002, and correction for multiple comparisons using FDR, **SA.D**; Fig 5.7A). Comparing performance on the MST for each hand, there was an increase in memory improvement following a LA-CLAS night compared to sham (p=0.019, **SA.E**; Fig 5.7B,C).

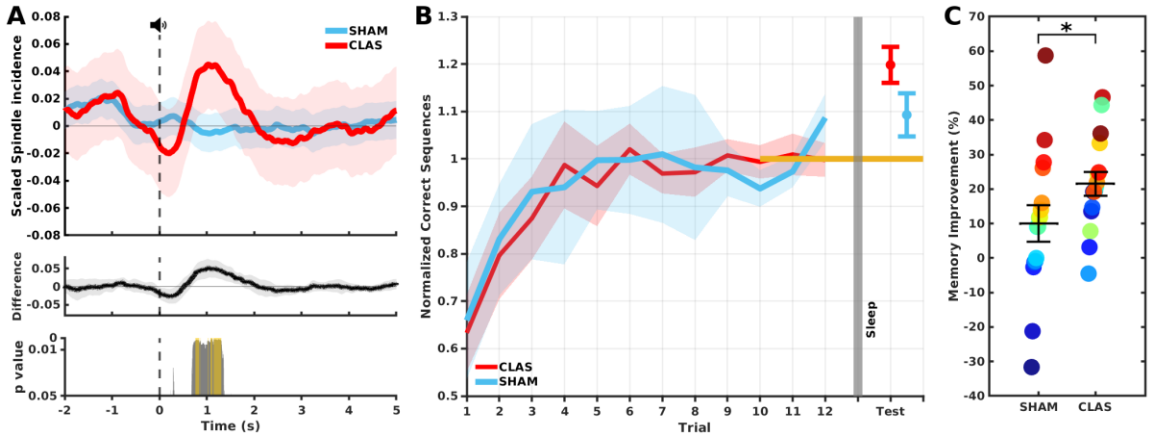

Figure 5.7. Spindle incidence and sleep-dependent memory improvement following LA-CLAS. A) There is a large increase in spindle incidence following LA-CLAS stimulation compared to sham nights. See caption of Figure 5.4 for description of panel elements. **B)** Subjects underdoing LA-CLAS or sham LA-CLAS showed normal learning curves with learning plateaus towards the later trials. Performance was normalized by the average of the last trials in training before sleep (orange line). **C)** LA-CLAS increases memory improvement compared to sham. In this panel, each dot indicates a subject, the thick horizonal line indicates the mean, and the thin horizontal lines indicate the standard error of the mean. *p=0.02.

4. Discussion

Through simultaneous scalp EEG and intracranial thalamic recordings, we investigated the impact, parameters, and mechanisms underlying CLAS-induced slow oscillations and sleep spindles, and the impact on memory function in patients with epilepsy. The observed increases in both cortical and thalamic SOs following CLAS indicate its potential as a modulatory tool for thalamocortical network dynamics during sleep.

We investigated the timing of CLAS relative to the upstate of SOs. We found that stimulation administered closer to the peak of the SO upstate yielded a higher number of

evoked SOs, suggesting a window of opportunity for enhancing the yield of this non-invasive technique. This temporal specificity aligns with theoretical frameworks positing that the upstate of SOs represents a period of increased neuronal excitability and synchronization, thereby amplifying the efficacy of sensory stimuli (Massimini *et al.*, 2004; Batterink, Creery and Paller, 2016).

Importantly, our study reveals a nuanced relationship between CLAS, SOs, and sleep spindles (SSs), crucial for memory consolidation. While CLAS targeting high-amplitude SOs disrupted SSs activity in the thalamus, stimulation targeting lower-amplitude SOs increased SS activity coupled with the evoked SOs. This differential modulation of SSs activity underscores the importance of considering SO characteristics in optimizing CLAS parameters for memory enhancement.

Furthermore, our investigation extends beyond the acute effects of CLAS to explore its implications for memory consolidation. We observed that CLAS targeting lower-amplitude SOs not only augmented SS activity but also translated into improved memory consolidation compared to CLAS targeting high-amplitude SOs. This finding underscores the translational potential of CLAS as a therapeutic intervention for addressing cognitive deficits in epilepsy and other neurological disorders.

Despite the promising findings, several questions warrant further exploration. Future studies could illuminate how CLAS implementations might influence memory function over time and explore individual variability in response to stimulation parameters.

Additionally, elucidating the underlying neural mechanisms mediating the observed effects of CLAS on thalamocortical dynamics would provide insights into its therapeutic efficacy and guide the development of targeted interventions.

5. Conclusion

In conclusion, the present study provides novel insights into the underlying mechanisms of closed-loop auditory stimulation (CLAS) and its potential as a non-invasive therapeutic modality for alleviating cognitive deficits in epilepsy. By elucidating the optimal timing and characteristics of stimulation, as well as its differential impact on thalamocortical dynamics and memory consolidation, our findings lay the groundwork for the development of personalized therapeutic interventions tailored to individual patient profiles. Future work to integrate this non-invasive therapeutic approach could lead to significant improvements in cognitive function and quality of life for epilepsy patients.

CHAPTER SIX: Conclusion

1. Short summary

In this thesis, we applied different methodologies to measure, predict, and manipulate electrographic markers of disease in patients with epilepsy. In four distinct studies, we examined techniques to improve the prediction of seizure risk (Chapter 2), understand thalamocortical circuit dysfunction (Chapter 3), explore the connection between sensory processing and attention deficits in the thalamus (Chapter 4), and optimize a potential non-invasive therapeutic intervention (Chapter 5).

2. Improved seizure risk prediction and understanding thalamocortical dysfunction

In Chapter 2, we investigated the challenge of seizure prediction in children with SeLECTS (self-limited epilepsy with centrotemporal spikes). To do so, we identified novel predictors estimated from features in the interictal discharges, such as spike height and slow wave characteristics. Predictions of seizure risk not only impact patient care, but also enhance our knowledge of the candidate neuronal mechanisms. Building on this, our second study (Chapter 3) considered abnormalities in the thalamocortical circuits of SeLECTS patients that persist even after seizures subside. Our results show that decreases in connectivity – inferred through increases in nerve conduction times – occur in children with resolved epilepsy. We also found a relationship between the ventral thalamus volume and conduction time, which supports the importance of changes in the thalamus in this

epilepsy and suggests a compensatory mechanism to enhance inhibitory processing and potentially suppress abnormal activity in the circuit. Future work should expand this study to include more subjects and investigate other types of epilepsies using similar methodology.

3. Thalamus: a key player in attention and biomarkers for dysfunction

In Chapter 4, we studied sensory gating in patients with drug-resistant epilepsy and the role of the thalamic reticular nucleus in sensory processing, spindle modulation, and attention control. We found the sensory gating response and spindle rate in the thalamus predicts patient accuracy in an attention task. These findings illuminate the complex interplay between thalamic function, sensory inhibition, and cognitive performance in epilepsy patients, potentially offering new directions for thalamocortical circuit understanding. This study highlights the potential of thalamic sensory gating, thalamic spindle rate and non-invasive scalp spindle rate as biomarkers for attention deficits and underscores the critical role of assessing thalamic function in managing epilepsy effectively. The next steps would be to examine how the sensory gating phenomenon fares across various brain regions, notably in the frontal lobe, hippocampus and temporal lobe.

4. Optimizing a novel therapeutic approach: closed-loop auditory stimulation (CLAS)

In Chapter 5, we implemented a novel therapeutic approach – Closed-Loop Auditory Stimulation (CLAS) – to address the cognitive symptoms in epilepsy. Existing work suggests CLAS enhances memory consolidation during sleep, suggesting its potential to improve cognitive outcomes and quality of life for individuals with epilepsy. We investigated strategies to optimize CLAS in patients with epilepsy and found that stimulation targeting lower amplitude slow oscillations supports sleep spindles and memory consolidation better than existing strategies. These results offer a blueprint for future studies, such as longitudinal investigating to examine long term effects. Additionally, investigating the potential synergistic effects of CLAS with other cognitive interventions, such as cognitive behavioral therapy or pharmacological treatments, could further enhance our understanding of its therapeutic efficacy and inform multimodal treatment approaches for epilepsy-related cognitive deficits.

5. Significance

In conclusion, in this thesis we investigate the impact of epilepsy on the brain's dynamics. To do so we applied different data recordings modalities, experiments, and stimulation approaches. We investigated the impact on behavior, linked the result to candidate pathophysiological mechanisms of epilepsy, and proposed a non-invasive

treatment strategy to improve cognitive symptoms. By offering insights into seizure prediction, thalamocortical dysfunction, sensory processing, attention deficits, and innovative therapies, we contribute to enhanced clinical practice and future research aimed at improving the lives of those living with epilepsy.

BIBLIOGRAPHY

Agarwal, R. *et al.* (2016) 'Thalamic abnormalities in children with continuous spike-wave during slow-wave sleep: An F-18-fluorodeoxyglucose positron emission tomography perspective', *Epilepsia*, 57(2), pp. 263–271. Available at: https://doi.org/10.1111/epi.13278.

Ahrens, S. *et al.* (2015) 'ErbB4 regulation of a thalamic reticular nucleus circuit for sensory selection', *Nature Neuroscience*, 18(1), pp. 104–111. Available at: https://doi.org/10.1038/nn.3897.

American Association of Neurological Surgeons (2024) *Epilepsy – Seizure Types, Symptoms and Treatment Options*. Available at: https://www.aans.org/ (Accessed: 4 June 2024).

Andrillon, T. *et al.* (2011) 'Sleep Spindles in Humans: Insights from Intracranial EEG and Unit Recordings', *The Journal of Neuroscience*, 31(49), pp. 17821–17834. Available at: https://doi.org/10.1523/JNEUROSCI.2604-11.2011.

Bagheri, E. *et al.* (2017) 'Interictal epileptiform discharge characteristics underlying expert interrater agreement', *Clinical Neurophysiology*, 128(10), pp. 1994–2005. Available at: https://doi.org/10.1016/j.clinph.2017.06.252.

Barkmeier, D.T. *et al.* (2012) 'High inter-reviewer variability of spike detection on intracranial EEG addressed by an automated multi-channel algorithm', *Clinical Neurophysiology*, 123(6), pp. 1088–1095. Available at: https://doi.org/10.1016/j.clinph.2011.09.023.

Batterink, L.J., Creery, J.D. and Paller, K.A. (2016) 'Phase of Spontaneous Slow Oscillations during Sleep Influences Memory-Related Processing of Auditory Cues', *The Journal of Neuroscience*, 36(4), pp. 1401–1409. Available at: https://doi.org/10.1523/JNEUROSCI.3175-15.2016.

Beenhakker, M.P. and Huguenard, J.R. (2009) 'Neurons that Fire Together Also Conspire Together: Is Normal Sleep Circuitry Hijacked to Generate Epilepsy?', *Neuron*, 62(5), pp. 612–632. Available at: https://doi.org/10.1016/j.neuron.2009.05.015.

Beghi, E. *et al.* (2019) 'Global, regional, and national burden of epilepsy, 1990–2016: a systematic analysis for the Global Burden of Disease Study 2016', *The Lancet Neurology*, 18(4), pp. 357–375. Available at: https://doi.org/10.1016/S1474-4422(18)30454-X.

Behrens, T. e. j. *et al.* (2003) 'Characterization and propagation of uncertainty in diffusion-weighted MR imaging', *Magnetic Resonance in Medicine*, 50(5), pp. 1077–1088. Available at: https://doi.org/10.1002/mrm.10609.

Benjamini, Y. and Hochberg, Y. (1995) 'Controlling the False Discovery Rate: A Practical and Powerful Approach to Multiple Testing', *Journal of the Royal Statistical Society. Series B (Methodological)*, 57(1), pp. 289–300.

Bennett, D.R. (1967) 'Spike-wave complexes in "normal" flying personnel', *Aerospace medicine*, 38(12), p. 1276.

Berg, A.T. *et al.* (2010) 'Revised terminology and concepts for organization of seizures and epilepsies: Report of the ILAE Commission on Classification and Terminology, 2005–2009', *Epilepsia*, 51(4), pp. 676–685. Available at: https://doi.org/10.1111/j.1528-1167.2010.02522.x.

Black, M.A. *et al.* (2000) 'Real-time Detection of Epileptiform Activity in the EEG: A Blinded Clinical Trial', *Clinical Electroencephalography*, 31(3), pp. 122–130. Available at: https://doi.org/10.1177/155005940003100304.

Blumenfeld, H. (2002) 'The Thalamus and Seizures', *Archives of Neurology*, 59(1), p. 135. Available at: https://doi.org/10.1001/archneur.59.1.135.

Bouma, P.A.D. *et al.* (1997) 'The course of benign partial epilepsy of childhood with centrotemporal spikes', *Neurology*, 48(2), pp. 430–437. Available at: https://doi.org/10.1212/WNL.48.2.430.

Bragin, A., Wilson, C.L. and Engel Jr, J. (2000) 'Chronic Epileptogenesis Requires Development of a Network of Pathologically Interconnected Neuron Clusters: A Hypothesis', *Epilepsia*, 41(s6), pp. S144–S152. Available at: https://doi.org/10.1111/j.1528-1157.2000.tb01573.x.

Bray Patrick F. *et al.* (1964) 'Evidence for a Genetic Etiology of Temporal-Central Abnormalities in Focal Epilepsy', *New England Journal of Medicine*, 271(18), pp. 926–933. Available at: https://doi.org/10.1056/NEJM196410292711803.

Bray, P.F. and Wiser, W.C. (1965) 'HEREDITARY CHARACTERISTICS OF FAMILIAL TEMPORAL-CENTRAL FOCAL EPILEPSY', *Pediatrics*, 36(2), pp. 207–211. Available at: https://doi.org/10.1542/peds.36.2.207.

Caciagli, L. *et al.* (2020) 'Thalamus and focal to bilateral seizures', *Neurology*, 95(17), pp. e2427–e2441. Available at: https://doi.org/10.1212/WNL.0000000000010645.

Callenbach, P.M.C. *et al.* (2010) ‘Long term outcome of benign childhood epilepsy with centrotemporal spikes: Dutch Study of Epilepsy in Childhood’, *Seizure*, 19(8), pp. 501–506. Available at: https://doi.org/10.1016/j.seizure.2010.07.007.

Carvill, G.L. *et al.* (2013) ‘GRIN2A mutations cause epilepsy-aphasia spectrum disorders’, *Nature Genetics*, 45(9), pp. 1073–1076. Available at: https://doi.org/10.1038/ng.2727.

Chang, W.-D. *et al.* (2016) ‘Detection of eye blink artifacts from single prefrontal channel electroencephalogram’, *Computer Methods and Programs in Biomedicine*, 124, pp. 19–30. Available at: https://doi.org/10.1016/j.cmpb.2015.10.011.

Chen, H. and Koubeissi, M.Z. (2019) ‘Electroencephalography in Epilepsy Evaluation’, *CONTINUUM: Lifelong Learning in Neurology*, 25(2), p. 431. Available at: https://doi.org/10.1212/CON.0000000000000705.

Chen, Z. *et al.* (2016) ‘Thalamic Circuit Mechanisms Link Sensory Processing in Sleep and Attention’, *Frontiers in Neural Circuits*, 9. Available at: https://doi.org/10.3389/fncir.2015.00083.

Ciumas, C. *et al.* (2014) ‘White matter development in children with benign childhood epilepsy with centro-temporal spikes’, *Brain*, 137(4), pp. 1095–1106. Available at: https://doi.org/10.1093/brain/awu039.

Cowan, N. (2008) ‘What are the differences between long-term, short-term, and working memory?’, *Progress in brain research*, 169, pp. 323–338. Available at: https://doi.org/10.1016/S0079-6123(07)00020-9.

Crabtree, J.W. (2018) ‘Functional Diversity of Thalamic Reticular Subnetworks’, *Frontiers in systems neuroscience*, 12, pp. 41–41. Available at: https://doi.org/10.3389/fnsys.2018.00041.

Davis, Z.W. *et al.* (2020) ‘Spontaneous Traveling Cortical Waves Gate Perception in Behaving Primates’, *Nature*, 587(7834), pp. 432–436. Available at: https://doi.org/10.1038/s41586-020-2802-y.

Desikan, R.S. *et al.* (2006) ‘An automated labeling system for subdividing the human cerebral cortex on MRI scans into gyral based regions of interest’, *NeuroImage*, 31(3), pp. 968–980. Available at: https://doi.org/10.1016/j.neuroimage.2006.01.021.

Eeg-Olofsson, O., Petersén, I. and Selldén, U. (1971) ‘The Development of the Electroencephalogram in Normal Children from the Age of 1 Through 15 Years –

Paroxysmal activity', *Neuropädiatrie*, 2(04), pp. 375–404. Available at: https://doi.org/10.1055/s-0028-1091791.

Ellenrieder, N. von *et al.* (2022) 'SleepSEEG: automatic sleep scoring using intracranial EEG recordings only', *Journal of Neural Engineering*, 19(2), p. 026057. Available at: https://doi.org/10.1088/1741-2552/ac6829.

Engel, A.K. *et al.* (2005) 'Invasive recordings from the human brain: clinical insights and beyond', *Nature Reviews Neuroscience*, 6(1), pp. 35–47. Available at: https://doi.org/10.1038/nrn1585.

Engel, J. (2011) 'Biomarkers in epilepsy: introduction', *Biomarkers in Medicine*, 5(5), pp. 537–544. Available at: https://doi.org/10.2217/bmm.11.62.

Epilepsy and Seizures | National Institute of Neurological Disorders and Stroke (2024). Available at: https://www.ninds.nih.gov/health-information/disorders/epilepsy-and-seizures (Accessed: 4 June 2024).

Epstein, J.N. *et al.* (2010) 'Examining predictors of reaction times in children with ADHD and normal controls', *Journal of the International Neuropsychological Society : JINS*, 16(1), pp. 138–147. Available at: https://doi.org/10.1017/S1355617709991111.

Fama, R. and Sullivan, E.V. (2015) 'Thalamic structures and associated cognitive functions: Relations with age and aging', *Neuroscience and biobehavioral reviews*, 54, pp. 29–37. Available at: https://doi.org/10.1016/j.neubiorev.2015.03.008.

Fedorov, A. *et al.* (2012) '3D Slicer as an image computing platform for the Quantitative Imaging Network', *Magnetic Resonance Imaging*, 30(9), pp. 1323–1341. Available at: https://doi.org/10.1016/j.mri.2012.05.001.

Feng, L. *et al.* (2017) 'Seizures and Sleep in the Thalamus: Focal Limbic Seizures Show Divergent Activity Patterns in Different Thalamic Nuclei', *The Journal of Neuroscience*, 37(47), pp. 11441–11454. Available at: https://doi.org/10.1523/JNEUROSCI.1011-17.2017.

Fernández, I.S. *et al.* (2015) 'Should epileptiform discharges be treated? Invited Review: Epilepsia', *Epilepsia*, 56(10), pp. 1492–1504. Available at: https://doi.org/10.1111/epi.13108.

Fischl, B. *et al.* (2002) 'Whole brain segmentation: automated labeling of neuroanatomical structures in the human brain', *Neuron*, 33(3), pp. 341–355. Available at: https://doi.org/10.1016/s0896-6273(02)00569-x.

Fischl, B. *et al.* (2004) ‘Sequence-independent segmentation of magnetic resonance images’, *NeuroImage*, 23 Suppl 1, pp. S69-84. Available at: https://doi.org/10.1016/j.neuroimage.2004.07.016.

Fischl, B. (2012) ‘FreeSurfer’, *NeuroImage*, 62(2), pp. 774–781. Available at: https://doi.org/10.1016/j.neuroimage.2012.01.021.

Fischl, B., Sereno, M.I. and Dale, A.M. (1999) ‘Cortical Surface-Based Analysis: II: Inflation, Flattening, and a Surface-Based Coordinate System’, *NeuroImage*, 9(2), pp. 195–207. Available at: https://doi.org/10.1006/nimg.1998.0396.

Fisher, R.S. *et al.* (2014) ‘ILAE Official Report: A practical clinical definition of epilepsy’, *Epilepsia*, 55(4), pp. 475–482. Available at: https://doi.org/10.1111/epi.12550.

Frauscher, B. *et al.* (2017) ‘High-frequency oscillations: The state of clinical research’, *Epilepsia*, 58(8), pp. 1316–1329. Available at: https://doi.org/10.1111/epi.13829.

FreeSurfer (no date) *FreeSurfer*. Available at: https://surfer.nmr.mgh.harvard.edu/ (Accessed: 22 April 2024).

Garcia-Ramos, C. *et al.* (2015) ‘Cognition and Brain Development in Children with Benign Epilepsy with Centrotemporal Spikes (BECTS)’, *Epilepsia*, 56(10), pp. 1615–1622. Available at: https://doi.org/10.1111/epi.13125.

Ghasemi, P., Sahraee, T. and Mohammadi, A. (2018) ‘Closed- and Open-loop Deep Brain Stimulation: Methods, Challenges, Current and Future Aspects’, *Journal of Biomedical Physics & Engineering*, 8(2), pp. 209–216.

Gotman, J. and Koffler, D.J. (1989) ‘Interictal spiking increases after seizures but does not after decrease in medication’, *Electroencephalography and Clinical Neurophysiology*, 72(1), pp. 7–15. Available at: https://doi.org/10.1016/0013-4694(89)90026-6.

Gotman, J. and Marciani, M.G. (1985) ‘Electroencephalographic spiking activity, drug levels, and seizure occurence in epileptic patients’, *Annals of Neurology*, 17(6), pp. 597–603. Available at: https://doi.org/10.1002/ana.410170612.

Gregory, D.L. and Wong, P.K. (1984) ‘Topographical Analysis of the Centrotemporal Discharges in Benign Rolandic Epilepsy of Childhood’, *Epilepsia*, 25(6), pp. 705–711. Available at: https://doi.org/10.1111/j.1528-1157.1984.tb03481.x.

Gregory, R.P., Oates, T. and Merry, R.T.G. (1993) ‘Electroencephalogram epileptiform abnormalities in candidates for aircrew training’, *Electroencephalography and Clinical*

Neurophysiology, 86(1), pp. 75–77. Available at: https://doi.org/10.1016/0013-4694(93)90069-8.

Grigg, -Damberger Madeleine *et al.* (2007) 'The Visual Scoring of Sleep and Arousal in Infants and Children', *Journal of Clinical Sleep Medicine*, 03(02), pp. 201–240. Available at: https://doi.org/10.5664/jcsm.26819.

Gupta, S. and Kadam, S.D. (2022) 'Interictal Discharges: All Roads Lead to Rome?', *Epilepsy Currents*, 22(4), pp. 252–254. Available at: https://doi.org/10.1177/15357597221098809.

Halford, J.J. (2009) 'Computerized epileptiform transient detection in the scalp electroencephalogram: Obstacles to progress and the example of computerized ECG interpretation', *Clinical Neurophysiology*, 120(11), pp. 1909–1915. Available at: https://doi.org/10.1016/j.clinph.2009.08.007.

Hamalainen, M.S. and Sarvas, J. (1987) 'Feasibility of the homogeneous head model in the interpretation of neuromagnetic fields', *Physics in Medicine & Biology*, 32(1), p. 91. Available at: https://doi.org/10.1088/0031-9155/32/1/014.

Haneef, Z. and Skrehot, H.C. (2023) 'Neurostimulation in generalized epilepsy: A systematic review and meta-analysis', *Epilepsia*, 64(4), pp. 811–820. Available at: https://doi.org/10.1111/epi.17524.

Herman, S.T. *et al.* (2011) 'Electroencephalography in clinical epilepsy research', *Epilepsy & Behavior*, 22(1), pp. 126–133. Available at: https://doi.org/10.1016/j.yebeh.2011.06.009.

Herrera, C.G. and Tarokh, L. (2024) 'A Thalamocortical Perspective on Sleep Spindle Alterations in Neurodevelopmental Disorders', *Current Sleep Medicine Reports*, 10(2), pp. 103–118. Available at: https://doi.org/10.1007/s40675-024-00284-x.

Hesdorffer, D.C. *et al.* (2004) 'ADHD as a Risk Factor for Incident Unprovoked Seizures and Epilepsyin Children', *Archives of General Psychiatry*, 61(7), pp. 731–736. Available at: https://doi.org/10.1001/archpsyc.61.7.731.

Holmes, G.L. (2015) 'Cognitive impairment in Epilepsy: The Role of Network Abnormalities', *Epileptic disorders : international epilepsy journal with videotape*, 17(2), pp. 101–116. Available at: https://doi.org/10.1684/epd.2015.0739.

Holstein, D.H. *et al.* (2013) 'Sensory and sensorimotor gating in adult attention-deficit/hyperactivity disorder (ADHD)', *Psychiatry Research*, 205(1–2), pp. 117–126. Available at: https://doi.org/10.1016/j.psychres.2012.08.013.

Horvath, A.A. *et al.* (2020) ‘Inhibiting Epileptiform Activity in Cognitive Disorders: Possibilities for a Novel Therapeutic Approach’, *Frontiers in Neuroscience*, 14, p. 557416. Available at: https://doi.org/10.3389/fnins.2020.557416.

Iglesias, J.E. *et al.* (2018) ‘A probabilistic atlas of the human thalamic nuclei combining *ex vivo* MRI and histology’, *NeuroImage*, 183, pp. 314–326. Available at: https://doi.org/10.1016/j.neuroimage.2018.08.012.

Jing, J. *et al.* (2020) ‘Development of Expert-Level Automated Detection of Epileptiform Discharges During Electroencephalogram Interpretation’, *JAMA Neurology*, 77(1), pp. 103–108. Available at: https://doi.org/10.1001/jamaneurol.2019.3485.

Johnson, H., Harris, G. and Williams, K. (2007) ‘BRAINSFit: Mutual Information Registrations of Whole-Brain 3D Images, Using the Insight Toolkit’, *The Insight Journal* [Preprint]. Available at: https://doi.org/10.54294/hmb052.

Judd, L.L. *et al.* (1992) ‘Sensory gating deficits in schizophrenia: new results’, *The American Journal of Psychiatry*, 149(4), pp. 488–493. Available at: https://doi.org/10.1176/ajp.149.4.488.

Kaculini, C.M., Tate-Looney, A.J. and Seifi, A. (2021) ‘The History of Epilepsy: From Ancient Mystery to Modern Misconception’, *Cureus* [Preprint]. Available at: https://doi.org/10.7759/cureus.13953.

Kanemura, H. *et al.* (2015) ‘EEG characteristics predict subsequent epilepsy in children with their first unprovoked seizure’, *Epilepsy Research*, 115, pp. 58–62. Available at: https://doi.org/10.1016/j.eplepsyres.2015.05.011.

Kanner, A.M. (2008) ‘Mood disorder and epilepsy: a neurobiologic perspective of their relationship’, *Dialogues in Clinical Neuroscience*, 10(1), pp. 39–45.

Kanoga, S., Nakanishi, M. and Mitsukura, Y. (2016) ‘Assessing the effects of voluntary and involuntary eyeblinks in independent components of electroencephalogram’, *Neurocomputing*, 193, pp. 20–32. Available at: https://doi.org/10.1016/j.neucom.2016.01.057.

Khani, A. *et al.* (2019) ‘Large-Scale Networks for Auditory Sensory Gating in the Awake Mouse’, *eNeuro*, 6(5), p. ENEURO.0207-19.2019. Available at: https://doi.org/10.1523/ENEURO.0207-19.2019.

Kim, S.E. *et al.* (2014) ‘Alterations in white matter microstructures and cognitive dysfunctions in benign childhood epilepsy with centrotemporal spikes’, *European*

Journal of Neurology, 21(5), pp. 708–717. Available at: https://doi.org/10.1111/ene.12301.

van Klink, N.E.C. *et al.* (2016) 'Ripples on rolandic spikes: A marker of epilepsy severity', *Epilepsia*, 57(7), pp. 1179–1189. Available at: https://doi.org/10.1111/epi.13423.

Kobayashi, K. *et al.* (2011) 'High-frequency oscillations in idiopathic partial epilepsy of childhood', *Epilepsia*, 52(10), pp. 1812–1819. Available at: https://doi.org/10.1111/j.1528-1167.2011.03169.x.

Kostin, A. *et al.* (2017) 'Sleep homeostasis', in *Reference Module in Neuroscience and Biobehavioral Psychology*. Elsevier Inc. Available at: https://doi.org/10.1016/B978-0-12-822963-7.00243-7.

Kramer, M. *et al.* (2021) 'Focal sleep spindle deficits reveal focal thalamocortical dysfunction and predict cognitive deficits in childhood epilepsy with centrotemporal spikes', *The Journal of Neuroscience*, 41, p. JN-RM. Available at: https://doi.org/10.1523/JNEUROSCI.2009-20.2020.

Kramer, M.A. *et al.* (2019) 'Scalp recorded spike ripples predict seizure risk in childhood epilepsy better than spikes', *Brain*, 142(5), pp. 1296–1309. Available at: https://doi.org/10.1093/brain/awz059.

Kural, M.A. *et al.* (2020) 'Criteria for defining interictal epileptiform discharges in EEG', *Neurology*, 94(20), pp. e2139–e2147. Available at: https://doi.org/10.1212/WNL.0000000000009439.

Kwon, H. *et al.* (2022) 'Transient, developmental functional and structural connectivity abnormalities in the thalamocortical motor network in Rolandic epilepsy', *NeuroImage: Clinical*, 35, p. 103102. Available at: https://doi.org/10.1016/j.nicl.2022.103102.

Laura Fernandez and Anitha Luthi (2019) *Sleep Spindles: Mechanisms and Functions*. Available at: https://doi.org/10.1152/physrev.00042.2018.

Lee, Y., Nelder, J.A. and Pawitan, Y. (2006) 'Generalized linear models with random effects : unified analysis via h-likelihood'. Available at: https://digital.library.tu.ac.th/tu_dc/frontend/Info/item/dc:16433 (Accessed: 23 April 2024).

Lemke, J.R. *et al.* (2013) 'Mutations in GRIN2A cause idiopathic focal epilepsy with rolandic spikes', *Nature Genetics*, 45(9), pp. 1067–1072. Available at: https://doi.org/10.1038/ng.2728.

Leszczyński, M. and Staudigl, T. (2016) ‘Memory-guided attention in the anterior thalamus’, *Neuroscience & Biobehavioral Reviews*, 66, pp. 163–165. Available at: https://doi.org/10.1016/j.neubiorev.2016.04.015.

Li, Q. *et al.* (2021) ‘Computational Evidence for a Competitive Thalamocortical Model of Spikes and Spindle Activity in Rolandic Epilepsy’, *Frontiers in Computational Neuroscience*, 15. Available at: https://doi.org/10.3389/fncom.2021.680549.

Li, Y. *et al.* (2020) ‘Distinct subnetworks of the thalamic reticular nucleus’, *Nature (London)*, 583(7818), pp. 819–824. Available at: https://doi.org/10.1038/s41586-020-2504-5.

Lijffijt, M. *et al.* (2009) ‘P50, N100, and P200 sensory gating: Relationships with behavioral inhibition, attention, and working memory’, *Psychophysiology*, 46(5), p. 1059. Available at: https://doi.org/10.1111/j.1469-8986.2009.00845.x.

Lindquist, B.E. *et al.* (2023) ‘Thalamocortical circuits in generalized epilepsy: Pathophysiologic mechanisms and therapeutic targets’, *Neurobiology of disease*, 181, p. 106094. Available at: https://doi.org/10.1016/j.nbd.2023.106094.

Löscher, W. *et al.* (2020) ‘Drug Resistance in Epilepsy: Clinical Impact, Potential Mechanisms, and New Innovative Treatment Options’, *Pharmacological Reviews*, 72(3), pp. 606–638. Available at: https://doi.org/10.1124/pr.120.019539.

Mamashli, F. *et al.* (2017) ‘Auditory processing in noise is associated with complex patterns of disrupted functional connectivity in autism spectrum disorder’, *Autism Research*, 10(4), pp. 631–647. Available at: https://doi.org/10.1002/aur.1714.

Martín-López, D. *et al.* (2017) ‘The Role of Thalamus Versus Cortex in Epilepsy: Evidence from Human Ictal Centromedian Recordings in Patients Assessed for Deep Brain Stimulation’, *International journal of neural systems*, 27(7), pp. 1750010-. Available at: https://doi.org/10.1142/S0129065717500101.

Massimini, M. *et al.* (2004) ‘The Sleep Slow Oscillation as a Traveling Wave’, *Journal of Neuroscience*, 24(31), pp. 6862–6870. Available at: https://doi.org/10.1523/JNEUROSCI.1318-04.2004.

Mazarati, A. (2008) ‘Epilepsy and Forgetfulness: One Impairment, Multiple Mechanisms’, *Epilepsy Currents*, 8(1), pp. 25–26. Available at: https://doi.org/10.1111/j.1535-7511.2007.00224.x.

McAlonan, K., Brown, V.J. and Bowman, E.M. (2000) ‘Thalamic Reticular Nucleus Activation Reflects Attentional Gating during Classical Conditioning’, *The Journal of*

Neuroscience, 20(23), pp. 8897–8901. Available at: https://doi.org/10.1523/JNEUROSCI.20-23-08897.2000.

McAlonan, K., Cavanaugh, J. and Wurtz, R.H. (2006) 'Attentional Modulation of Thalamic Reticular Neurons', *The Journal of neuroscience*, 26(16), pp. 4444–4450. Available at: https://doi.org/10.1523/JNEUROSCI.5602-05.2006.

Micoulaud-Franchi, J.-A. *et al.* (2015) 'Perceptual abnormalities related to sensory gating deficit are core symptoms in adults with ADHD', *Psychiatry Research*, 230(2), pp. 357–363. Available at: https://doi.org/10.1016/j.psychres.2015.09.016.

Moeller, F. *et al.* (2013) 'EEG-fMRI in atypical benign partial epilepsy', *Epilepsia*, 54(8), pp. e103–e108. Available at: https://doi.org/10.1111/epi.12243.

Mölle, M. and Born, J. (2011) 'Chapter 7 - Slow oscillations orchestrating fast oscillations and memory consolidation', in E.J.W. Van Someren et al. (eds) *Progress in Brain Research*. Elsevier (Slow Brain Oscillations of Sleep, Resting State and Vigilance), pp. 93–110. Available at: https://doi.org/10.1016/B978-0-444-53839-0.00007-7.

Nabbout, R. and Kuchenbuch, M. (2020) 'Impact of predictive, preventive and precision medicine strategies in epilepsy', *Nature Reviews Neurology*, 16(12), pp. 674–688. Available at: https://doi.org/10.1038/s41582-020-0409-4.

Nakajima, M., Schmitt, L.I. and Halassa, M.M. (2019) 'Prefrontal Cortex Regulates Sensory Filtering through a Basal Ganglia-to-Thalamus Pathway', *Neuron*, 103(3), pp. 445-458.e10. Available at: https://doi.org/10.1016/j.neuron.2019.05.026.

National Institute of Neurological Disorders and Stroke (2024) *Curing the Epilepsies: The Promise of Research | National Institute of Neurological Disorders and Stroke*. Available at: https://www.ninds.nih.gov/current-research/focus-disorders/epilepsy-research/curing-epilepsies-promise-research (Accessed: 4 June 2024).

Nemtsas, P. *et al.* (2017) 'Source localization of ictal epileptic activity based on high-density scalp EEG data', *Epilepsia*, 58(6), pp. 1027–1036. Available at: https://doi.org/10.1111/epi.13749.

Ngo, H.-V.V. *et al.* (2013) 'Auditory Closed-Loop Stimulation of the Sleep Slow Oscillation Enhances Memory', *Neuron*, 78(3), pp. 545–553. Available at: https://doi.org/10.1016/j.neuron.2013.03.006.

Ngo, H.-V.V. *et al.* (2015) 'Driving Sleep Slow Oscillations by Auditory Closed-Loop Stimulation—A Self-Limiting Process', *Journal of Neuroscience*, 35(17), pp. 6630–6638. Available at: https://doi.org/10.1523/JNEUROSCI.3133-14.2015.

Nguyen, Q.-A., Moolchand, P. and Soltesz, I. (2020) ‘Connecting Pathological Cellular Mechanisms to Large-Scale Seizure Structures’, *Trends in Neurosciences*, 43(8), pp. 547–549. Available at: https://doi.org/10.1016/j.tins.2020.04.006.

Nicolai, J. *et al.* (2012) ‘The cognitive effects of interictal epileptiform EEG discharges and short nonconvulsive epileptic seizures’, *Epilepsia*, 53(6), pp. 1051–1059. Available at: https://doi.org/10.1111/j.1528-1167.2012.03491.x.

Ostendorf, A.P. and Gedela, S. (2017) ‘Effect of Epilepsy on Families, Communities, and Society’, *Seminars in Pediatric Neurology*, 24(4), pp. 340–347. Available at: https://doi.org/10.1016/j.spen.2017.10.007.

Ostrowski, L.M. *et al.* (2019) ‘Dysmature superficial white matter microstructure in developmental focal epilepsy’, *Brain Communications*, 1(1), p. fcz002. Available at: https://doi.org/10.1093/braincomms/fcz002.

Portas, C.M. *et al.* (1998) ‘A Specific Role for the Thalamus in Mediating the Interaction of Attention and Arousal in Humans’, *Journal of Neuroscience*, 18(21), pp. 8979–8989. Available at: https://doi.org/10.1523/JNEUROSCI.18-21-08979.1998.

Potter, S.M., El Hady, A. and Fetz, E.E. (2014) ‘Closed-loop neuroscience and neuroengineering’, *Frontiers in Neural Circuits*, 8. Available at: https://doi.org/10.3389/fncir.2014.00115.

‘Proposal for Revised Classification of Epilepsies and Epileptic Syndromes’ (1989) *Epilepsia*, 30(4), pp. 389–399. Available at: https://doi.org/10.1111/j.1528-1157.1989.tb05316.x.

Prueter, C. and Norra, C. (2005) ‘Mood Disorders and Their Treatment in Patients With Epilepsy’, *The Journal of Neuropsychiatry and Clinical Neurosciences*, 17(1), pp. 20–28. Available at: https://doi.org/10.1176/jnp.17.1.20.

van Rijckevorsel, K. (2006) ‘Cognitive problems related to epilepsy syndromes, especially malignant epilepsies’, *Seizure*, 15(4), pp. 227–234. Available at: https://doi.org/10.1016/j.seizure.2006.02.019.

Ross, E.E. *et al.* (2020) ‘The natural history of seizures and neuropsychiatric symptoms in childhood epilepsy with centrotemporal spikes (CECTS)’, *Epilepsy & Behavior*, 103, p. 106437. Available at: https://doi.org/10.1016/j.yebeh.2019.07.038.

Sánchez Fernández, I. *et al.* (2017) ‘Reduced thalamic volume in patients with Electrical Status Epilepticus in Sleep’, *Epilepsy Research*, 130, pp. 74–80. Available at: https://doi.org/10.1016/j.eplepsyres.2017.01.010.

Scheffer, I.E. *et al.* (2017) ‘ILAE classification of the epilepsies: Position paper of the ILAE Commission for Classification and Terminology’, *Epilepsia*, 58(4), pp. 512–521. Available at: https://doi.org/10.1111/epi.13709.

Scheuer, M.L., Bagic, A. and Wilson, S.B. (2017) ‘Spike detection: Inter-reader agreement and a statistical Turing test on a large data set’, *Clinical Neurophysiology*, 128(1), pp. 243–250. Available at: https://doi.org/10.1016/j.clinph.2016.11.005.

Schiller, K. *et al.* (2022) ‘Focal epilepsy disrupts spindle structure and function’, *Scientific Reports*, 12(1), p. 11137. Available at: https://doi.org/10.1038/s41598-022-15147-0.

Schlafly, E.D. *et al.* (2022) ‘Multiple Sources of Fast Traveling Waves during Human Seizures: Resolving a Controversy’, *The Journal of Neuroscience*, 42(36), pp. 6966–6982. Available at: https://doi.org/10.1523/JNEUROSCI.0338-22.2022.

Shi, J. *et al.* (2013) ‘Sustained Attention in Intellectually Gifted Children Assessed Using a Continuous Performance Test’, *PLOS ONE*, 8(2), p. e57417. Available at: https://doi.org/10.1371/journal.pone.0057417.

Shi, W. *et al.* (2023) ‘Spike ripples localize the epileptogenic zone better than other leading biomarkers: a multicenter intracranial study’. medRxiv, p. 2023.04.25.23289111. Available at: https://doi.org/10.1101/2023.04.25.23289111.

Shinnar, S. *et al.* (1994) ‘Discontinuing antiepileptic drugs in children with epilepsy: A prospective study’, *Annals of Neurology*, 35(5), pp. 534–545. Available at: https://doi.org/10.1002/ana.410350506.

Sisterson, N.D. *et al.* (2019) ‘Closed-Loop Brain Stimulation for Drug-Resistant Epilepsy: Towards an Evidence-Based Approach to Personalized Medicine’, *Neurotherapeutics*, 16(1), pp. 119–127. Available at: https://doi.org/10.1007/s13311-018-00682-4.

Sitaram, R. *et al.* (2017) ‘Closed-loop brain training: the science of neurofeedback’, *Nature Reviews Neuroscience*, 18(2), pp. 86–100. Available at: https://doi.org/10.1038/nrn.2016.164.

Sonnleitner, A. *et al.* (2012) ‘Alpha spindles as neurophysiological correlates indicating attentional shift in a simulated driving task’, *International Journal of Psychophysiology*, 83(1), pp. 110–118. Available at: https://doi.org/10.1016/j.ijpsycho.2011.10.013.

Sovierzoski, M.A., Argoud, F.I.M. and De Azevedo, F.M. (2008) ‘Identifying eye blinks in EEG signal analysis’, in *2008 International Conference on Technology and*

Applications in Biomedicine. *2008 International Conference on Technology and Applications in Biomedicine (ITAB)*, Shenzhen, China: IEEE, pp. 406–409. Available at: https://doi.org/10.1109/ITAB.2008.4570605.

Specchio, N. *et al.* (2022) 'International League Against Epilepsy classification and definition of epilepsy syndromes with onset in childhood: Position paper by the ILAE Task Force on Nosology and Definitions', *Epilepsia*, 63(6), pp. 1398–1442. Available at: https://doi.org/10.1111/epi.17241.

Spencer, E.R. *et al.* (2022) 'Source EEG reveals that Rolandic epilepsy is a regional epileptic encephalopathy', *NeuroImage : Clinical*, 33, p. 102956. Available at: https://doi.org/10.1016/j.nicl.2022.102956.

Stafstrom, C.E. and Carmant, L. (2015) 'Seizures and Epilepsy: An Overview for Neuroscientists', *Cold Spring Harbor Perspectives in Medicine*, 5(6), p. a022426. Available at: https://doi.org/10.1101/cshperspect.a022426.

Staley, K.J. and Dudek, F.E. (2006) 'Interictal Spikes and Epileptogenesis', *Epilepsy Currents*, 6(6), pp. 199–202. Available at: https://doi.org/10.1111/j.1535-7511.2006.00145.x.

Steriade, M. *et al.* (1987) 'The deafferented reticular thalamic nucleus generates spindle rhythmicity', *Journal of Neurophysiology*, 57(1), pp. 260–273. Available at: https://doi.org/10.1152/jn.1987.57.1.260.

Stroink, H. *et al.* (2006) 'Interobserver reliability of visual interpretation of electroencephalograms in children with newly diagnosed seizures', *Developmental Medicine & Child Neurology*, 48(5), pp. 374–377. Available at: https://doi.org/10.1017/S0012162206000806.

Tamilia, E. *et al.* (2021) 'Noninvasive Mapping of Ripple Onset Predicts Outcome in Epilepsy Surgery', *Annals of Neurology*, 89(5), pp. 911–925. Available at: https://doi.org/10.1002/ana.26066.

de Bourbon-Teles, J. *et al.* (2014) 'Thalamic Control of Human Attention Driven by Memory and Learning', *Current Biology*, 24(9), pp. 993–999. Available at: https://doi.org/10.1016/j.cub.2014.03.024.

Tenney, J.R. *et al.* (2016) 'Longitudinal stability of interictal spikes in benign epilepsy with centrotemporal spikes', *Epilepsia*, 57(5), pp. 805–811. Available at: https://doi.org/10.1111/epi.13367.

Thorn, E.L. *et al.* (2020) ‘Persistent abnormalities in Rolandic thalamocortical white matter circuits in childhood epilepsy with centrotemporal spikes’, *Epilepsia*, 61(11), pp. 2500–2508. Available at: https://doi.org/10.1111/epi.16681.

Toosy, A.T., Mason, D.F. and Miller, D.H. (2014) ‘Optic neuritis’, *The Lancet Neurology*, 13(1), pp. 83–99. Available at: https://doi.org/10.1016/S1474-4422(13)70259-X.

Trapp, S., Schroll, H. and Hamker, F.H. (2012) ‘Open and closed loops: A computational approach to attention and consciousness’, *Advances in Cognitive Psychology*, 8(1), pp. 1–8. Available at: https://doi.org/10.2478/v10053-008-0096-y.

Truccolo, W. *et al.* (2014) ‘Neuronal Ensemble Synchrony during Human Focal Seizures’, *Journal of Neuroscience*, 34(30), pp. 9927–9944. Available at: https://doi.org/10.1523/JNEUROSCI.4567-13.2014.

Tucker, M.A., Nguyen, N. and Stickgold, R. (2016) ‘Experience Playing a Musical Instrument and Overnight Sleep Enhance Performance on a Sequential Typing Task’, *PLOS ONE*, 11(7), p. e0159608. Available at: https://doi.org/10.1371/journal.pone.0159608.

Understanding different kinds of seizures (2024) *NIH MedlinePlus Magazine*. Available at: https://magazine.medlineplus.gov/article/understanding-different-kinds-of-seizures (Accessed: 4 June 2024).

Urakami, Y. *et al.* (2012) ‘Sleep Spindles – As a Biomarker of Brain Function and Plasticity’, in *Advances in Clinical Neurophysiology*. IntechOpen. Available at: https://doi.org/10.5772/48427.

Vadlamudi, L. *et al.* (2006) ‘Analyzing the Etiology of Benign Rolandic Epilepsy: A Multicenter Twin Collaboration’, *Epilepsia*, 47(3), pp. 550–555. Available at: https://doi.org/10.1111/j.1528-1167.2006.00466.x.

Vantomme, G. *et al.* (2019) ‘Regulation of Local Sleep by the Thalamic Reticular Nucleus’, *Frontiers in Neuroscience*, 13, p. 576. Available at: https://doi.org/10.3389/fnins.2019.00576.

Vaughn, A. *et al.* (2011) ‘Relation Between Outcomes on a Continuous Performance Test and ADHD Symptoms Over Time’, *Journal of abnormal child psychology*, 39(6), pp. 853–864. Available at: https://doi.org/10.1007/s10802-011-9501-y.

Webber, W.R.S. *et al.* (1993) 'Automatic EEG spike detection: what should the computer imitate?', *Electroencephalography and Clinical Neurophysiology*, 87(6), pp. 364–373. Available at: https://doi.org/10.1016/0013-4694(93)90149-P.

White, A. *et al.* (2010) 'EEG spike activity precedes epilepsy after kainate-induced status epilepticus', *Epilepsia*, 51(3), pp. 371–383. Available at: https://doi.org/10.1111/j.1528-1167.2009.02339.x.

Wickens, S., Bowden, S.C. and D'Souza, W. (2017) 'Cognitive functioning in children with self-limited epilepsy with centrotemporal spikes: A systematic review and meta-analysis', *Epilepsia*, 58(10), pp. 1673–1685. Available at: https://doi.org/10.1111/epi.13865.

Williams, A.E. *et al.* (2016) 'Epilepsy and attention-deficit hyperactivity disorder: links, risks, and challenges', *Neuropsychiatric Disease and Treatment*, 12, pp. 287–296. Available at: https://doi.org/10.2147/NDT.S81549.

Wimmer, D. *et al.* (2015) 'Thalamic control of sensory selection in divided attention', *Nature*, 526(7575), pp. 705-709M. Available at: https://doi.org/10.1038/nature15398.

Wirrell, E.C. (1998) 'Benign Epilepsy of Childhood With Centrotemporal Spikes', *Epilepsia*, 39(s4), pp. S32–S41. Available at: https://doi.org/10.1111/j.1528-1157.1998.tb05123.x.

Wodeyar, A. *et al.* (2024) 'Thalamic epileptic spikes disrupt sleep spindles in patients with epileptic encephalopathy', *Brain*, p. awae119. Available at: https://doi.org/10.1093/brain/awae119.

World Health Organization (2024) *Epilepsy*. Available at: https://www.who.int/news-room/fact-sheets/detail/epilepsy (Accessed: 4 June 2024).

Wright, N.F. *et al.* (2015) 'A Critical Role for the Anterior Thalamus in Directing Attention to Task-Relevant Stimuli', *Journal of Neuroscience*, 35(14), pp. 5480–5488. Available at: https://doi.org/10.1523/JNEUROSCI.4945-14.2015.

Wunderlin, M. *et al.* (2021) 'Modulating overnight memory consolidation by acoustic stimulation during slow-wave sleep: a systematic review and meta-analysis', *Sleep*, 44(7), p. zsaa296. Available at: https://doi.org/10.1093/sleep/zsaa296.

Xie, W. *et al.* (2018) 'Timing matters: Impact of anticonvulsant drug treatment and spikes on seizure risk in benign epilepsy with centrotemporal spikes', *Epilepsia Open*, 3(3), pp. 409–417. Available at: https://doi.org/10.1002/epi4.12248.

Zhang, W. *et al.* (2023) ‘Childhood absence epilepsy patients with cognitive impairment have decreased sleep spindle density’, *Sleep Medicine*, 103, pp. 89–97. Available at: https://doi.org/10.1016/j.sleep.2023.01.012.

Zrenner, C. *et al.* (2016) ‘Closed-Loop Neuroscience and Non-Invasive Brain Stimulation: A Tale of Two Loops’, *Frontiers in Cellular Neuroscience*, 10, p. 92. Available at: https://doi.org/10.3389/fncel.2016.00092.

CURRICULUM VITAE